Modelling force behaviour and contributions of metallic extrusion dampers for seismic energy dissipation

Vishnupriya

A thesis
presented for the Degree
of
Doctor of Philosophy
in
Mechanical Engineering
at the
University of Canterbury
Christchurch, New Zealand

———————

University of Canterbury
2019

To my daughter Neerja
The centre of my universe.

Abstract

Supplemental energy dissipation devices are increasingly used to protect structures, limiting loads transferred to structures and absorbing significant response energy without sacrificial structural damage. HF2V, or high force to volume, devices are a successful form of relatively low-cost, robust supplemental dissipation devices. The displacement of the HF2V device bulged shaft plastically deforms a working material, dissipating significant energy.

HF2V devices are metallic extrusion dampers, currently designed using limited precision models, so there is variability in force prediction, which makes design difficult and time consuming. Furthermore, while a device force is predicted, the knowledge of the exact internal mechanisms occuring within these devices is lacking, limiting insight and predictive accuracy in device design. As a result, there is a need for significant analysis to develop and improve means of designing HF2V devices to deliver specific design required dissipation forces.

This thesis develops a first precision HF2V design model based on the sum of friction and extrusion forces modelled as a function of device dimensions. Specifically, the Area Ratio (AR), shaft Surface Area (SA), and Bulge Area (AB). Multiplicative coefficients for these terms in 14 linear and linear-quadratic models are calculated using regression analysis on data from 18 experimental devices with and without bulges. Pearson correlation coefficient values (R^2) summarise model completeness and the error between experimental and model predicted force. Leave k=3 out validation for random and specific groups of devices assesses model robustness to the device data used to identify the model. The overall results provide a simple, generalisable model capturing all relevant mechanics for precise design of HF2V devices to a specific quasi-static force capacity, as well as a good starting point for more specific and detailed mechanics models.

Upper bound and lower bound analytical models are then derived by matching the HF2V device geometric parameters to direct and indirect extrusion design parameters from the metal forming industry. Six design based analytical models provide maximum and minimum loads produced in HF2V devices based on plasticity theorem, and results are compared to experimental device forces. The models exhibit an operational range for the devices within which the HF2V devices operate during plastic deformation. All the experimental device forces lie under the direct extrusion upper bound values and above the lower bound values. The indirect extrusion model forces broadly match the experimental HF2V device forces. A further method to achieve approximate HF2V device forces from these analytical boundary equations is developed using combinations of UB and LB force models. Device parameters directly influencing damper forces are identified through analysis, which is valuable for future HF2V design selection, and provide an accurate, and more complex analytical modelling approach from this thesis, as well as boundary limits useful in design.

Finally, a generic finite element model is developed using ABAQUS, to better understand force generation and aid in precision device design, thus speeding up the overall design and implementation process for uptake and use. The model is applied to experimental HF2V devices of various sizes. The highly nonlinear, large-deflection analysis is run using ABAQUS/Explicit with automatic increments to balance higher accuracy and computational time. The total force output is sum of the friction forces between the lead working material and the steel device components, due to the contact pressure forces acting between moving shaft and displaced lead. The results are accurate to ±20% for *Typical* and *Large* devices, yielding a third model, which also provides insight into internal device motion and strain in the working material, which has not previously been known.

Overall, three modelling approaches developed for lead extrusion dampers are presented in this thesis. The generalized and design based models can predict specific force capacities of the HF2V devices in the design stage and can serve as an optimization tool for design modifications. Design parameters affecting the device forces in the devices are identified and provide a guideline for future design of the devices.

Acknowledgements

I wish to thank all the people whose assistance was a milestone in the completion of this project.

I would like to express my deepest gratitude to Professor Geoffrey Chase and Professor Geoffrey Rodgers, my research supervisors, for their patient guidance, enthusiastic encouragement and useful critiques of this research work. I am truly grateful for your continued support and optimism throughout the entirety of this research project.

I would like to express my very great appreciation to Professor John B. Mander, for his valuable and constructive suggestions during this research work, presented in Chapter 2 of this thesis. His willingness to give his time so generously has been very much appreciated.

I would also like to extend my thanks to Dr. Sid Becker and Annie Homewood for offering me the space and resources for my office, which allowed me to carry forward my research without hindrances. My thanks to my fellow doctoral students for their cooperation and friendship that made this journey memorable.

I am thankful to the friends that turned into family, loved ones and family members who brought sunshine to my life in the toughest times. My mother-in-law and sister, I can never thank you enough for the support. Thanks to my parents for giving me the courage to take on challenges and accepting nothing less than excellence from me.

My steadfast husband: Thank you for your patience, love, believing in me more than myself and being the anchor in my life.

Table of Contents

Abstract……i
Acknowledgements…….. ..v
List of Figures……ix
List of Tables……..……..xi

Chapter 1: Introduction.....**1**

1.1. Seismic Protection.....1
1.2. Lead Extrusion Devices 3
1.3. High Force to Volume (HF2V) Devices 6
1.4. Problem Statement 10
1.5. Research Scope 11
1.6. Preface.....12
1.7. Summary 13

Chapter 2: Design based specific force modelling: An Empirical Model.....**14**

2.1. Introduction 14
2.2. Methods.....14
2.2.1. HF2V device modelling.....*14*
2.2.2. Relevant mechanics factors.....*16*
2.2.3. Proposed Models *19*
2.2.4. Devices and data.....*21*
2.2.5. Model Identification.....*22*
2.2.6. Analysis and validation.....*23*
2.2.7. Model proposal to analysis : Sketch *28*
2.3. Results and Discussion.....29
2.4. Summary 40

Chapter 3: Upper bound and Lower bound: Analytical Modelling **42**

3.1. Introduction 42
3.1.1. Direct and Indirect Extrusion Analogy.....*42*
3.1.2. Limit Loads *45*
3.2. Methods.....46
3.2.1. . Direct extrusion based HF2V UB Modelling.....*46*
3.2.1.1. UB Model 1 ($F_{UB,1}$) *49*
3.2.1.2. UB Model 2 ($F_{UB,2}$) *50*
3.2.2. Indirect Extrusion based HF2V UB modelling.....*50*
3.2.3. Lower bound equation (F_{LB}) *54*
3.2.1.5. Modified Lower Bound Equation ($F_{LB,1}$).....*55*
3.2.4. Friction force (F_f) modelling *55*
3.2.5. Summary of UB and LB Equations *57*
3.3. Analysis.....58
3.4. Results 64

3.4.1. UB and LB forces and plots *64*
3.4.2. Key Design Parameters *69*
3.5. Precise force calculation method from UB and LB models 74
3.5.1. Method 1 : Average of forces *74*
3.5.2. Method 2: Linear equation from plots *77*
3.5.3. Method 3: Specific force from direct extrusion UB model ($F_{UB,1}$) *80*
3.6. UB Model Improvement 82
3.7. Summary 84

Chapter 4: Nonlinear finite element modelling for HF2V device force prediction: A Computational Model 85

4.1. Introduction 85
4.2. Methods 86
4.2.1. Finite element modelling *86*
4.2.2. FE model description *87*
4.2.3. Device information *95*
4.2.4. Analysis *96*
4.3. Results and Discussion 97
4.3.1. HF2V Simulations and Qualitative Validation *97*
4.3.2. Force Deflection Plot comparisons: Quantitative Validation *101*
4.3.3. FEM: Force prediction: Quantitative Validation *105*
4.3.4. Overall assessment *108*
4.4. Summary 109

Chapter 5: Summary of HF2V models proposed 111

5.1. Introduction 111
5.2. Model comparison 111
5.2.1. Force estimation *111*
5.2.2. Advantages and Disadvantages *119*
5.3. Summary 120

Chapter 6: Conclusion 121

Chapter 7: Future Work 124

7.1. Experimental testing and validation 124
7.2. Study of frictional effects 125
7.3. Velocity Dependence 125
7.4. Design of Experiments and Optimization 126
7.5. Automated HF2V modelling 127

List of Figures

Figure 1.1. Comparison of pre-optimized and post-optimized lead extrusion dampers.....7

Figure 1.2. Force displacement plots for the HF2V devices from testing 8

Figure 2.1. External view of an HF2V damper.....17

Figure 2.2. Cross sectional view of an HF2V device and design parameters with areas relevant to the forces produced.....17

Figure 2.3. Schematic representation of steps undertaken for model identification and validation.....29

Figure 2.4. Plots for F_{exp} vs F_{cal} for Model 2 and 4, where a dashed blue line indicates the actual fit of the model, and a dotted red line is the 1:1 line for the perfect model.....35

Figure 3.1. (a) Direct extrusion (b) Indirect Extrusion (c) HF2V device. 44

Figure 3.2. (a) Direct extrusion parameters from equation (b) Direct extrusion geometry mapping to HF2V devices. 47

Figure 3.3. HF2V lead extrusion damper parameters.....49

Figure 3.4. (a) Indirect extrusion parts (b) Geometric mapping of parameters onto the HF2V devices.....52

Figure 3.5. Plots for HF2V device UB and LB force ranges from results in Table 3.5. ..68

Figure 3.6. Devices ranked on values of key device parameters. 72

Figure 3.7. Plots for UB and LB model forces vs $F_{exp.}$.....79

Figure 3.8. Comparison of model ($F_{UB,1\_specific}$) outcome to experimental device forces. 81

Figure 4.1. Axisymmetric 2D model of HF2V damper 88

Figure 4.2. Boundary conditions applied on HF2V model.....90

Figure 4.3. Mesh applied on deformable lead part. 92

Figure 4.4. Stress distribution in lead with shaft displacement (upwards) at the input displacements noted for Device 10.....100

Figure 4.5. Comparisons of plots between experimental results and finite element models for few HF2V devices.....102

Figure 4.6. Plots of the FEM results for Device 17 for different modelling choices.....104

Figure 4.7. Plot of the experimental device forces against FEM analysis results. Standard Deviation representation of the devices. R^2=0.96 for the linear 1:1 line. The spread accounts for variability in device force due to manufacturing variability by $\pm$ 1, 2, 3 SEs. 107

Figure 5.1. Empirical, FEM, UB and LB forces for Devices 1-22. 113

Figure 5.2. Plots of $F_{empirical}$ and F_{FEM} plotted against F_{exp} along with UB and LB model forces 115

Figure 5.3. HF2V device forces for *Typical* HF2V devices from empirical, FEM, experimental, UB and LB models.....117

Figure 5.4. Model forces (FEM, $F_{empirical}$, $F_{UB,3}$ and $F_{LB,1}$) plotted over the hysteresis plots from experimental test data. 118

List of Tables

Table 2.1. Potential models investigated. 20

Table 2.2. Experimental HF2V device data with associated design parameters. 21

Table 2.3. Device data parameters used for independent external validation. 28

Table 2.4. R^2 values for the models, best values are in bold for each case. Invalid indicates that negative coefficients were found for that model. 30

Table 2.5. Leave k=3 out (N=15 repetitions) validation results for Models 2, 3 and 4. R^2 is about the best fit line in Figure 2.4. 31

Table 2.6. Model 2 and 4 comparison for leave k = 3 (same set) out (N = 22 repetitions). 32

Table 2.7. Comparison of Model 4 and Model 2 leave k= 3 (same set) validation results excluding *Small* devices. 33

Table 2.8. Force calculation and contributions for Model 4: $\mathbf{F = \alpha 0 AR.Dcyl + \alpha 1\ SA + \alpha 2 AB}$ with $\boldsymbol{\alpha 0}$ = 7.4, $\boldsymbol{\alpha 1}$= 0.003 and $\boldsymbol{\alpha 2}$= 0.037. 36

Table 2.9. Force prediction using Model 4 for independent device data from Table 2.3. 38

Table 3.1. The HF2V UB and LB equations used for analysis. 58

Table 3.2. HF2V device parameters. 59

Table 3.3. The yield strength values of pure lead form Equation (3-22). 60

Table 3.4. Yield strength values for LB calculations using Equation (3-24). 62

Table 3.5. Comparison of HF2V LB and UB forces to experimental forces. 65

Table 3.6. Average model forces and corresponding errors for HF2V devices with respect to mean HF2V peak force. 75

Table 3.7. Comparison of maximum achieved experimental device force to average analytical model forces and corresponding errors for HF2V devices. 76

Table 3.8. HF2V force approximation based on linear equations from plots. 80

Table 3.9. Comparison of precise force from $F_{UB,1}$ and average F_{exp} 81

Table 4.1. Elastic properties of lead used for modelling [287] 89

Table 4.2. Plastic data of lead used for models [284] 89

Table 4.3. Device data used for modelling and analysis. Device design parameters are defined and illustrated in Chapters 2-3. 95

Table 4.4. Comparison of forces from experiments and finite element modelling 106

Table 5.1. HF2V device forces from all the proposed models 112

Chapter 1: Introduction

1.1. Seismic Protection

Earthquakes can occur regularly in seismically active areas. While major events are more rarely occurring, they can arise in cycles of 50-100 years, creating significant risk to the built environment. However, there is no reliable method for earthquake forecasting the strength or occurrence of an earthquake [1-3].

Severe earthquakes subject structures to large energy inputs, due to ground motions causing significant structural response, leading to any or all of, cracks, dislodgement of non-structural elements, major structural damage, and in some cases collapse. However, even more frequent, moderately severe earthquakes can cause devastating damage in sites with poorly constructed buildings and dense populations. For example, the earthquakes that caused structural collapse and a large number of fatalities in Iran (2003), Christchurch (2011) and Italy (2016) were of moderate intensities [4-6].

The cost associated with the repair, service disruption, and loss of infrastructure causes significant economic loss and can cripple economic developments [7-9]. This impact is particularly severe in economically poorer countries [10-12]. While, infrastructure may be eventually reestablished, damages to cultural heritage [13-15] and loss of life are the irreversible and devastating consequences of earthquakes. Overall, the social and economic after effects of a seismic event may be severe, leaving lasting socioeconomic [16-18] and psychological impact [19-24] on the society.

To mitigate social disruption, economic loss, and ensure life safety a structure needs to remain largely damage free. Many seismic design methodologies are developed and adapted to improve earthquake resistance of structures [25-27]. As these codes modernize and evolve, they increasingly favor better design and systems over accepting significant sacrificial damage to preserve life safety [28-32].

Structural protective systems can be broadly classified into three types: seismic base isolation, passive energy dissipation devices and active devices [33-39]. While base isolation systems provide both damping capacity and restoring force, they are not necessarily suitable for structures on soft soils and high-rise buildings [40-44]. Passive energy dissipation devices include viscous fluid dampers and friction-based energy dissipation mechanisms, among many others [25, 45-48]. Viscous fluid dampers can reduce seismic response by creating resistive forces which are dissipated as heat within the dampers to improve seismic response of structures [47, 49, 50]. Likewise, sliding friction connections can be used to absorb seismic response energy and provide inelastic displacement capacity at beam-column joints [51-54] and at column-base connections [55, 56].

Some modern structures also use active or semi- active control systems to control or modify structural response motions using external power supply. In addition to being complex, the requirement for an external power supply renders this technology expensive and vulnerable to power failure in an event of a major earthquake, potentially making them less robust [33, 57]. Semi-active systems require minimal power input and are strictly dissipative, but still add significant complexity and thus potential lack of robustness [37, 58-62]. Passive damping systems improve structural strength and damping capacity without the use of an external power

source or complex technology for a wide range of ground velocities s[33, 35, 39, 56, 63, 64], providing more robust options in this space using specifically designed devices [65, 66].

While several new structures in seismically active regions are designed and built to meet the seismic requirements of the zone, older structures are prone to greater earthquake damage. These structures may be retrofitted to withstand seismic loads using combinations of suitable earthquake protection systems discussed above [67, 68].

Under this approach, a damaged supplemental device is easier to replace than repairing an entire damaged structure [45]. However, an undamaged supplemental dissipation device requires no checking or replacement, reducing cost and downtime, and increasing resilience. Thus, damage free supplemental dampers offers greater advantages compared to solutions shifting sacrificial damage to replaceable elements, such as yielding fuses [69-71].

1.2. Lead Extrusion Devices

Lead extrusion dampers (LED) are supplemental energy devices utilizing the hysteretic properties of lead to reduce response of a structure to earthquake loading. They were developed by Robinson and Greenbank at the Physics and Engineering Laboratory, DSIR [72, 73]. Two designs were proposed for these lead extrusion dampers based on how the lead is extruded.

The first design, known as the ‘constricted tube lead extrusion damper’, consists of a concentric cylinder with lead filled in between the walls. The outer cylinder has bulged inner walls which creates an annular restriction and deforms the lead during relative axial displacement between the central shaft and the containing cylinder [72, 74]. The other type of damper is called a

‘bulged shaft lead extrusion damper’, where lead is contained in a cylindrical housing and is deformed by axial motion of a centrally bulged shaft [72]. Both types of devices designed on the principles of extrusion [75-77], where extrusion occurs in these devices when the lead, which is a relatively soft metal is forced to pass through constricted area formed by the bulges, produces repeatable dissipative forces [72].

In comparison to the constricted type extrusion damper, bulged shaft lead extrusion dampers are easier and cheaper to manufacture [78, 79] and provide a ‘squarer’ force-displacement curve similar to coulomb damping plots [72]. The hysteresis loop, which is an important characterizing property of a damping device, depicts the maximum force absorbed at a given displacement. A rectangle/square loop represents constant energy dissipation throughout a sinusoidal response cycle or displacement. For these reasons, bulged shaft lead extrusion dampers have found more applications than the constricted type [80-84].

Pure lead (Pb) has low yield strength, low melting point and high ductility, all of which are desirable properties for an extrusion damper metal [85, 86]. It also, possesses a unique property to recrystallize immediately after deformation at room temperatures by grain growth and recovery. The recrystallization property of lead repairs the damage due to the extrusion working process by atomic mobility. The recrystallization temperature of lead is as low (10°C) due to low melting point (327°C). The other metal with similar mechanical and recrystallization properties is tin (Sn) [86]. However, it is very expensive and not as readily available as lead. Finally, unlike other metals, the repeated deformation of lead at ambient temperature neither increases the mechanical properties of the metal by strain hardening nor decreases the overall strength by onset of creep and low cycle fatigue [85, 87]. Hence, lead extrusion offers repeatable “damage-free” working material for energy dissipation devices. They have also been

used as the damping element in base isolation [88-90], telescopic lead yielding dampers [91], compressive/tensile load dampers [92], lead viscoelastic damper [93, 94], combined steel-lead damper [95, 96], clapboard type lead dampers [97] and other damping devices [98, 99].

Thus, LEDs have the capacity to retain their original mechanical properties despite undergoing large inelastic deformation by rapid recrystallization of lead before the next stroke, making them suitable for a wide range of applications [72, 100]. The first application of lead extrusion dampers (constricted tube type) were in 1976 at the Aurora Terrace and Bolton Street Overbridges in Wellington. Each bridge had 6 dampers installed of ~140kN capacity [72, 73, 90, 101, 102]. The constricted type LEDs also found application in the Wellington Central Police station and the Bannockburn Bridge in South Island of New Zealand in 1988 for seismic protection [90, 101-104]. The constricted type design was selected for applications for all these structures due to the earlier manufacturing experience by the Auckland Nuclear Accessories Company in New Zealand [73, 104].

In Japan, a high rise building fitted with lead extrusion dampers for seismic protection has withstood numerous major earthquakes and has exhibited excellent response during a M9.0 earthquake, leaving the structure undamaged [105, 106]. Similarly, the devices have found satisfactory applications in nuclear power plants for protection of steam generators at NUPEC, Tokyo [107, 108]. Finally, other versions have been used in Christchurch rebuild [109].

Although invented for the purpose of seismic isolation of structures, these devices may be used as micro-isolators for damping structural motions due to strong winds or vibrations of heavy machinery and washing machines or cancelling undesirable vibrations [100].

1.3. High Force to Volume (HF2V) Devices

The large sizes of the original LEDs, negate their use within typical structural connections [72, 104, 110, 111]. Also, devices with large stroke length pose a risk of buckling under loading and require large shaft sizes to overcome this issue [72]. In recent years, the bulged type LED have been optimized to a smaller volumetric size with equal or higher force capacities. These devices are referred to as high force to volume (HF2V) devices [112, 113].

In the HF2V devices, lead in the cylinder is compressed the by method of pre-stressing. Pre-stressing improves the overall force produced depending on the size of the damper, and peak forces are achieved at smaller displacements [82, 83]. This methodology of prestressing lead extrusion dampers has been followed by researchers to obtain improved force capacities in lead extrusion dampers [114-120].

HF2V devices have the similar force capacity of 100kN-1000kN as their predecessors for a much smaller geometry. In addition to pre-stressing, understanding the effect of the shaft bulge size in varying force capacities helped in achieving higher forces. A 150kN HF2V device has stroke length of 110mm and cylinder diameter of 89mm [112]. While, early lead extrusion dampers of 150kN had stroke length of 500mm and cylinder diameter of 150mm [73]. Similarly, a 400mm long damper with 200mm cylinder diameter would generate forces of only 250kN [104]. Thus, HF2V devices can produce the same force for smaller dimensions of 160mm length and 60mm cylinder diameter [112]. A comparison of the sizes of the lead extrusion devices with similar capacity before and after optimization are seen in Figure 1.1. The earlier LED of force capacities 700kN (larger device) and 100kN (smaller device) is seen

in Figure 1.1.(a) [110], while after optimization a significantly smaller device is capable of producing 120kN force as shown in Figure 1.1. (b) [121].

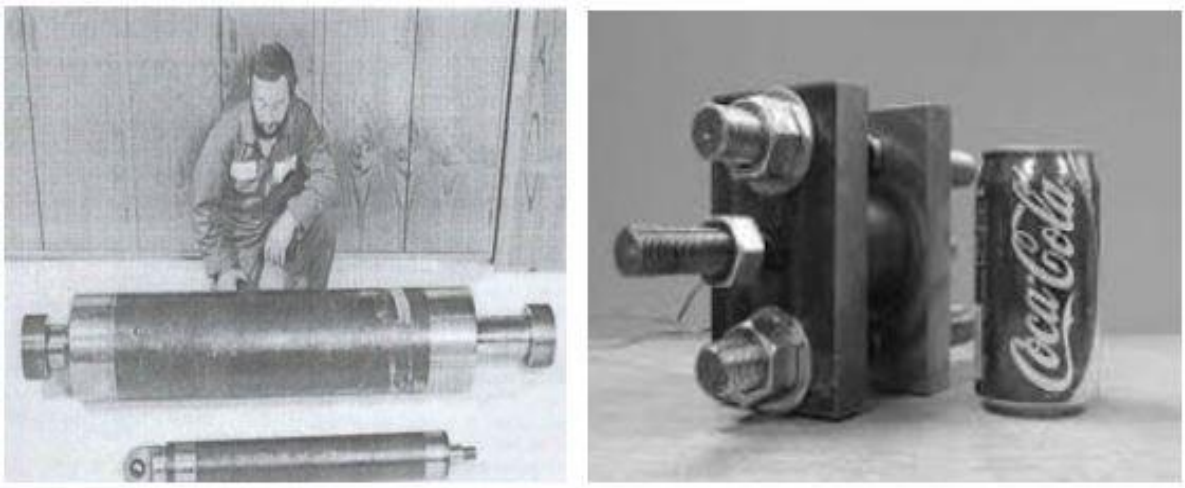

(a) LEDs before optimization [110] (b) Optimized HF2V devices [121]

Figure 1.1. Comparison of pre-optimized and post-optimized lead extrusion dampers

Devices of similar dimensions in length and cylinder diameter can also produce different forces by varying the bulge diameters relative to cylinder diameter. For example, a 110mm long device with cylinder diameter of 89 mm can develop force of 170kN for a 40mm bulge diameter and 320kN peak force for 360kN with a 58 mm bulge diameter [83, 112]. This flexibility of forces for the same external geometry and the possibility of higher forces for smaller geometry makes it a desirable earthquake mitigation device for applications in structures in seismically active regions of the world. More importantly, the larger forces for smaller geometries allow HF2V devices to be directly fitted into structural connections in new or retrofit designs.

The force-displacements plots obtained from quasi-static loading of the HF2V dampers are shown i**n** Figure 1.2. During shaft displacement, stresses rise rapidly in the cylinder due to lead deformation by the bulged shaft and frictional forces at the shaft-lead interface. After the attaining peak forces, steady forces are reached.

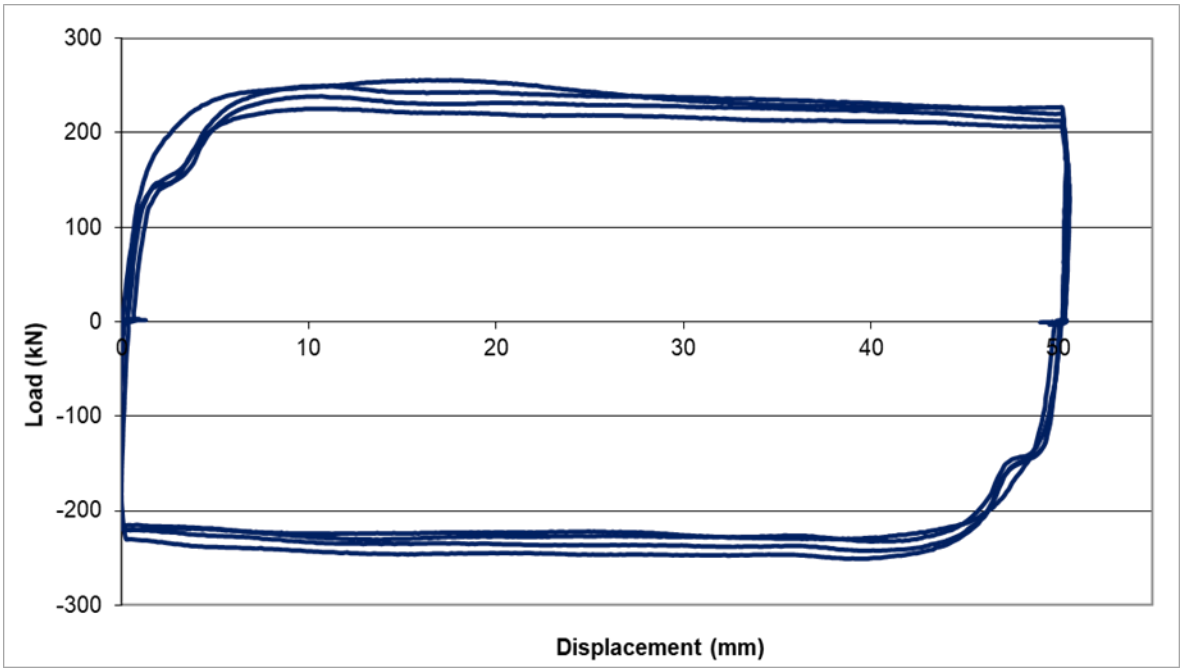

Figure 1.2. Force displacement plots for the HF2V devices from testing

Previous research shows the efficacy of HF2V devices in structural applications by computational and experimental methods on large-scale subassembly experiments, device only (component) testing, and in full-scale structural analyses [121-128]. HF2V devices can be used in combinations with other devices to achieve the benefits of both the devices and for greater structural response reductions. The analyses of HF2V devices has been undertaken along with semi-active devices [129-131], ring spring dampers [132-134], sliding hinge joints [55, 56, 135]. Research shows HF2V devices can be incorporated into structural systems like concrete frames [126, 136, 137], braced structures [138], steel moment frames [124, 139], steel connections[128, 140, 141], beam-column joints [139, 142], wooden frame structures [116, 143], joints of frames in large structures [117, 124, 144, 145] and slotted beam assemblies [146, 147] for effective damage resilience.

The suitability of these devices is primarily due to low velocity dependence [148], making them suitable for both near-field and far-field earthquakes and the ability to achieve predictable

and repeatable performance [149]. Low maintenance requirements also make them a favourable choice for building applications, particularly considering they do not need replacement after a major event.

The HF2V devices have found numerous applications in numerous commercial buildings recently. The Forté Health at Kilmore Street in Christchurch have been applied with 96 HF2V devices [118, 120, 149]. The predominantly steel structure is provide passive dissipation by the HF2V devices, with 32 devices of 120mm stroke and 64 devices with 140mm stroke. Similarly, in San Francisco a residential building for the economically vulnerable senior citizens has been installed with the HF2V dampers to provide seismic protection to the 9-story structure [150]. Most recent application was at the Tūranga Central Library in Christchurch, which is five-floor building supplemented by 20 HF2V devices. Each device has a force capacity of approximately 700kN [109, 151]. The low damage structural design of the Tūranga was recognized globally and presented with Seismic Resilience Award for low damage design by New Zealand Society for Earthquake Engineering (NZSEE) and Structures in Extreme Conditions by Institution of Structural Engineers (IStructE), among numerous others.

One drawback of this device and all LED devices is the inability to recentre. It thus requires an external force to return to the original position. This issue is resolved by forming hybrid devices, in combination with ring spring devices [133, 134, 152-154]. However, the residual displacements were not large and can be mitigated by seismic frames [124, 144]. The overall structure may have recentering ability from other sources and the device may recentre, even if it does not have static recentering capability.

Originally, a common problem encountered during HF2V operations was the formation of air pockets in the working material due to its shrinking after filling and cooling. This issue led to a delay in the development of the peak force in the device during shaft displacement due to the formation of trailing voids in the working material. Appropriate pre-stressing can expel air voids and forms a compact and fully lead-filled damper, eliminating this problem [82, 83].

1.4. Problem Statement

A great deal of research focuses on seismic design of structures using lead extrusion dampers [80, 84, 155-158]. It is evident extensive research has carried out on the application methods of HF2V devices to structures. However, research focusing on a design methodology for these devices is limited for manufacturing and application. The exact reaction mechanisms generating forces beyond extrusion or bulk/shear modulus of lead are not fully known in an HF2V device and no accurate predictive models exist.

As a result, devices are currently designed using very simple models with limited precision [82, 83]. They are then manufactured based on previous designs of similar force capacities and tested to determine if the exact force capacities match the design goal before application. This approach potentially necessitates redesign if initial prototype devices do not provide a good match to the design needs [149]. For seismic protection of large structures, a great number of HF2V devices of varying sizes and force capacities may be required according to the structural design requirement [107, 108, 118, 120].

Thus, there is a major need for a modelling methodology to better estimate device force capacity in the design phase itself, without reliance on prior experimental results and testing to

correct design. A better understanding of the device mechanics and the influence of device parameters on force generation mechanisms would allow for easier design techniques.

1.5. Research Scope

This research seeks to addresse the design requirements of HF2V devices with the focus on understanding and improving the device mechanisms by answering the following questions:

a) What device design dimensions and factors contribute towards the device resistive forces and how are they affected?

b) How can a specific force be attained from a HF2V device?

c) Do the experimental results match the analytical predictions of response?

d) Can a generic modelling method be achieved that is applicable to HF2V devices of varying sizes and force capacities?

The study focuses on several key areas to achieve the answers to the above given questions:

a) Modelling of HF2V device reaction mechanics to understand the contribution of various factors towards resistive reaction mechanics.

b) Upper bound and lower bound limit analysis by applying plasticity theorems.

c) Nonlinear, large displacement finite element modelling of the HF2V dampers as a tool for force prediction and design optimization.

d) Studying device mechanisms and stress distributions by simulating device operations and force displacement plots.

Overall, this research seeks to develop a design or modelling approach for the HF2V damping devices through an empirical, analytical and computational study of the devices that can be easily taken up by researchers and engineers for design applications. Experimental test data and results from previous research are considered for modelling, analysis and comparison in this study, thus reducing the reliance on additional experimental testing and validation.

1.6. Preface

Chapter 2 presents the development of a generic design based empirical model relating the device geometries to the reaction mechanisms for predicting the device force capacity. The empirical model is fitted to experimental results from previous research. Model validation is done using a *leave k out* methodology and external validation. The results are compared to experimental results to assess the prediction capacity of the model.

Chapter 3 relates the conventional extrusion forming process to the HF2V extrusion process to develop upper bound and lower bound force limit models. This analytical study predicts the maximum and minimum expected forces from the HF2V devices during plastic deformation inside the devices based on device geometries and plasticity theorem. It also assesses which theoretical approaches provide the closest bounds with the lowest error.

Chapter 4 presents a finite element computational study of the devices to study the large inelastic deformations and stress distributions within the devices during operation. A simple

and generic finite element model is developed using ABAQUS for force estimation of the HF2V devices. Results are evaluated against previously collected experimental results.

Chapter 5 presents a comparative study of the results from the empirical, analytical and computational modelling from the previous chapters to outline an overall design methodology for the HF2V devices.

Chapter 6 presents the overall conclusions to the research.

Chapter 7 discusses the possible extensions of the current research and future work.

1.7. Summary

This chapter has presented the motivation for this research and an introduction to the device studied and modelled in this research. Overall, earthquakes are unpredictable natural disasters that can cause severe structural damage. Supplemental damping improves structural resilience by dissipating energy from structures during ground motions. High force to volume lead extrusion dampers offer repeatable and consistent performance by energy dissipation under earthquake loading. The development of a simple and generic force prediction and design methodology for these lead extrusion dampers would enable ease of manufacture and design for structural application.

Chapter 2: Design based specific force modelling: An Empirical Model

2.1. Introduction

Chapter 1 discusses the merits, and prior research, and ongoing applications of HF2V devices. However, to date, the delineation of force contributions and the exact reaction mechanisms generating these forces, beyond estimates based on simple extrusion or linear bulk/shear modulus of lead, are not fully known for HF2V devices. This issue makes device design difficult for specific applications.

This chapter discusses research done on modelling HF2V lead extrusion dampers for specific force capacities by identifying the key parameters contributing to the resistive forces during shaft loading. The key device parameters are related to expected mechanisms of lead extrusion damper operations, and thus device force is calculated. The model developed is verified for accuracy, consistency, and generalizability using typical validation methods.

2.2. Methods

2.2.1. HF2V device modelling

HF2V devices are low maintenance form of supplemental energy dissipators, which are relatively easy to manufacture and assemble. The lack of a design based model to estimate the specific force capacities of these devices in the design phase itself makes it difficult to build devices to pre-specified, application specific force capacities. The current practice of approximating forces based on previous designs prior to building and testing is costly and

unreliable, resulting in a build-test approach, that might require iteration.

In the early development of the lead extrusion dampers, equations used to determine extrusion pressures in the metal processing industry were directly used to approximate damper extrusion forces [72]. Tsai et al. consider temperature effects during extrusion while modelling lead extrusion dampers [159]. However, the impact of manufacturing pre-stress of the lead working material and other manufacturing variabilities are also not considered in existing device design models [160].

Existing research relies on the Betzalel's extrusion formula for modelling lead extrusion damper forces [67, 80, 81, 161], which is used to estimate extrusion pressures in the bulk forming technology. However, this model has not been tested on lead extrusion devices of varying sizes and force capacities to establish its reliability and prediction capacity.

An overall device-based force-velocity relationship proposed by Pekcan et al [162] was applied for the HF2V devices for determining the forces developed in the device [82, 83, 127]. However, later studies suggest HF2V devices are more weakly velocity dependent due to resistive force contributions from both extrusion and friction [121, 148]. However, these effects have not previously been delineated explicitly. Another model of the HF2V device mechanics was suggested by Rodgers using Mohr-Coulomb failure criteria [82, 83, 112], but does not account for friction along the device shaft, which is seen in the forces generated in devices without a bulge [163, 164]. Hence, precision design of devices to achieve a specified quasi-static force capacity is not yet possible, but is also a necessary first step towards more regular design uptake and use of these devices.

Better design models are required for increased uptake, as well as increased understanding of the force contribution of different mechanical aspects of the device. These force contributions need to be linked to device design parameters and dimensions to enable precision design to specified force levels for any given application. This study uses existing experimental data from a diverse range of existing prototype devices to create a simplified, more precise, general design model based on the device dimension inputs, as related to physically reasonable and expected reaction mechanisms.

2.2.2. Relevant mechanics factors

An HF2V device has a simple design, consisting of a bulged shaft within a cylinder, filled with lead, secured within the cylinder using endcaps. Energy is dissipated through a reversible extrusion process when lead flows through the annular orifice between the bulged shaft and the cylinder walls. The cylinder length (L_{cyl}) is the length of the cylinder within the endcaps where lead flows. Figure 2.1. presents an external image of an HF2V damper. The diameter of the bulge on the shaft (D_{blg}) determines the annular orifice area of a device, where the dimensions are shown in detail in Figure 2.2.

A bulged shaft extrusion damper derives its total resistive force from a combination of two basic forces, extrusion and friction forces The key device design parameters associated with the extrusion force are the annular orifice area between the bulge and the cylinder wall, the projected annular bulge area (AB), and the cylinder diameter (D_{cyl}) [160]. Friction forces arise due to relative motion between the entrapped lead or working material and the moving shaft.

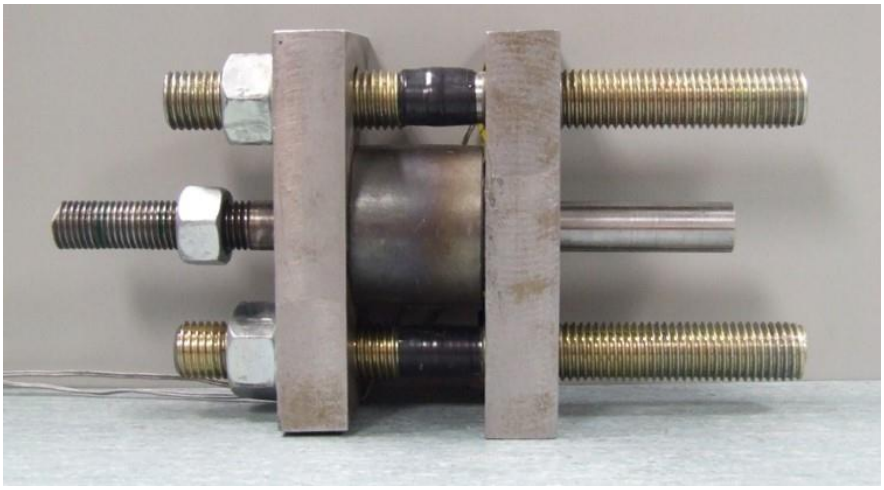

Figure 2.1. External view of an HF2V damper.

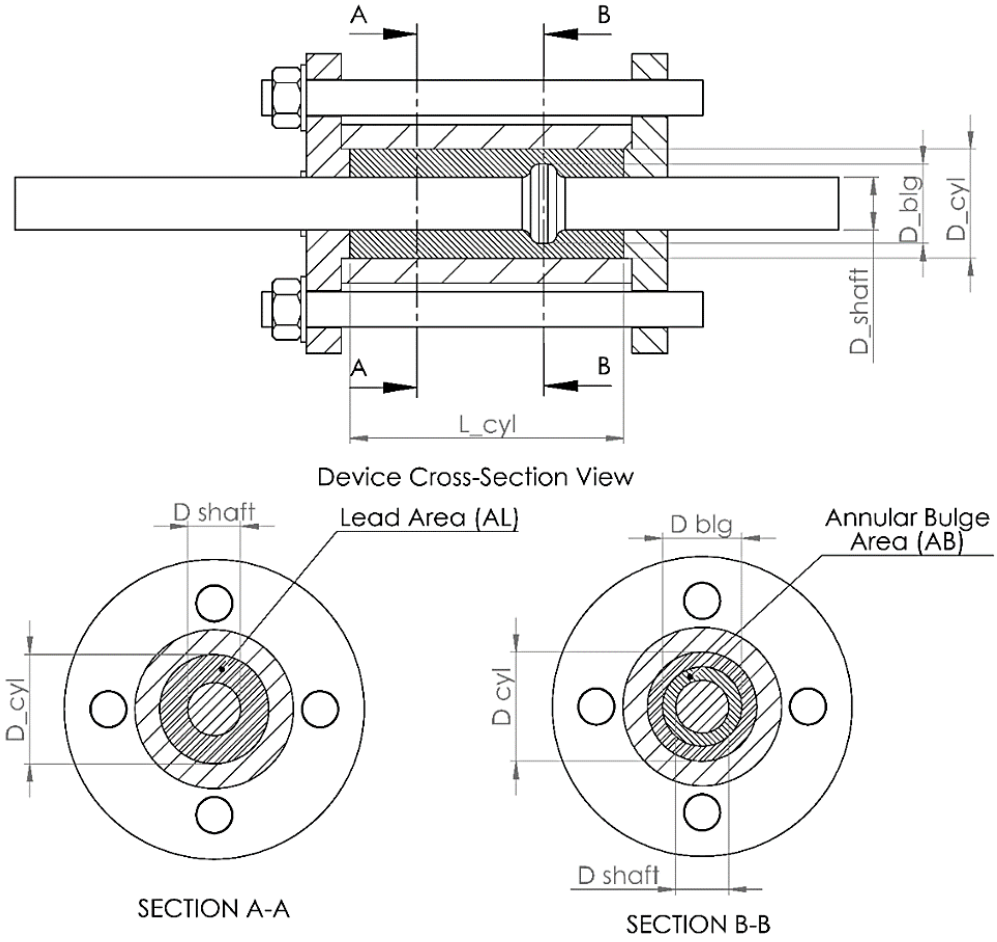

Figure 2.2. Cross sectional view of an HF2V device and design parameters with areas relevant to the forces produced.

Some HF2V devices considered in this chapter have a no-bulge shaft with a constant diameter along the entire shaft [163, 164]. In no-bulge HF2V devices ($D_{blg} = D_{shaft}$), the annular orifice area is considered as the area between the shaft and the cylinder wall. Unlike the typical lead extrusion damping devices, the resistive forces produced in these devices are independent of the extrusion process. However, they are capable of producing significant resistive forces through friction between the shaft and the lead during axial motion of the shaft through the lead. Friction force arises from the relative motion between the lead and shaft surface area (SA) [112]. Inclusion of no-bulge devices in modelling and analysis enables isolating and understanding frictional force contributions better.

In particular, extrusion force is best related to the area ratio between the projected annular bulge area (AB) and the annular lead area around the shaft (AL), which in this study is referred to as the area ratio (AR) [160]. An area ratio of 1.0 indicates the limiting case of a bulge, that goes all the way to the cylinder wall (no orifice area), and thus AB = AL, and conversely, a shaft with no bulge has AR = 0.0. It is also possible to have devices with a negative bulge area, where a recess or reduced diameter is machined into the shaft, but such devices are not considered here [163, 164]. The associated device design parameter for a no-bulge HF2V device relying solely on friction is the shaft surface area (SA). It is used to explain the force produced in devices with AR = 0.0 or with a very small bulge [163].

Figure 2.2**.** illustrates these device parameters for a generic HF2V device, and, in particular, relates them to device design dimensions to meet the overall goal of relating device dimensions to force capacity. Area Ratio (AR), Surface Area (SA), and Bulge Area (AB), are functions of device dimensions: Cylinder Diameter (D_{cyl}); Bulge Diameter (D_{blg}); and Cylinder Length (L_{cyl}), yielding:

$$\boldsymbol{AB = \frac{\pi}{4}\left(D_{blg}{}^{2} - D_{shaft}{}^{2}\right)} \quad \text{2-1}$$

$$AR = \frac{AB}{AL} = \frac{\left(\frac{\pi}{4}\right)\left(D_{blg}{}^{2} - D_{shaft}{}^{2}\right)}{\left(\frac{\pi}{4}\right)\left(D_{cyl}{}^{2} - D_{shaft}{}^{2}\right)} = \frac{D_{blg}{}^{2} - D_{shaft}{}^{2}}{D_{cyl}{}^{2} - D_{shaft}{}^{2}} \quad \text{2-2}$$

$$\boldsymbol{SA = \pi D_{shaft} L_{cyl}} \quad \text{2-3}$$

2.2.3. Proposed Models

Based on the assumption that the total device forces produced in the HF2V devices arise primarily from a combination of friction forces and extrusion forces, analytical models are proposed utilizing device design parameters to estimate the resistive device force. The goal is a model to accurately predict the quasi-static forces produced in the devices based on device dimensions using Equations (1)-(3). This model would thus explain the contribution of these device design parameters to the type of device and overall forces produced.

Fourteen general models are proposed, where each assumes frictional forces and extrusion forces comprise the total resistive forces produced by the device. Table 2.1. lists the models proposed, where the model device force (F) is a linear and/or quadratic function of any of the input parameters AR, SA and AB, and α_i are weighting coefficients identified by fitting the models to a range of experimental device data. Missing terms assume $\alpha_i = 0$ in a given model. This broad range of possible models assess all possible linear and quadratic combinations of force contributions from which the best model can be selected.

A common problem associated with modelling is the lack of associated parameters and interactions of parameters in prediction [165]. Hence, a broad range of models with possible

combinations of parameters contributing to the total resistive forces is considered in**.**Table 2.1. Multivariable models are great tools for making predictions when the terms are chosen carefully to represent the relevant (possible) associated mechanics [165].

Table 2.1. Potential models investigated.

1	F =	$\alpha_0 AR$	$+\alpha_1 SA$	_	_	_
2	F =	$\alpha_0 AR.\, D_{cyl}$	$+\alpha_1 SA$	_	_	_
3	F =	$\alpha_0 AR$	$+\alpha_1 SA$	$+\alpha_2 AB$	_	_
4	F =	$\alpha_0 AR.\, D_{cyl}$	$+\alpha_1 SA$	$+\alpha_2 AB$	_	_
5	F =	$\alpha_0 AR.\, D_{blg}$	$+\alpha_1 SA$	_	_	_
6	F =	$\alpha_0 AR.\, D_{cyl}^2$	$+\alpha_1 SA$	_	_	_
7	F =	$\alpha_0 AR.\, D_{cyl}^2$	$+\alpha_1 SA$	$+\alpha_2 AB$	_	_
8	F =	$\alpha_0 AR$	$+\alpha_1 SA$	_	$+\alpha_3 AR^2$	_
9	F =	$\alpha_0 AR.\, D_{cyl}$	$+\alpha_1 SA$	_	$+\alpha_3 AR^2$	_
10	F =	$\alpha_0 AR.\, D_{cyl}^2$	$+\alpha_1 SA$	_	$+\alpha_3 AR^2$	_
11	F =	$\alpha_0 AR.\, D_{cyl}^2$	$+\alpha_1 SA$	_	$+\alpha_3 AR^2.\, D_{cyl}^2$	_
12	F =	$\alpha_0 AR$	$+\alpha_1 SA$	$+\alpha_2 AB$	$+\alpha_3 AR^2$	_
13	F =	$\alpha_0 AR$	$+\alpha_1 SA$	_	$+\alpha_3 AR^2$	$+\alpha_4 SA^2$
14	F =	$\alpha_0 AR$	$+\alpha_1 SA$	_	_	$+\alpha_4 SA^2$

The quadratic AR^2 terms in the Models 8-13 allows quadratic extrusion effects as AR increases. The SA^2 terms in Models 13-14 allow for the possibility of nonlinear friction contributions. The AB terms may better capture differences between devices with similar Area Ratio (AR), but different absolute device size. AR is multiplied by D_{cyl} and D_{blg} in Models 2, 4, 5 and 9 based on prior work showing their use as a device scale parameter in normalizing results between different devices [112]. Finally, multiplying D_{cyl}^2 to AR in Models 6, 7, 10 and 11 makes them dimensionally consistent, allowing for scalability. Overall, the models in Table 2.1. provides a comprehensive set of possible generalized design models.

2.2.4. Devices and data

Significant experimental research work has been done in recent years on HF2V devices. The data of HF2V devices manufactured and used in previous research work and structural applications have provided a key set of experimental results for this research [112, 116, 118, 163, 164]. These devices were tested quasi-statically at a constant velocity within a range of 0.1 - 0.5mm/s. Experimental and design data from 18 HF2V devices of different sizes, configurations and forces are considered in the study for modelling, shown in Table 2.2.

Table 2.2. Experimental HF2V device data with associated design parameters.

	Device	F_{exp} (kN)	AR	SA (mm^2)	D_{cyl} (mm)	D_{blg} (mm)	D_{shaft} (mm)	AB (mm^2)
SMALL	1	55	0	2260	17	12	12	0
	2	74	0	4020	20	16	16	0
	3	55	0.17	2260	17	13	12	20
	4	85	0.23	4020	20	17	16	26
TYPICAL								
	5	140	0.10	9896	89	40	30	550
	6	250	0.23	9896	89	50	30	1257
	7	320	0.35	9896	89	58	30	1935
	8	175	0.20	12250	66	40	30	550
	9	310	0.46	12250	66	50	30	1256
	10	130	0.30	3141	50	32	20	490
	11	150	0.30	4400	50	32	24	490
	12	155	0.34	7540	50	35	33	509
	13	260	0.25	16590	60	42	24	497
	14	155	0.34	7536	50	35	30	510
	15	250	0.35	7065	70	48	30	1102
LARGE								
	16	145	0.14	27130	54	35	30	228
	17	165	0.20	27130	54	36	30	310
	18	185	0.27	27130	54	38	30	427

In Table 2.2, F_{exp} is the experimentally measured force. Devices are categorized as *Small, Typical or Large*. Devices 1- 4 have very small or zero bulge sizes (AB, AR= 0 or small) and small SA in comparison to the other devices, and are thus categorized as *Small*, with associated lower experimental force, F_{exp} = 55 - 85kN. Devices 16-18 have relatively large SA, but relatively low to average F_{exp} = 145 - 185kN, and are categorized as *Large* devices. These two groups capture potentially outlying device designs. The remaining devices are grouped as '*Typical*' devices with F_{exp} = 130 - 320kN.

2.2.5. Model Identification

Models are identified using linear least squares regression. For each model in Table 2.1, a linear regression problem is created to find all non-zero $\alpha_{0,1,2,3,4}$ values. For example, this problem is defined for Model 1:

$$[\mathbf{AR}_{\bar{n}\times 1} \quad \mathbf{SA}_{\bar{n}\times 1}]_{\bar{n}\times 2} \quad \begin{bmatrix}\boldsymbol{\alpha_0}\\ \boldsymbol{\alpha_1}\end{bmatrix}_{2\times 1} = \mathbf{F}_{\bar{n}\times 1} \qquad 2\text{-}4$$

where, $AR_{\bar{n}\times 1}$ is a $\bar{n} \times 1$ vector of AR values, $SA_{\bar{n}\times 1}$ is a $\bar{n} \times 1$ vector of SA values and $F_{\bar{n}\times 1}$ is the $\bar{n} \times 1$ vector of the experimental force values in Table 2.2 for $\bar{n}$ =18 devices. The 2x1 vector contains α_0 and α_1, the two unknowns to be identified, with α_{2-4}= 0 assumed by definition for this model. Adding other columns and α_i values, and following the same pattern, creates similar over-determined identification problems for the other models in Table 2.1.

Importantly, a model identifying a value of α_i <0 is considered "invalid" [166]. In particular, the models of Table 2.1. implicitly assume positive contributions to device force from each term ($\alpha_i \geq 0$). Thus, negative coefficients are not physically reasonable, and likely reflect a

model fitting error relative to the device data available.

Thus, model identification is an iterative process, requiring modifications to simple models by addition or removal of contributing device parameters to obtain a relevant model with "valid" $\alpha_i > 0$ values. An ideal model has valid relationships between variables (device parameters) and a regression equation that not just gives a good fit of data, but can also outline the physics of the device operation.

2.2.6. Analysis and validation

Model validation is a key step in evaluating the effectiveness in repeatable prediction capability of the model for different data set [167]. Modelling techniques applied without subsequent analysis for performance can result in imprecise models that are not applicable to future data [168]. Thus, the measuring predictive accuracy and efficiency of models is an important step in model identification. Thus, models are assessed and validated in this section for the following purposes:

- To assess the goodness of model fit.
- To identify models with stable predictor terms or coefficients.
- To check the prediction accuracy.
- To ensure if the model is capable of repeatable predictions for different data sets.
- To verify the dependency of model results on any particular device set.
- To evaluate if the model predicts well for new data set.

After identifying the α_i values for a given model using MATLAB, the experimental data can be plotted against the model device forces. The resulting Pearson correlation coefficient (R^2) can be calculated. However, the 1:1 line is also shown as it provides a measure of the ideal model goal ($F_{model} = F_{exp}$), where a y-intercept close to zero and a slope ~ 1.0 is the optimal best fit model. The value of R^2 indicates model completeness, as $(1-R^2)\times100$ is the percent of the variance between experimental and model device forces not captured by the model. Experimental versus model device force errors can also be calculated and included to quantify model validity.

Correlation coefficients around the 1:1 line of experimental and model force assess accuracy (R^2) and completeness ($(1-R^2) \times 100$). However, very big or small values of device parameters can dominate the models in Table 2.1. when including the *Large* and *Small* device groups. Thus, the analyses are repeated ignoring *Small* Devices 1-4, and again ignoring *Large* Devices 16-18. Finally, both *Small* and *Large* devices are excluded in subsequent analyses investigating only *Typical* devices. This overall analysis approach thus assesses robustness and variation across specific ranges of device design parameters, including and excluding potential outliers, as well as for all devices. From these results, the 'better' models are selected from a subset of valid models.

To establish the most robust and accurate model, a series of validation analyses is undertaken. Internal and external validation are validation methods where the former uses data from the same population for validation, while the latter uses external or excluded data for validation purposes [169]. Internal validation methods verify the model's robustness and repeatability in prediction. While, external validation techniques ensure generalizability of a model by testing it on data which was not included in any phase of modelling [170, 171]. The popular methods

of internal validation methods are *leave k out validation*, *k-fold-cross-validation*, and *hold out methods* [172-175].

2.2.6.1. Internal Validation

The 'better' models demonstrating higher R^2 values, smaller intercepts and valid coefficient values are considered for this validation. The *leave k out method* is used for validation in this study [176-178]. In this cross validation technique, from the data available for modelling (*d*), k = 3 devices are excluded and the remaining data (*d-3*) is used for training/modelling the data. It is a method generally used when the data is not particularly very large for splitting, training and testing [178, 179].

Repeated model validation is a well-suited strategy for small data sets to identify models extremely dependent on a particular data set [180-182]. By calibrating a prediction model to various combinations of device ensures the predictive capacity of the devices is not dependent on a particular device data. Thus leave k tests are performed for N times to verify the robustness of the model. Thus, from the data available for modelling (*d = 18*), devices are randomly excluded (k = 3) from the analysis and the modelling is performed on the remaining data (*d-3*) for multiple times (N).

The leave k validation test is performed on 3 instances during the model analysis. It is performed each time better predicting models are selected, for identifying stable models, overall performance, choosing the best of the better models and to establish the independence of model on *Small* devices.

The first leave k validation is done in particular on 'better models' (with high R^2 values), to test model robustness for the best valid models, α_i values are compared across 15 sets of models created by randomly excluding k=3 of 18 devices, where consistency of α_i values in a 'leave k=3 out' (N= 15) analysis indicates a more robust model. In particular, this consistency indicates a lesser reliance of the model on any one or few experimental devices. It also assesses the predictive capacity of the models for the k=3 devices not used in creating the model, providing an independent cross validation. Overall, models resulting in very similar errors and α_i values when tested repeatedly by excluding groups of k=3 randomly selected devices are more robust and less biased by the specific data used. They are and thus more likely to be general. The value of k=3 devices left out are identified randomly using Microsoft excel and are different for each validation test conducted. The best performing models are chosen from this analysis.

The second leave k validation is done on the 'best models' based on the outcomes of the first leave k validation results (N= 15 times), models with stable coefficients and consistent predictions are considered for further leave k out validation. The leave k=3 out analysis is repeated for N= 22 times for the final 'best models'. In this validation process, the randomly chosen k=3 devices for exclusion from analysis is kept common for final best models considered for repeated validation. From the outcomes of leave k= 3 (N=22 times) for the final best models, the R^2 values, slopes and intercept values evaluated. This detailed validation ensures the model adequacy and predictive capacity.

The third leave k validation is done on the 'best models' considered for the second round of leave k validation. Here the test is repeated for N= 10 times for best models by excluding *Small* devices. The mechanisms producing resistive forces produced in the *Small* devices do not

exactly match the force generation mechanisms in other devices due to their small to no-bulge geometry. Hence, a repeated leave common k= 3 device (N=10) analysis further verifies the validity and robustness of the model even after exclusion of sets of devices that may alter the overall results of the analysis.

The model repeatedly predicting with higher R^2 values, smaller intercepts and slopes $\simeq 1$ and better performance from the exclusion of *Small* devices can be considered the final best prediction model.

2.2.6.2. External Validation

The final model resulting from the internal validation is tested using independent data. This ascertains the prediction capacity of the final model for new data. The similarity or difference in performance is an indicator of the generalizability or adaptability of the model for future predictions [183-185].

For external data validation, device data was obtained for few HF2V devices manufactured and tested for other research [116] and applications, given in Table 2.3**.** Devices 19 and 20 can be classified as *Typical* devices due to moderate surface area and average device forces compared to devices in Table 2.2. However, Device 21 has small surface area and relatively smaller forces from *Typical* devices seen in Table 2.2, despite having a large AR. Device 22 is a very large device with largest surface area and force capacity on comparison to all the devices considered in this study. Inclusion of a very large device would enable to understanding of whether the model predicts well for devices of larger sizes which are not included in modelling.

None of the devices considered for modelling in Table 2.2. have AR>0.35. The testing of the model on these devices will show the efficiency of the model to predict forces for *Typical* and any *atypical* devices. Repeatability and ability to predict for a new data set is a concern while prediction modelling using a small data set. The testing of the model on an independent data set can negate this concern.

Table 2.3. Device data parameters used for independent external validation**.**

	Device	F_{exp} (kN)	AR	SA (mm^2)	D_{cyl} (mm)	D_{blg} (mm)	D_{shaft} (mm)	AB (mm^2)
TEST SET	19	125	0.27	6280	40	27	20	285
	20	170	0.37	12063	48	35	24	509
	21	107	0.52	2951	40	32	20	489
	22	500	0.38	29390	89	62	36	2548

2.2.7. Model proposal to analysis : Sketch

Figure 2.3**.** summarizes all the steps undertaken under Section 2.2**.** towards identification of a achieving a valid, robust, consistent, repeatable and generalizable model for specific force capacities.

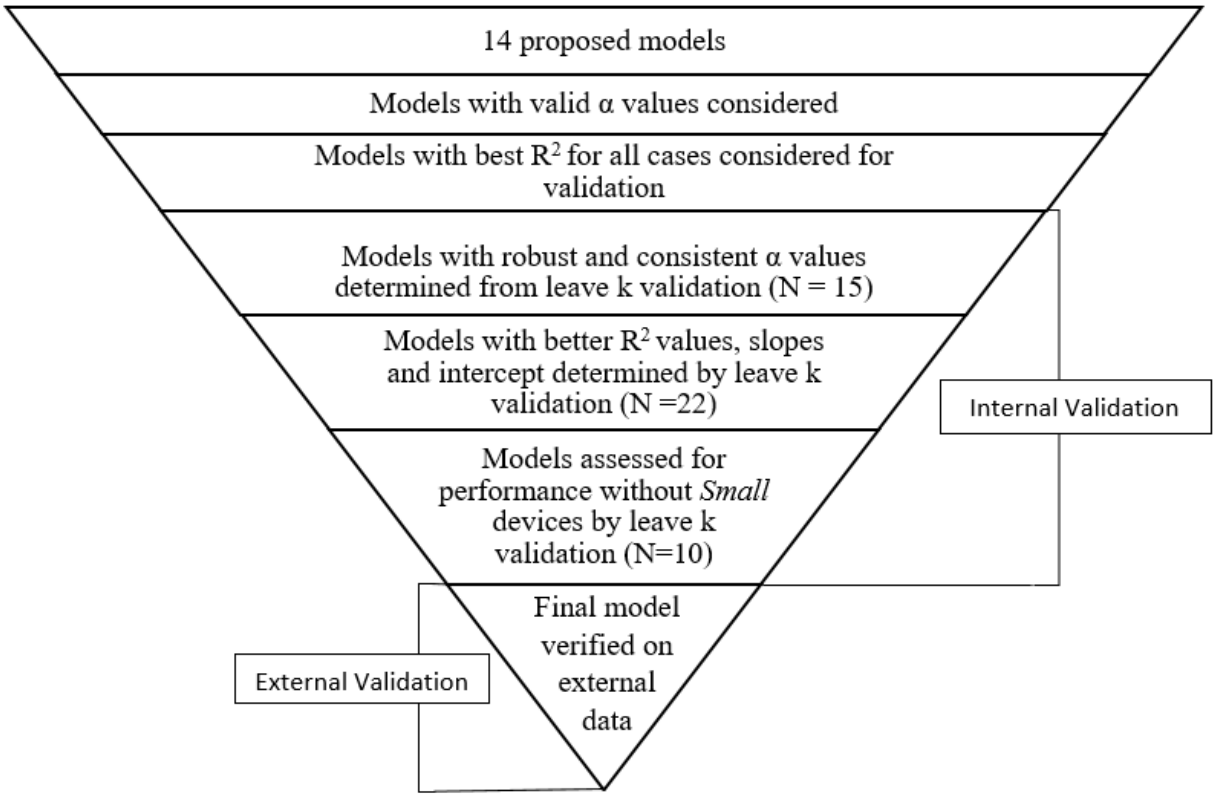

Figure 2.3. Schematic representation of steps undertaken for model identification and validation.

2.3. Results and Discussion

Table 2.4. gives R^2 values for all 14 models of Table 2.1. Only 7 of 14 proposed models are valid for all groups. Model 1 is essentially the same as Model 2, but the normalization of AR with D_{cyl} in Model 2 makes a measurable improvement in R^2 (from 0.56 to 0.89), particularly for the group without the *Small* devices with AR = 0 or small, where R^2 increased to 0.82 from 0.32. Similarly, normalization of AR by D_{blg} in Model 5 gives better R^2 values compared to Model 1. Normalisation by D_{cyl}^2 makes the results of Model 6 better that Models1, 2 and 4. The addition of AB to Models 1 and 2 yields Models 3 and 4, respectively, which deliver better R^2 values. The role of AB in modeling experimentally measured device forces thus appears significant.

Table 2.4. R^2 values for the models, best values are in bold for each case. Invalid indicates that negative coefficients were found for that model.

Model No.	Model	R^2 All devices	R^2 w/o *Large* devices	R^2 w/o *Small* devices	R^2 w/o *Small* &*Large* devices
1	$F = \alpha_0 AR + \alpha_1 SA$	0.56	0.79	0.32	0.62
2	$F = \alpha_0 AR.D_{cyl} + \alpha_1 SA$	0.89	**0.95**	0.82	0.84
3	$F = \alpha_0 AR + \alpha_1 SA + \alpha_2 AB$	0.89	**0.96**	0.85	**0.95**
4	$F = \alpha_0 AR.D_{cyl} + \alpha_1 SA + \alpha_2 AB$	**0.91**	**0.96**	**0.91**	**0.95**
5	$F = \alpha_0 AR.D_{blg} + \alpha_1 SA$	0.86	**0.93**	0.73	0.86
6	$F = \alpha_0 AR.D_{cyl}^2 + \alpha_1 SA$	0.90	**0.91**	0.83	**0.91**
7	$F = \alpha_0 AR.D_{cyl}^2 + \alpha_1 SA + \alpha_2 AB$	Invalid	Invalid	Invalid	Invalid
8	$F = \alpha_0 AR + \alpha_1 SA + \alpha_3 AR^2$	0.59	0.81	Invalid	0.62
9	$F = \alpha_0 AR.D_{cyl} + \alpha_1 SA + \alpha_3 AR^2$	Invalid	Invalid	Invalid	Invalid
10	$F = \alpha_0 AR.D_{cyl}^2 + \alpha_1 SA + \alpha_3 AR^2$	**0.91**	**0.96**	0.85	**0.94**
11	$F = \alpha_0 AR.D_{cyl}^2 + \alpha_1 SA + \alpha_3 AR^2.D_{cyl}^2$	Invalid	**0.96**	Invalid	**0.93**
12	$F = \alpha_0 AR + \alpha_1 SA + \alpha_2 AB + \alpha_3 AR^2$	Invalid	**0.96**	Invalid	**0.95**
13	$F = \alpha_0 AR + \alpha_1 SA + \alpha_3 AR^2 + \alpha_4 SA^2$	Invalid	Invalid	Invalid	Invalid
14	$F = \alpha_0 AR + \alpha_1 SA + \alpha_4 SA^2$	Invalid	Invalid	Invalid	Invalid

Table 2.5. presents the leave k=3 out validation (N=15 combinations) analysis assessing predictive accuracy of Models 2-4 and 10 (the 'better' models). The range of α_i values in Table 4 are most consistent for Models 2 and 4 with relatively small differences between maximum and minimum α_i values across all combinations. Model 2 is a highly robust model, yielding the same α_i values for all 15 leave k=3 out validations, even while modelling with or without any *Large* or *Small* atypical devices. Model 4 on the other hand gives very high R^2 values for all leave k=3 out validations in Table 4 with relatively low variation in the α_0 and α_1 values. In contrast, Models 3 and 10 are valid for all leave 3 out validations. However, values of α_{2min}= 2.5 and α_{2max} = 604 for Model 10, shows very large variability in this identified model parameter, and thus a less general and robust model too dependent upon the the specific device

data used. Similarly, α_{0min} = 194 and α_{0max} = 345 indicate a similar inconsistency in coefficient values and issue for Model 3.

Table 2.5. Leave k=3 out (N=15 repetitions) validation results for Models 2, 3 and 4. R^2 is about the best fit line in Figure 2.4.

Model No.	Model	$\alpha_{i\ min}$	$\alpha_{i\ max}$	R^2 for all devices
2	$F = \alpha_0 AR.D_{cyl} + \alpha_1 SA$	α_0= 9.0 α_1= 0.003	α_0= 9.5 α_1= 0.0036	0.89
3	$F = \alpha_0 AR + \alpha_1 SA + \alpha_2 AB$	α_0= 345 α_1= 0.0025 α_2= 0.10	α_0= 194 α_1= 0.004 α_2= 0.14	0.89
4	$F = \alpha_0 AR.D_{cyl} + \alpha_1 SA + \alpha_2 AB$	α_0= 5.8 α_1= 0.003 α_2= 0.02	α_0= 8.3 α_1= 0.004 α_2= 0.08	0.91
10	$F = \alpha_0 AR.D_{cyl}^2 + \alpha_1 SA + \alpha_3 AR^2$	α_0= 0.08 α_1= 0.003 α_2= 2.5	α_0= 0.13 α_1= 0.006 α_2= 604	0.91

The overall outcomes of this validation analysis indicate the stability, robustness and validity of both Models 2 and 4, as well as their good predictive capability for devices not used in creating the model. However, Models 3 and 10 can be excluded from further analysis due to large variations found in the coefficient values especially for α_0 in Model 3 and α_3 in Model 10. Overall, Model 2 is more robust in comparison to Model 4, while Model 4 has higher R^2 values and relatively smaller model force errors, especially for *Large* devices.

In Table 2.6., the results from the leave k = same 3 devices for both Models 2 and 4 shows Model 4 gives better R^2 values for 21 of 22 analyses and one case of equal values of R^2 for leave k validation. Model 4 intercepts are lesser than Model 2 equations only for 6 cases and equal for 4 others. The slope is almost equal to 1 for both the models in all cases except two.

Table 2.6. Model 2 and 4 comparison for leave k = 3 (same set) out (N = 22 repetitions).

Device	Model 4 $F = \alpha_0 AR.D_{cyl} + \alpha_1 SA + \alpha_2 AB$	Model 2 $F = \alpha_0 AR.D_{cyl} + \alpha_1 SA$
1.	y = 1.0952x - 24.08 R^2 = 0.89	y = 1.0677x - 21.05 R^2 = 0.82
2.	y = 1.2283x - 48.61 R^2 = 0.97	y = 1.173x - 39.79 R^2 = 0.87
3.	y = 1.1075x - 27.53 R^2 = 0.91	y = 1.0588x - 26.30 R^2 = 0.86
4.	y = 1.1266x - 33.11 R^2 = 0.90	y = 0.9918x - 20.19 R^2 = 0.84
5.	y = 1.0789x - 27.61 R^2 = 0.91	y = 1.0503x - 22.63 R^2 = 0.87
6.	y = 1.107x - 26.65 R^2 = 0.90	y = 1.055x - 25.95 R^2 = 0.84
7.	y = 1.1018x - 30.82 R^2 = 0.90	y = 1.1171x - 34.29 R^2 = 0.88
8.	y = 1.0956x - 29.31 R^2 = 0.92	y = 1.0584x - 30.92 R^2 = 0.88
9.	y = 1.1631x - 32.16 R^2 = 0.90	y = 1.0805x - 32.36 R^2 = 0.85
10.	y = 1.0839x - 14.49 R^2 = 0.86	y = 1.0344x - 18.21 R^2 = 0.79
11.	y = 1.2121x - 40.51 R^2 = 0.96	y = 1.1825x - 38.81 R^2 = 0.92
12.	y = 1.0383x - 18.27 R^2 = 0.88	y = 1.0296x - 20.76 R^2 = 0.82
13.	y = 1.1161x - 26.90 R^2 = 0.89	y = 0.9873x - 17.07 R^2 = 0.83
14.	y = 1.1002x - 28.34 R^2 = 0.92	y = 1.0592x - 28.82 R^2 = 0.88
15.	y = 1.1837x - 42.25 R^2 = 0.96	y = 1.123x - 33.69 R^2 = 0.87
16.	y = 1.1185x - 28.97 R^2 = 0.88	y = 1.0628x - 20.64 R^2 = 0.86
17.	y = 0.8238x + 33.53 R^2 = 0.92	y = 1.0388x - 19.17 R^2 = 0.91
18.	y = 1.0809x - 22.98 R^2 = 0.90	y = 1.0447x - 16.71 R^2 = 0.89
19.	y = 1.125x - 31.76 R^2 = 0.91	y = 1.1165x - 31.65 R^2 = 0.91
20.	y = 1.1127x - 26.69 R^2 = 0.88	y = 1.1009x - 20.19 R^2 = 0.86
21.	y = 1.1181x - 26.77 R^2 = 0.91	y = 1.0907x - 25.96 R^2 = 0.91
22.	y = 1.1716x - 40.32 R^2 = 0.96	y = 1.1821x - 30.4 R^2 = 0.93

Similar results are observed for leave k= 3 out (same set of devices) validation after excluding small devices in Table 2.7. Model 4 gives better R^2 and intercept values compared to Model 2 in all the cases. This result excluding small devices show the validation results from Model 4 are independent of *Small* devices and display better correlation compared to Model 2.

Table 2.7. Comparison of Model 4 and Model 2 leave k= 3 (same set) validation results excluding *Small* devices.

Device	Model 4 $F = \alpha_0 AR.D_{cyl} + \alpha_1 SA + \alpha_2 AB$	Model 2 $F = \alpha_0 AR.D_{cyl} + \alpha_1 SA$
1.	y = 1.0537x - 14.08 R^2 = 0.97	y = 0.9276x + 13.27 R^2 = 0.92
2.	y = 0.9253x + 9.26 R^2 = 0.84	y = 0.9183x + 15.78 R^2 = 0.82
3.	y = 0.924x + 10.82 R^2 = 0.84	y = 0.8949x + 20.48 R^2 = 0.83
4.	y = 1.0544x - 24.86 R^2 = 0.82	y = 0.8055x + 38.18 R^2 = 0.81
5.	y = 0.8994x + 16.68 R^2 = 0.80	y = 0.8121x + 40.26 R^2 = 0.76
6.	y = 1.0419x - 9.93 R^2 = 0.96	y = 0.97x + 10.38 R^2 = 0.91
7.	y = 0.8949x + 18.65 R^2 = 0.82	y = 0.8385x + 28.72 R^2 = 0.77
8.	y = 0.9276x + 12.58 R^2 = 0.85	y = 0.879x + 28.07 R^2 = 0.83
9.	y = 0.8588x + 25.12 R^2 = 0.82	y = 0.7697x + 37.59 R^2 = 0.75
10.	y = 1.0622x - 12.57 R^2 = 0.98	y = 0.9133x + 19.68 R^2 = 0.84

Figure 2.4 shows correlation plots for Models 2 and 4 for all cases (All, w/o small, w/o *Large* and w/o *Small* and *Large* devices). Model 4 has a higher R^2 value in all four cases. The y-intercept and slope values for the best fit of both models are comparable, and very close to the ideal slope of 1.0 and low intercept (ideally equal to 0), indicating good models. Both models have 10% experimental error bars [160] overlapping the 1:1 line, although the *Small* devices are not as well captured as they rely primarily on a single model term (SA). Error bars

overlapping the 1:1 slope line indicate the model captures the point when one standard deviation of experimental error is considered.

Even though, the plots for both Models 2 and 4 show similar arrangement along the 1:1 line in all cases, Model 4 without the *Large* and *Small* devices is a nearly perfect model for *Typical* devices, as the error bars of these 11 devices cross the 1:1 line. In contrast, Model 2 error bars for 3 of 11 '*Typical*' devices miss the 1:1 line for the perfect device model, thus capturing only 70% of these devices.

Based on the following observations from the analyses, Model 4 is considered the best device design model based on the device data available:

- Model 4 provides higher values of R^2 values compared to Model 2 of leave k validation for different sets of devices as shown in Table 2.5.
- The leave k= 3 (same set of devices) out validation, showed that Model 4 had smaller values of intercept in most cases and higher R^2 in almost all cases, compared to Model 2, given in Table 2.6.
- Leave k = 3 (same set of devices) out validation excluding Small devices showed better R^2 and intercept values in all the cases of validation, shown in Table 2.7.
- Model 4 captures device forces better than Model 2 without *atypical* devices as shown in Figure 2.4.

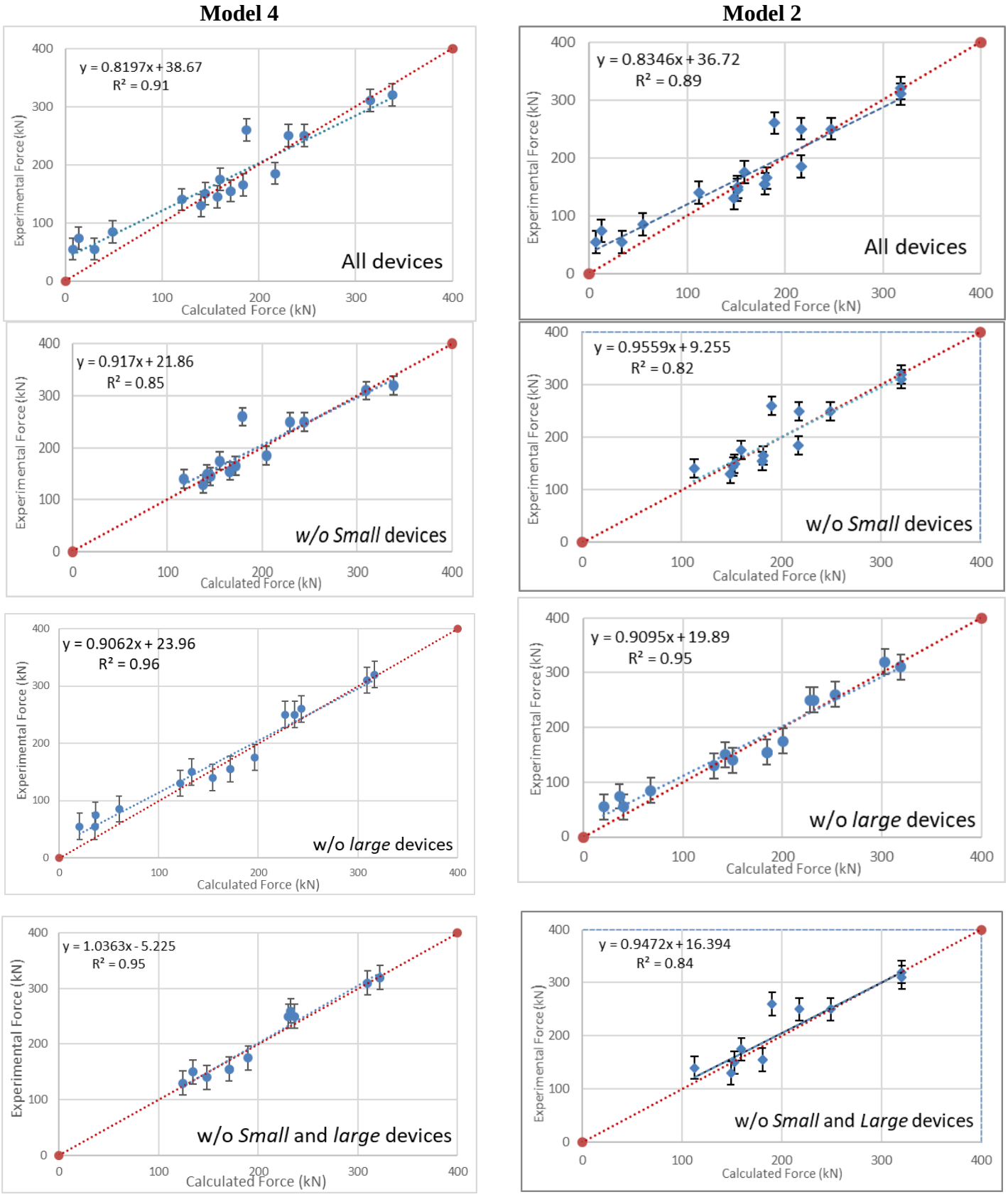

Figure 2.4. Plots for F_{exp} vs F_{cal} for Model 2 and 4, where a dashed blue line indicates the actual fit of the model, and a dotted red line is the 1:1 line for the perfect model.

The α_i values are obtained from repeated leave k validation. The coefficient values $\alpha_0 = \sim 7.4$, $\alpha_1 = \sim 0.003$ and $\alpha_2 = \sim 0.037$ were achieved consistently during repeated leave k validation for Model 4. The forces produced by each device are estimated using Model 4 in Table 2.8**.** The percentage contribution of parameters $\alpha_0 AR.D_{cyl}$, $\alpha_1 SA$ and $\alpha_2 AB$ to the total force in each case are also given. The percentage error for the predicted total device force is also presented.

Table 2.8. Force calculation and contributions for Model 4: $\mathbf{F = \alpha_0 AR.D_{cyl} + \alpha_1 SA + \alpha_2 AB}$ with $\boldsymbol{\alpha_0}$ = 7.4, $\boldsymbol{\alpha_1}$= 0.003 and $\boldsymbol{\alpha_2}$= 0.037.

Device	$\alpha_0 AR.D_{cyl}$	% Force from $AR.D_{cyl}$	$\alpha_1 SA$	% Force from SA	$\alpha_2 AB$	% Force from AB	F_{cal} (kN)	F_{exp} (kN)	Error
1	0	0%	7.7	100%	0	0%	7.6	55	82%
2	0	0%	13.7	100%	0	0%	13.7	74	82%
3	21.5	72%	7.7	26%	0.7	2%	29.9	55	46%
4	34.2	70%	13.7	28%	0.9	2%	48.8	85	43%
5	66.2	55%	33.7	28%	20.3	17%	120.2	140	24%
6	150.3	65%	33.7	15%	46.5	20%	230.4	250	15%
7	232.4	69%	33.7	10%	71.6	21%	337.6	320	0%
8	98.2	61%	41.6	26%	20.3	13%	160.2	175	10%
9	226.9	72%	41.6	13%	46.4	15%	314.9	310	3%
10	111.6	79%	10.7	8%	18.1	13%	140.4	130	13%
11	111.6	77%	14.9	10%	18.1	13%	144.6	150	2%
12	126.5	74%	25.6	15%	18.8	11%	170.9	155	14%
13	112.5	60%	56.4	30%	18.4	10%	187.3	260	37%
14	126.5	74%	25.6	15%	18.8	11%	171.0	155	14%
15	182.3	74%	24.0	10%	40.7	17%	247.1	250	0%
16	56.2	36%	92.2	59%	8.4	5%	157.0	145	4%
17	80.3	44%	92.2	50%	11.4	6%	184.0	165	9%
18	108.6	50%	92.2	43%	15.8	7%	216.7	185	15%

The model prediction is precise for both *Large* and *Typical* devices with larger errors (>15%) for only two cases. Device 13 is a clear outlier, generating prediction errors of 37%. Errors for Devices 1-4 are due to the large difference in the scale of the size of the devices from the rest of the 14 devices, and the relatively very small (or no) bulges that make them unique and limit the model terms that can model this behaviour. The model is thus less accurate for *Small* devices, as it has to rely almost entirely or solely upon the single SA term, which while effective in general, is not effective as the only term in this case.

Errors from the model can be attributed to variations in the applied pre-stress and imperfectly controlled quasi-static test velocity on older manually controlled testing machines [112], as well as to potential inconsistency over devices in assembly and/or manufacture. The error for *Small* devices shows SA is a valuable, but imperfect parameter. Relying entirely or almost entirely on this parameter for devices with very small bulges, or no bulge, contributes to the greater error seen in these *Small* devices where a single, simple, linear SA parameter cannot capture the device forces for all such cases, as well as the smaller SA contribution of the other devices. Finally, the results may vary for devices with large AR (AR>0.5), which were not available for this analysis and would be relatively very large force devices.

The percentage contribution of the $\alpha_0 AR.D_{cyl}$ term in Table 2.8indicates AR, as normalized, contributes a significant part of the forces produced in the device. The *Typical* devices and the *Small* devices with a very small bulge show this term contributes ~70% of device force based on extrusion of lead over the bulge. The no bulge Devices 1-2 have zero force from extrusion, as expected, and the *Large* devices have a greater contribution from SA and friction, also as expected based on their dimensions. The considerable forces produced in devices with no-bulge

are thus explained by the role of SA in capturing the friction based mechanics for these *Small* devices with no bulge.

The percentage contribution of α_0 AR.D_{cyl} decreases with the addition of the AB term compared to Model 2 (results not shown). The contribution of α_2.AB is almost equal to the percentage contribution of SA for some devices in Table 2.8., which shows the AB term is a significant contributor to modelling experimental device forces. The AB term captures bulge size directly as a part of the overall extrusion forces exerted. The contributions of AB and AR are thus primarily about extrusion force, where large bulges will deliver more force for the same AR across devices, thus explaining the need for this added term.

The results of the application of Model 4 to an independent set of data of Table 2.3. is tabulated in Table 2.9. The model predicts forces for Devices 19 and 20 very well with only 10% and 12% errors respectively. However, a large error of 70% is observed for Device 21, which has a small surface area. Device 21 has large AR (>0.5), but small a surface area. This outcome shows this model depends heavily on the SA of a device for force prediction and predicts less well for devices with relatively small SA. The model error is only 11% for very large device 22, indicating the suitability of the application for very large device force prediction.

Table 2.9. Force prediction using Model 4 for independent device data from Table 2.3.

Device	α_0AR. D_{cyl}	% Force from AR.D_{cyl}	α_1SA	% Force from SA	α_2AB	% Force from AB	F_{cal} (kN)	F_{exp} (kN)	Error
19	79.9	72%	18.8	19%	10.6	9%	109.3	125	10%
20	131.4	68%	36.2	21%	18.8	10%	186.4	170	12%
21	153.9	85%	8.9	5%	18.1	10%	182.8	107	70%
22	251	56%	99	22%	94	21%	445.8	500	11%

The force contribution percentages for Device 19 and 20 are as observed in Table 2.9., with majority of force contributed by $\alpha_0 AR.D_{cyl}$ term (~70%) in both devices. The output from $\alpha_1.SA$ and $\alpha_2.AB$ terms are ~20% and 10% respectively for both device 19 and 20. The results are similar to the results for *Typical* devices in Table 2.8. From earlier analyses of the 18 devices, for *Small* devices, maximum forces were attained due to SA contributions due to their small bulge or no-bulge geometry. However, the maximum force contribution from Device 21 is from the term α_0 AR.D_{cyl} like the *Typical* or *Large* devices. This result can be attributed to the large area ratio of the device. From the force contribution evaluation, it is understood Model 4 does not capture the SA force contributions of the Device 21 completely, producing larger error (~70%) in predicting device force. The percentage contribution of forces by each parameter for Device 22 matches the results from other devices shown in Table 2.8.

These outcomes suggest that Model 4 requires calibration of the $\alpha_1.SA$ term to be able to fully capture the SA force contributions of *Small* devices. The model needs to be used with caution for predicting forces for devices with relatively small surface areas. However, the validation results predict consistently well with small errors for *Typical* and *Large* devices. It thus also shows the overall model obtained is relatively general and independent of the device data used to create it, and thus provides a useful guideline for a wide range of devices.

Limitations include the fact the experimental results from large AR devices (AR> 0.5) were not available in creating the model. The *Small* devices used here are atypical, particularly those with no bulge, and thus a model excluding them might give better results, as seen in Models 3 and 4. The reliance on a single parameter, SA, for Devices 1-2 with AR = 0 and largely so for Devices 3-4, is limiting when considering the other 14 devices. Hence, the *Small* devices used here could skew the model, but the models chosen were robust to this effect, as seen in Tables

2.3-2.6. and Figure 2.4.

The overall model (Model 4) remains to be prospectively tested on wide range and large number of devices. However, the external validation shows the prediction is good for independent test results not used to create the device force model. Equally, it shows the overall model obtained is relatively general and independent of the device data used to create it, and thus provides a useful guideline for a wide range of devices.

2.4. Summary

This chapter has presented a simple precision design model using device and experimental data from 18 HF2V devices with and without bulges. From 14 proposed models, identification and analysis assessing independent prediction accuracy, model completeness and robustness resulted in two very good models, from which one was slightly better. Model 4: $F = \alpha_0 AR.D_{cyl} + \alpha_1 SA + \alpha_2 AB$, was identified as the best model as it produced the highest R^2 = 0.91, and its addition of the annular bulge area (AB) term indicates the necessity of this term. Delineation of the force in this model indicates that extrusion terms deliver 78% of the total force on average across all devices, with 22% due to friction.

The model tested on independent data, predicts very well for *Typical* and *Large* devices. The overall model is very general and provides a far more precise design tool linking device dimensions and quasi-static device force. It thus enables easier uptake by practitioners, as well as first indications on more specific and precise mechanics modelling of these devices.

Overall, this chapter has presented an empirical fit of models using key device parameters to

experimental results. The next step will be to consider other models using first principles, rather than empirical fits.

Chapter 3: Upper bound and Lower bound: Analytical Modelling

3.1. Introduction

The specific design force and displacement capacity requirements for a damper for a given structure will depend upon a number of structural design parameters. Therefore, there is a need to be able to reliably predict damping device forces for any given required force capacity. Having methods able to predict upper and lower bounds of the final device performance will eliminate the need for iterative design and experimental testing to achieve a final desired device performance.

While Chapter 2 presented empirical models, this chapter will investigate the application of conventional extrusion models to predict HF2V device forces. This chapter presents equations to provide upper bound and lower bound force limits for a device design. It is based on analogies with bulk extrusion methods, which is a comparable mechanism to the HF2V devices. Existing extrusion force models are classified as direct and indirect. They are modified in derivation to match geometric parameters of the HF2V device designs. The upper and lower bound load estimations are then calculated. Performance and limitations of the models individually or in combinations are assessed.

3.1.1. Direct and Indirect Extrusion Analogy

Extrusion is a forming process in which the working material is forced between dies by an external load. Generally, in direct extrusion processes, the ram moves forward to push the metal billet through the die orifice at room temperature, extruding the metal in the same direction as

the ram. The metal is sheared and compressed between the dies to create plastic deformation to produce metal parts. Typical direct extrusion examples are shown in Figure 3.1. (a).

In indirect metal forming processes, the stamp head is forced through the working material by application of force on the stamp, useful for forming hollow tubes. Unlike direct extrusion, the entire work piece is not displaced by the ram to pass through an orifice. The stamp pushes through the work piece, so the working material compresses and shears passing in the opposite direction to the direction of displacement of the stamp, as shown in Figure 3.1 .(b).

The extrusion process in a HF2V device, as shown in Figure 3.1. (c), is a closed container operation, in which the working material can be repeatedly extruded by shaft displacement. In a prestressed HF2V device, lead is plastically deformed during extrusion and regains its mechanical properties through recrystallization behind the bulge [87]. The working material is forced to flow against the shaft behind the bulge [112]. The working material remains within the containing cylinder after extrusion and does not cause changes in overall configuration of the working material in the HF2V devices, unlike metal forming extrusion processes.

Despite the fact the reversible extrusion process used within these devices does not strictly match conventional extrusion processes, close analogies exist between them. The bulges in the HF2V devices are analogous to the stamp head in indirect extrusion processes and to the die in direct extrusion. The functions of the bulge, stamp head and die are to deform the metal during the extrusion process. Compression and shear forces are produced from deformation of metal and friction between the metal and moving parts in both the processes. Thus, there are strong analogies.

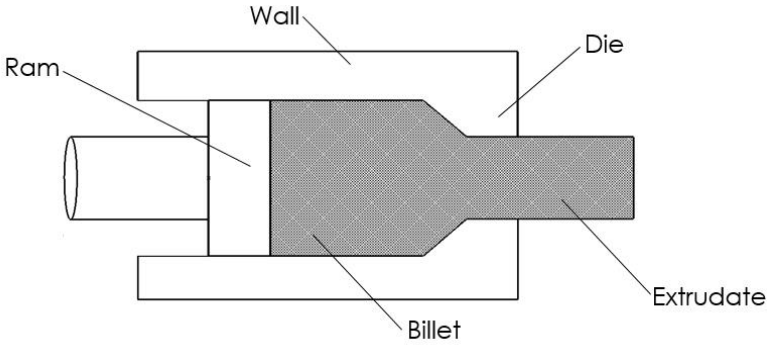

(a)

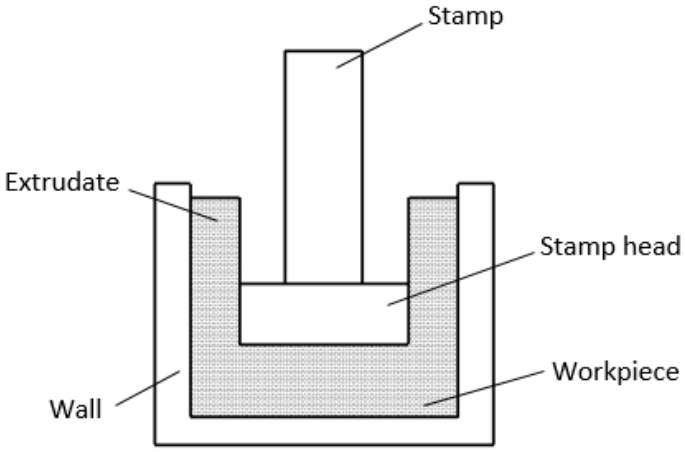

(b)

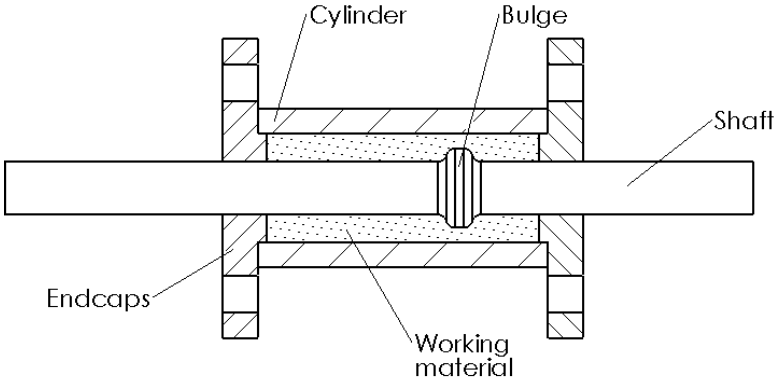

(c)

Figure 3.1. (a) Direct extrusion (b) Indirect Extrusion (c) HF2V device.

The exact interaction of working material (lead) with the cylinder walls of the HF2V devices is uncertain. In particular, there is no simple methodology to observe the actual flow of lead

during shaft displacement in the devices, limiting information. Due to the ambiguity regarding the forces due to wall friction as lead flows, two assumptions are considered in this study:

Assumption 1: Intermetallic shear occurs in lead during the shaft displacement, shearing lead only along the shaft during displacement and the lead along the wall is not displaced [186]. Thus, there are no frictional forces from the cylinder walls, and all force is due to internal shear within the lead.

Assumption 2: Friction forces are produced from the flow of lead along the cylinder walls during shaft displacement, thus contributing to overall HF2V device forces.

3.1.2. Limit Loads

Due to the inherent complexity of the extrusion process, exact prediction of extrusion forces can be difficult. Instead, most methods seek to approximate upper and lower limits on the extrusion forces [187-189]. Upper bound (UB) theorems estimate maximum forces based on yield criteria and geometric self-consistency. Lower bound (LB) theorems determine the minimum forces produced, neglecting geometric self-consistency [189, 190].

Plain strain theory can be applied to metal forming processes with axisymmetric geometry for predicting approximate extrusion forces [76, 191-193]. The upper bound forces can also be estimated using the slip line field theory, which is a graphical method of determining the working load during metal deformation by assuming polycrystalline metals always slip in the direction of maximum shear stress. Thus, the slip-line field theory shows a graphical representation of directions of maximum shear at every point in the deforming body [188].

However, the construction of slip-line field and hodographs for force estimation is complex, and unreliable if the slip-line fields are inaccurate or not to scale [76, 192, 194, 195].

Overall, there are several generalized models available for upper limit approximations of axisymmetric direct and indirect extrusion forces [196-202]. However, only a few models are based on geometric parameters influenced by the frictional conditions involved in extrusion [203]. As HF2V device operation is based on extrusion, the device parameters are matched to equations for direct and indirect metal extrusion processes to obtain upper and lower bound force capacities for these devices. The goal is to provide insight into their operating mechanics and design.

Thus, the limit analysis of the HF2V devices can provide an estimate of the maximum or minimum forces that can be produced by the metal extrusion damper. The UB model predicts the upper force limit or capacity of an HF2V device by considering all types of deformation occurring in the device during operation, including friction forces. The LB model of an HF2V device computes only the force produced due to extrusion of lead between the bulge and the wall, without considering other forces produced during lead deformation.

3.2. Methods

3.2.1. Direct extrusion based HF2V UB Modelling

Upper bound models are proposed based on existing upper bound models for extrusion upper bound force calculations. A simplified, efficient upper bound (UB) extrusion solution for lead and aluminium alloys is considered in this analysis due to the simplified, direct analogy

between the extrusion model and HF2V device operation [196-198]. It is a generalized upper bound model independent of velocity fields and slip line fields [76], defined:

$$\mathbf{F_d = 2k\left[4\mu\left(\frac{H}{D}+\frac{h}{d}\right)+\left(\frac{\mu}{\sin\alpha}+1\right)\ln\frac{D^2}{d^2}\right]\frac{\pi D^2}{4}} \quad (3\text{-}1)$$

Where, *k* is the maximum stress, *D* is the billet container diameter, *H* is the length of billet in the container, *d* is the diameter of the extruded metal, *h* is the length of the die land, μ is the friction coefficient and *α* is the die angle [198, 204] as shown in Figure 3.2.(a). For the direct extrusion comparison to the HF2V device, geometric device parameters are mapped on to the HF2V devices for UB modelling as shown in Figure 3.2.(b).

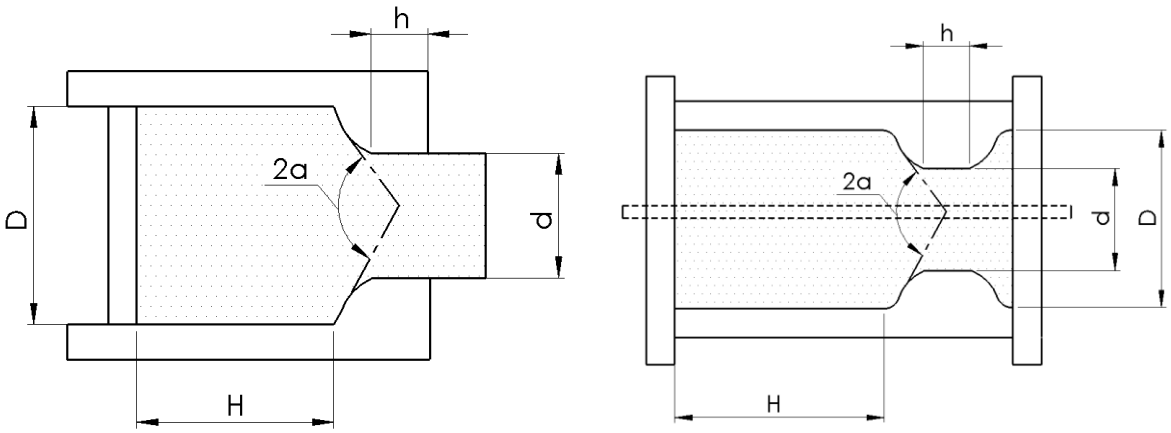

(a) (b)

Figure 3.2. (a) Direct extrusion parameters from equation (b) Direct extrusion geometry mapping to HF2V devices.

The following initial assumptions are made for modelling:

a. The bulges of the HF2V damper are assumed to be on the walls of the devices as shown in Figure 3.2. (b), similar to the constricted tube extrusion damper [72, 74, 100, 110], or that this equivalent analogy would provide the same forces.

b. Additionally, friction from a no-bulge shaft is considered in modelling.
c. The ram moves and lead is extruded between the two bulges on the walls creating extrusion and friction forces.
d. Friction between the endplates is neglected.

Based on Figure 3.2. (b), Equation (3-1) can be modified to match the geometric parameters defining HF2V devices. The additional friction force (F_f) from the shaft is added to the modified UB equation, which is then defined:

$$F_{UB,direct} = 2Y_o \frac{\pi(D_{cyl}-D_{sh})^2}{4}\left[4\mu\left(\frac{L_{cyl}-L_{blg}}{D_{cyl}-D_{sh}} + \frac{L_{flat\ blg}}{D_{cyl}-D_{blg}}\right) + \left(\frac{\mu}{sin\alpha}+1\right)\ln\left(\frac{D_{cyl}-D_{sh}}{D_{cyl}-D_{blg}}\right)^2\right] + F_F \quad (3\text{-}2)$$

where, Y_o is the yield strength of lead, μ is the coefficient of friction between the lead and the steel shaft surface, L_{cyl} is the length of the cylinder, L_{blg} is the length of the bulge, $L_{flat\ blg}$ is the length of the flat surface of the bulge similar to the die land of direct extrusion, D_{cyl} is the cylinder diameter, D_{blg} is the bulge diameter, D_{sh} is the shaft diameter, α is the bulge angle. All HF2V device geometric parameters in Equation (3-2) are shown in Figure 3.3

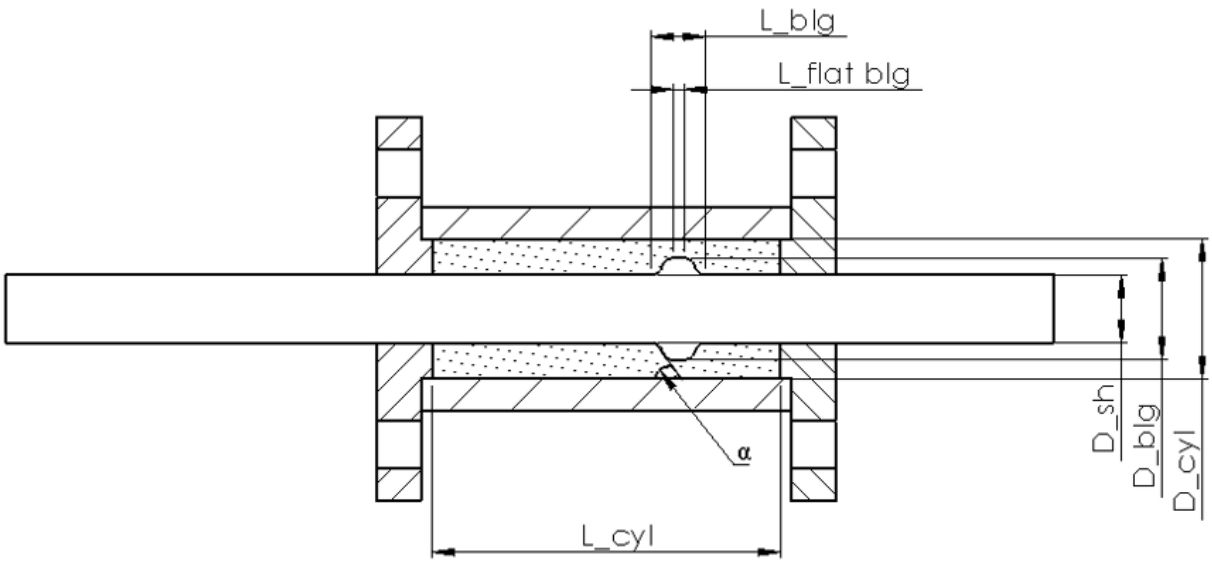

Figure 3.3. HF2V lead extrusion damper parameters.

During shaft displacement, large deformations occur in the lead working material due to shearing by the bulge as it passes through the lead. To attain the maximum possible HF2V device force to calculate an upper bound, the yield strength (Y_o) of the material is considered instead of the maximum stress (k). The value of F_f and the friction coefficient considered for modelling are discussed in detail in Section 3.2.4.

3.2.1.1.UB Model 1 ($F_{UB,1}$)

The friction forces produced in the HF2V devices between the cylinder walls and the lead are neglected in this model following Assumption 1. However, the friction forces attained from friction between the lead and the shaft (F_f) are captured in this model, defined:

$$F_{UB,1} = 2Y_o \frac{\pi(D_{cyl}-D_{sh})^2}{4}\left[4\mu\left(\frac{L_{cyl}-L_{blg}}{D_{cyl}-D_{sh}} + \frac{L_{flat\ blg}}{D_{cyl}-D_{blg}}\right)\ln\left(\frac{D_{cyl}-D_{sh}}{D_{cyl}-D_{blg}}\right)^2\right] + F_f \quad (3\text{-}3)$$

Where, F_f is the friction of lead along the entire shaft, defined in Section 3.2.4. As the friction forces produced at the cylinder walls are neglected in this equation, the minimum friction coefficient can be considered 0.05 between lead and walls for calculation [205, 206] of $F_{UB,1}$. The friction coefficient (μ) is μ = 0.25, and assumed constant at all points of interaction between the lead and shaft surface [207, 208].

3.2.1.2. UB Model 2 ($F_{UB,2}$)

Following Assumption 2, the $F_{UB,2}$ model accounts for the friction forces from lead-wall interaction [209, 210]. The friction coefficient at the lead-wall and lead-shaft interaction are considered as μ = 0.25 in Equation (3-1) for $F_{UB,2}$ modelling [207, 208]. The modified UB equation under Assumption 1 is defined:

$$F_{UB,2} = 2Y_o \frac{\pi(D_{cyl}-D_{sh})^2}{4}\left[4\mu\left(\frac{L_{cyl}-L_{blg}}{D_{cyl}-D_{sh}} + \frac{L_{flat\ blg}}{D_{cyl}-D_{blg}}\right)\ln\left(\frac{D_{cyl}-D_{sh}}{D_{cyl}-D_{blg}}\right)^2\right] + F_{f\_sh} \quad (3\text{-}4)$$

Where, F_{f_sh} is the friction forces from the non-bulged shaft, which is explicitly defined in Section 3.2.4. The friction forces along the bulged shaft have already been captured in the model.

3.2.2. Indirect Extrusion based HF2V UB modelling

The overall geometry in the indirect extrusion case is similar to the geometry of the HF2V devices seen in Figure 4. The stamp head compresses and shears the metal, and passes through

the working piece, similar to the bulged shaft in the HF2V devices. The shaft bulge is analogous to the stamp and the container wall and work piece are compared to the cylinder walls and working material (lead), respectively. However, the extruded work piece does not flow over to the shaft behind the stamp head. In typical indirect extrusion, the extruded work piece retains the die geometry.

A constitutive approach is considered for indirect extrusion force modelling, where the sum of forces dissipated in the extrusion process is considered [195, 199, 211-213]. The forces produced by indirect extrusion are from friction between the work piece-stamp (F_p), workpiece- cylinder wall (F_m), compression of the work piece (F_r) and deformation of work piece (F_{def}) [199], defined:

$$F_i = \left(8\mu k \,.\frac{h_p}{d}\,\frac{D^2}{D^2-d^2}.\frac{\pi d^2}{4}\right)_{Fp} + \left(8\mu k\, D.\frac{h_m+\frac{h}{2}}{D^2-d^2}.\frac{D^2}{d^2}\,.\frac{\pi d^2}{4}\right)_{Fm} + \left[2k.\frac{\pi d^2}{4}.\left(1+\frac{\mu d}{H}\right)\right]_{Fr} + \left(2k\,.\frac{D^2}{d^2}\,.\frac{\pi d^2}{4}\,\ln\frac{D^2}{D^2-d^2}\right)_{Fdef} \quad (3\text{-}5)$$

Where, k is the maximum stress, D is the diameter of container, d is diameter of stamp head, h_p is the height of the stamp, h_m is length of extruded work piece behind the stamp, H is the height of non-deformed work piece [199] and h is defined:

$$h = \frac{\boldsymbol{D+d}}{\boldsymbol{2}}\frac{\sqrt{\boldsymbol{D^2-d^2}}}{\boldsymbol{d}} \quad (3\text{-}6)$$

These geometric parameters for indirect extrusion can be mapped to the HF2V devices for modelling the UB forces, as shown in Figure 3.4**.**

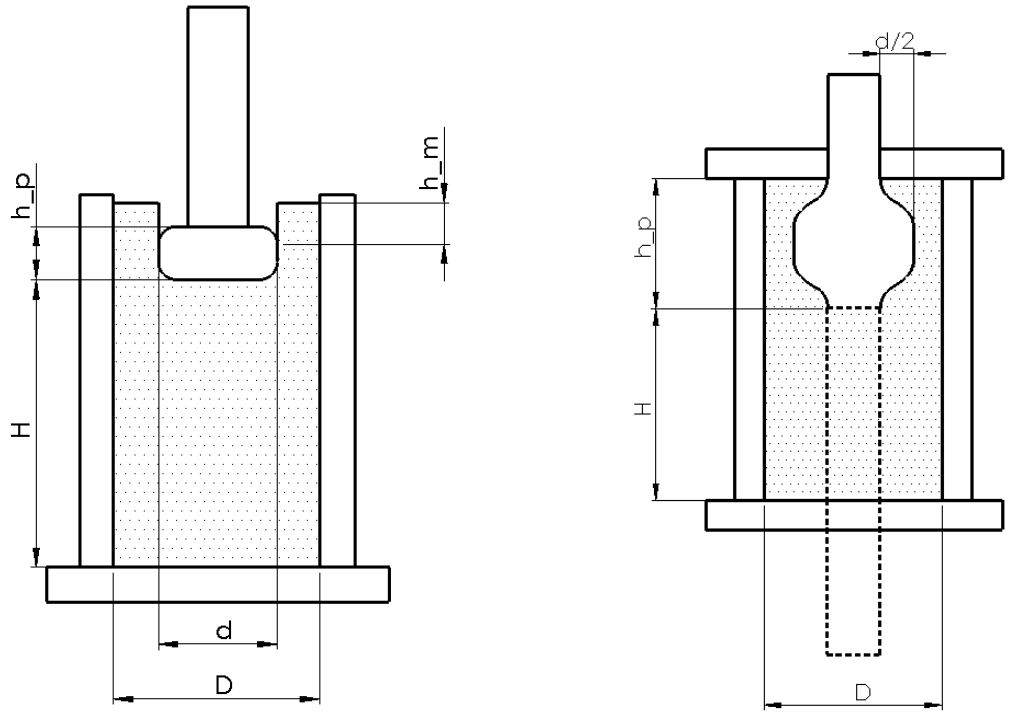

(a) (b)

Figure 3.4. (a) Indirect extrusion parts (b) Geometric mapping of parameters onto the HF2V devices.

Using the indirect extrusion modelling methodology, the upper bound limits of the total HF2V device forces can be calculated from the sum of upper limits of friction forces from lead-bulge *(F_{f_blg})*, lead-shaft *(F_{f_sh})* and lead-wall *(F_{f_wall})* interactions, compression forces *(F_{comp})*, deformation forces *(F_{def})* and extrusion force *(F_{ext})* from area reduction. Equations (3-3)-(3-5) is adapted and modified to match the geometric parameters of the HF2V devices and the UB forces from the HF2V devices can be calculated using:

$$\boldsymbol{F_{UB,indirect} = F_{comp} + F_{def} + F_{f\_blg} + F_{f\_sh} + F_{f\_wall} + F_{ext}} \quad (3\text{-}7)$$

The expression for compressive forces for HF2V devices is defined:

$$F_{comp} = 2Y_o \left(1 + \mu \frac{D_{blg} - D_{sh}}{L_{cyl} - L_{blg}}\right) \frac{\pi (D_{blg} - D_{sh})^2}{4} \quad (3\text{-}8)$$

The deformation forces are defined:

$$F_{def} = 2Y_o \frac{{D_{cyl}}^2}{(d)^2} \frac{\pi d^2}{4} \ln \frac{{D_{cyl}}^2}{{D_{cyl}}^2 - (D_{blg} - D_{sh})^2} \quad (3\text{-}9)$$

The force produced from the friction between the bulged shaft and the working material is calculated:

$$F_{f\_blg} = 8\mu Y_o \frac{(L_{blg})}{D_{blg} - D_{sh}} \frac{\pi \left(D_{blg} - D_{sh}\right)^2}{4} \frac{{D_{cyl}}^2}{{D_{cyl}}^2 - \left(D_{blg} - D_{sh}\right)^2} \quad (3\text{-}10)$$

The working material flows against the wall creating friction forces between the wall and working material, which are defined:

$$F_{f\_wall} = 8\mu Y_o \frac{L_{blg} + {}^{h}/_{2}}{{D_{cyl}}^2 - \left(D_{blg} - D_{sh}\right)^2} \frac{\pi \left(D_{blg} - D_{sh}\right)^2}{4} \frac{{D_{cyl}}^2}{{D_{cyl}}^2 - \left(D_{blg} - D_{sh}\right)^2} \quad (3\text{-}11)$$

Where, h is defined:

$$\boldsymbol{h} = \frac{\boldsymbol{D_{cyl} + (D_{blg} - D_{sh})}}{\mathbf{2}} + \frac{\sqrt{\boldsymbol{{D_{cyl}}^2 - {D_{sh}}^2}}}{\mathbf{2}} \quad (3\text{-}12)$$

in accordance to the indirect extrusion force calculation from Equation (3-6) [199].

The extrusion forces (F_{ext}) can be estimated using equations given in Section 3.2.3**.** The shaft friction force (F_{f_sh}) can be calculated as derived in Section 3.2.4.

3.2.1.1. UB Model 3 ($F_{UB,3}$)

The UB force calculation using the indirect extrusion process with the assumption of no friction between at lead-wall boundary (Assumption 1) yields $F_{UB,3}$, which considers the friction forces generated from the interaction of lead and shaft, defined:

$$F_{UB,3} = F_{comp} + F_{def} + F_{f\_blg} + F_{ext} + F_{f\_sh} \quad (3\text{-}13)$$

3.2.2.2. UB Model 3 ($F_{UB,4}$)

Following Assumption 2, the working material flows against the direction of motion against the wall, creating friction forces between the wall and lead, which are calculated using Equation (3-5). The modified UB force model $F_{UB,4}$ considering wall friction forces in HF2V devices is defined:

$$F_{UB,4} = F_{comp} + F_{def} + F_{f\_blg} + F_{f\_sh} + F_{ext} + F_{f\_wall} \quad (3\text{-}14)$$

3.2.3. Lower bound equation (F_{LB})

Lower bound extrusion forces can be estimated based on work models used to obtain metalworking loads, which assumes homogenous deformation and zero friction [76, 211, 214]:

$$F_{LB} = A_o Y'_o \ln \frac{A_o}{A_f} \quad (3\text{-}15)$$

Where, Y'_o is the yield stress is from power law, A_o is the area of lead before extrusion, A_f is the lead area after extrusion, defined for HF2V devices using Figure 3.3:

$$A_o = \pi \frac{(D_{cyl} - D_{sh})^2}{4};\ A_f = \pi \frac{(D_{cyl} - D_{blg})^2}{4} \tag{3-16}$$

Power law calculates yield strength under low stresses, which is ideal for lower bound force calculations. This model assumes pure extrusion with ideal deformation, no friction and no redundant work [214, 215]. Based on this reasoning, this model can be used to estimate extrusion forces from the device when the friction between the steel parts and lead is negligible. This condition can occur, for example, when surfaces are lubricated. Neglecting these terms is an appropriate simplifying assumption when calculating a lower bound. Thus, $F_{LB} = F_{ext}$.

3.2.1.3. Modified Lower Bound Equation ($F_{LB,1}$)

From previous research, actual HF2V forces are obtained from extrusion forces and friction forces [209, 210]. Hence, the force required to overcome friction for shaft displacement needs to be considered for LB modelling. The overall lower bound force developed in the HF2V damper can be obtained by adding F_f to Equation (3-15), yielding:

$$F_{LB,1} = A_o Y_o' \ln \frac{A_o}{A_f} + F_f \tag{3-17}$$

3.2.4. Friction force (F_f) modelling

Accounting frictional effects at the contact surface is complex and several studies have been undertaken to understand the mechanics involved at the contact boundary [216-220]. The Coulomb friction model is the earliest and most frequently used friction model in extrusion. It

is only dependent on load and direction of velocity, and estimates the dynamic friction forces from sliding [221].

A Coulomb friction based model is used to calculate friction forces from lead-shaft interface [222-225]:

$$F_F = m\pi DL\frac{Y_o}{\sqrt{3}} \tag{3-18}$$

The friction model considered in Equation (3-18), assumes shear stresses are proportional to the normal flow stress [218, 222-226] according to Von Mises friction law. The true estimation of the shear forces in the devices can be determined only if the actual area of contact between the lead and the shaft/container is known [227]. Industrial extrusion processes assume constant friction exists at all points of contact between working material and die/container [161, 218].

The length of the shaft in contact with lead is equal to the length of the cylinder (L_{cyl}), the frictional force component for the entire shaft is thus defined:

$$F_f = m\pi D_{sh}\frac{Y_o}{\sqrt{3}}L_{cyl} \tag{3-19}$$

The length of the bulge, L_{blg} is excluded in Equation (4) as the friction contribution by the bulge is already captured. The frictional force component is defined:

$$F_{f\_sh} = m\pi D_{sh}\frac{Y_o}{\sqrt{3}}(L_{cyl} - L_{blg}) \tag{3-20}$$

3.2.5. Summary of UB and LB Equations

Equations (3-1) to (3-20) present and revise several equations for UB and LB forces under a variety of conditions. To avoid confusion, they are summarised in

Table 3.1.

Table 3.1. The HF2V UB and LB equations used for analysis.

UB without wall friction from Direct extrusion	$F_{UB,1} = 2Y_o \frac{\pi(D_{cyl}-D_{sh})^2}{4}\left[4\mu\left(\frac{L_{cyl}-L_{blg}}{D_{cyl}-D_{sh}} + \frac{L_{flat\ blg}}{D_{cyl}-D_{blg}}\right)\ln\left(\frac{D_{cyl}-D_{sh}}{D_{cyl}-D_{blg}}\right)^2\right] + m\pi D_{sh}\frac{Y_o}{\sqrt{3}}L_{cyl}$
UB with wall friction from Direct extrusion	$F_{UB,2} = 2Y_o \frac{\pi(D_{cyl}-D_{sh})^2}{4}\left[4\mu\left(\frac{L_{cyl}-L_{blg}}{D_{cyl}-D_{sh}} + \frac{L_{flat\ blg}}{D_{cyl}-D_{blg}}\right)\ln\left(\frac{D_{cyl}-D_{sh}}{D_{cyl}-D_{blg}}\right)^2\right] + m\pi D_{sh}\frac{Y_o}{\sqrt{3}}(L_{cyl}-L_{blg})$
UB without wall friction from Indirect extrusion	$F_{UB,3} = Y_o\left[2\left(1+\mu\frac{D_{blg}-D_{sh}}{L_{cyl}-L_{blg}}\right)\frac{\pi(D_{blg}-D_{sh})^2}{4} + 2\frac{{D_{cyl}}^2}{(d)^2}\frac{\pi d^2}{4}\ln\frac{{D_{cyl}}^2}{{D_{cyl}}^2-(D_{blg}-D_{sh})^2} + 8\mu\frac{(L_{blg})}{D_{blg}-D_{sh}}\frac{\pi(D_{blg}-D_{sh})^2}{4}\frac{{D_{cyl}}^2}{{D_{cyl}}^2-(D_{blg}-D_{sh})^2} + A_o\ln\frac{A_o}{A_f} + m\pi D_{sh}\frac{L_{cyl}}{\sqrt{3}}\right]$
UB with wall friction from Indirect extrusion	$F_{UB,4} = Y_o\left[2\left(1+\mu\frac{D_{blg}-D_{sh}}{L_{cyl}-L_{blg}}\right)\frac{\pi(D_{blg}-D_{sh})^2}{4} + 2\frac{{D_{cyl}}^2}{(d)^2}\frac{\pi d^2}{4}\ln\frac{{D_{cyl}}^2}{{D_{cyl}}^2-(D_{blg}-D_{sh})^2} + 8\mu\frac{(L_{blg})}{D_{blg}-D_{sh}}\frac{\pi(D_{blg}-D_{sh})^2}{4}\frac{{D_{cyl}}^2}{{D_{cyl}}^2-(D_{blg}-D_{sh})^2} + A_o\ln\frac{A_o}{A_f} + m\pi D_{sh}\frac{L_{cyl}}{\sqrt{3}} + 8\mu\frac{L_{blg}+{}^{h}/_{2}}{{D_{cyl}}^2-(D_{blg}-D_{sh})^2}\frac{\pi(D_{blg}-D_{sh})^2}{4}\frac{{D_{cyl}}^2}{{D_{cyl}}^2-(D_{blg}-D_{sh})^2}\right]$
LB without friction from shaft and wall	$F_{LB} = A_o Y_o'\ln\frac{A_o}{A_f}$
LB with friction from shaft	$F_{LB,1} = A_o Y_o'\ln\frac{A_o}{A_f} + m\pi D_{sh}\frac{Y_o'}{\sqrt{3}}L_{cyl}$

3.3. Analysis

The UB and LB models in Table 3.1. are applied to 15 HF2V lead extrusion dampers whose experimental test data are available from previous research [125, 160, 228]. Some devices from Chapter 2 are considered in this study, whose relevant geometric values are known. The 15 devices considered are defined in Table 3.2. The following assumptions are made for the UB analysis:

i. The friction coefficient (μ) is μ = 0.25, and assumed constant at all points of interaction between the lead and shaft surfaces .

ii. The forces of compression behind the bulge slope after extrusion are neglected.

iii. The velocity of the shaft relative to the outer casing is assumed 0.5mm /s for all the devices.

iv. The effect of temperature is not considered in this analysis.

Table 3.2. HF2V device parameters.

Devices	L_{cyl} (mm)	L_{blg} (mm)	D_{cyl} (mm)	D_{blg} (mm)	D_{shaft} (mm)	α (degrees)
5.	110	30	89	40	30	68.2
6.	110	30	89	50	30	51.3
7.	110	30	89	58	30	41.8
8.	130	30	66	40	30	68.2
9.	130	30	66	50	30	51.3
10.	50	23.3	50	32	20	56.8
11.	70	20	50	32	20	56.3
12.	100	30	50	35	24	66.3
13.	160	20	60	42	33	62.1
14.	100	23	50	35	24	59.9
15.	75	30	70	48	30	54.2
16.	160	20	54	35	30	73.6
17.	160	20	54	36	30	70.6
18.	160	20	54	38	30	64.8
19.	100	17.2	40	27	20	65.3

For the UB analysis, the following expression is considered for calculating the yield stress (Y_o):

$$Y_o = 2\bar{Y} \tag{3-21}$$

The average or flow stress ($\bar{\boldsymbol{Y}}$) is the mean value of stresses from the beginning to end of deformation, defined [215]:

$$\bar{Y} = \frac{K\varepsilon^n}{1+n} \quad (3\text{-}22)$$

Where, K is the strength coefficient, ε is the strain during the deformation process, and n is the strain-hardening component. K = 26.4 and n = 0.28 for commercially pure lead [229]. The corresponding Y_o values calculated are given in Table 3.3.

Table 3.3. The yield strength values of pure lead form Equation (3-22).

Devices	ε	Y_o (N/mm^2)
5.	0.17	25.09
6.	0.34	30.47
7.	0.47	33.48
8.	0.28	28.82
9.	0.56	34.99
10.	0.40	31.92
11.	0.40	31.92
12.	0.42	32.42
13.	0.33	30.33
14.	0.42	32.42
15.	0.45	32.99
16.	0.21	26.59
17.	0.25	27.98
18.	0.33	30.33
19.	0.35	30.74

The strain hardening component in Equation (3-22) allows for estimation of forces developed in HF2V devices during strain hardening of lead, capturing peak forces produced during plastic deformation [215]. The Y_o values calculated Equation (3-22) for all the devices are comparable to experimental yield stress values of pure lead at 20 °C [230].

For the LB analysis, the yield stress for lead under shear and compression respectively can be estimated based on power law of stress strain relationship, which is used to calculate flow stresses under low stresses [229, 231-233]. Using the stress-stain relationship based on power law for commercially pure lead at room temperature [229, 232], flow stress at low stresses is defined:

$$\bar{Y}' = k'\bar{\varepsilon}^{n}\dot{\bar{\varepsilon}}^{m} \tag{3-23}$$

Where, *k'* is the stress constants (MPa), ε is the strain during the deformation process, *n* is the strain-hardening component and $\dot{\bar{\varepsilon}}$ is the strain rate. The yield stress values can be calculated using the respective parameter values from previous research [229, 232], given as *k'*= 33 MPa, *n* =0.30 and *m* = 0.091. Thus, corresponding yield stress is calculated using:

$$Y'_o = 2\bar{Y}' \tag{3-24}$$

The yield stresses for LB force calculations calculated using equation (3-24) is tabulated in Table 3.4**.** The device forces calculated using low stresses from power law would provide a rough estimate of the lowest forces produced in the devices before recrystallization after initial work hardening [215].

Table 3.4. Yield strength values for LB calculations using Equation (3-24).

Devices	ε	Y_o' (N/mm^2)
5.	0.17	20.63
6.	0.34	27.03
7.	0.47	30.83
8.	0.28	25.01
9.	0.56	32.78
10.	0.40	28.84
11.	0.40	28.84
12.	0.42	29.47
13.	0.33	26.86
14.	0.42	29.47
15.	0.45	30.19
16.	0.21	22.36
17.	0.25	24.01
18.	0.33	26.86
19.	0.35	27.37

The friction factor, *m*, also known as the interface friction shear factor is a quantitative index for determining friction stresses at interface [224]. The friction factor, m = 0.866 and is calculated using the following relationship [222, 234]:

$$\boldsymbol{m = 2\,\mu\sqrt{3}} \tag{3-25}$$

A total of 15 HF2V experimental device forces (F_{exp}) are compared against the estimated upper bound and lower bound forces. The resulting UB and LB forces are compared to the peak forces from experimental tests. The experimental forces are expected to lie between the UB and LB forces [195].

To better understand the dependency of the HF2V device forces and the estimated UB and LB forces on the device parameters, the devices are plotted on basis of increasing values of key HF2V geometric parameters of the empirical model (Model 4) from Chapter 2**.** In addition, based on existing research parameters influencing the extrusion forces in bulk forming industry, geometric parameters crucial in producing HF2V device forces are identified by comparison.

The UB models are analyzed to identify the reliable model giving closest predictions. UB and LB models provide a rough estimation of a broad range of maximum and minimum expected forces from HF2V devices. For practical applications, it will be helpful in determining device design forces.

To attain a closer approximation to actual device forces the following three methods are applied

i. Average UB and LB model forces are calculated based on the models presented and error based on experimental forces are calculated. The model combination showing the smallest error can be used for device force calculation.
ii. The model forces are plotted against experimental forces, with UB model force on the X-axis and experimental force on the Y axis. The model correlation coefficient is determined. The models showing excellent correlation, R^2 (> 0.85) with experimental values are assumed best, based on a trend line drawn for the plot and equation:

$$Y = AX + B \tag{3-26}$$

where, Y is the experimental force and X is the model force. A is the gradient of the line and B is the intercept. The equation is used to calculate expected HF2V device forces. The results are compared with experimental forces for corresponding devices.

$$F_{UB,1\text{precision}} = 2\frac{Y_o}{2}\frac{\pi\left(D_{cyl} - D_{sh}\right)^2}{4}\left[4\mu\left(\frac{L_{cyl-}L_{blg}}{D_{cyl} - D_{sh}} + \frac{L_{flat\ blg}}{D_{cyl} - D_{blg}}\right)\ln\left(\frac{D_{cyl} - D_{sh}}{D_{cyl} - D_{blg}}\right)^2\right]$$

$$+m\pi D_{sh}\frac{Y_o}{2}L_{cyl} \tag{3-27}$$

The HF2V device geometric parameters are applied to this model to attain precise device forces.

3.4. Results

3.4.1. UB and LB forces and plots

Experimental HF2V device forces are compared to UB and LB estimates of HF2V devices using the equations from

Table 3.1. The results are compared in Table 3.5 and

Figure 3.5. The experimental forces (F_{exp}) are smaller than the direct extrusion UB force values ($F_{UB,1}$ and $F_{UB,2}$) as expected, shown in Figure 3.5 (a). $F_{UB,1}$ predictions are closer to experimental test forces. The addition of wall friction makes the predictions of UB forces from $F_{UB,2}$ larger than FUB,1 as expected.

The results from the indirect extrusion model shows the upper bound forces without wall friction ($F_{UB,3}$) are lower than the experimental forces except for device 16, where the UB force is greater than the experimental peak force. However, on considering the wall friction between lead and cylinder, the upper bound forces ($F_{UB,4}$) are greater than the experimental forces for all 15 devices. The devices forces from experiments are plotted with UB forces from indirect extrusion ($F_{UB,3}$, $F_{UB,4}$)

Figure **3.5**.(b).

Table 3.5. Comparison of HF2V LB and UB forces to experimental forces.

Devices	F_{LB} (kN)	$F_{LB,1}$ (kN)	F_{exp} (kN)	$F_{UB,3}$ (kN)	$F_{UB,4}$ (kN)	$F_{UB,1}$ (kN)	$F_{UB,2}$ (kN)
5.	20.94	127.08	160	134.8	319.8	273.6	444.3
6.	61.16	200.25	285	245.4	477.1	486.5	702.4
7.	108.42	267.01	390	370.9	636.3	704.2	947.8
8.	16.56	168.66	200	174.5	316.0	288.6	436.6
9.	54.09	253.39	346	300.2	482.7	492.4	687.1
10.	20.81	65.77	130	77.7	172.0	155.3	208.8
11.	20.81	83.76	150	98.4	183.9	178.5	245.3
12.	17.21	127.49	155	132.5	245.3	219.9	311.4
13.	12.46	233.55	260	247.5	349.3	344.2	497.2
14.	17.21	127.49	155	136.8	231.0	220.8	315.9
15.	45.34	151.26	250	180.5	362.7	339.8	443.6
16.	4.72	172.05	170	185.2	261.2	251.0	369.2
17.	6.25	185.91	200	198.0	278.2	269.7	394.7
18.	9.85	210.84	260	222.4	310.1	305.6	442.0
19.	7.41	92.76	125	97.6	151.4	146.3	215.2

The lower bound forces from F_{LB} and $F_{LB,1}$ are lower than all the experimental forces except Device 16, which is almost equal to the experimental force shown in

Figure **3.5**(c). However, the values from F_{LB} are very low, as it neglects the forces from friction. This result shows the significance of friction force in HF2V devices. It also matches results in Chapter 2 of friction forces contributing between 10-60% total device forces in the *Typical* and *Large* devices.

Figure **3.5**.(d) shows the UB and LB force ranges for all the HF2V devices plotted along with the peak experimental device forces. Based on the results, as expected all the UB model force ranges lie above the experimental forces, except $F_{UB,3}$. The UB force values from the direct extrusion analogy are much larger than the UB forces calculated from indirect extrusion models, as the estimated forces required to overcome friction are higher due to the assumption entire billet moves through the cylinder with ram displacement [76, 215, 235]. The $F_{UB,1}$ model over estimates the device forces by 38- 60%.

However, results from the direct extrusion model without the wall friction ($F_{UB,1}$) and indirect extrusion model considering wall friction ($F_{UB,4}$) are very close, with UB ranges seeming to overlap each other. Although $F_{UB,4}$ considers wall friction forces, only the friction between the lead displaced by the bulge and the wall is captured by the F_{f_wall} term in the model. Thus, the wall friction forces are not over estimated similar to $F_{UB,1}$.

From the results shown in Table 3.5and

Figure 3.5(d) the UB force range from $F_{UB,3}$ lies very close to the experimental forces. All the forces from this model are smaller than the peak experimental forces as the model does not account for the HF2V device forces produced form prestressing, friction between shaft and endcaps. However the forces predicted are greater than $F_{LB,1}$ model forces for all the devices. Thus, $F_{UB,3}$ and $F_{LB,1}$ forces could be used for approximate prediction of average forces and the minimum HF2V device forces, respectively.

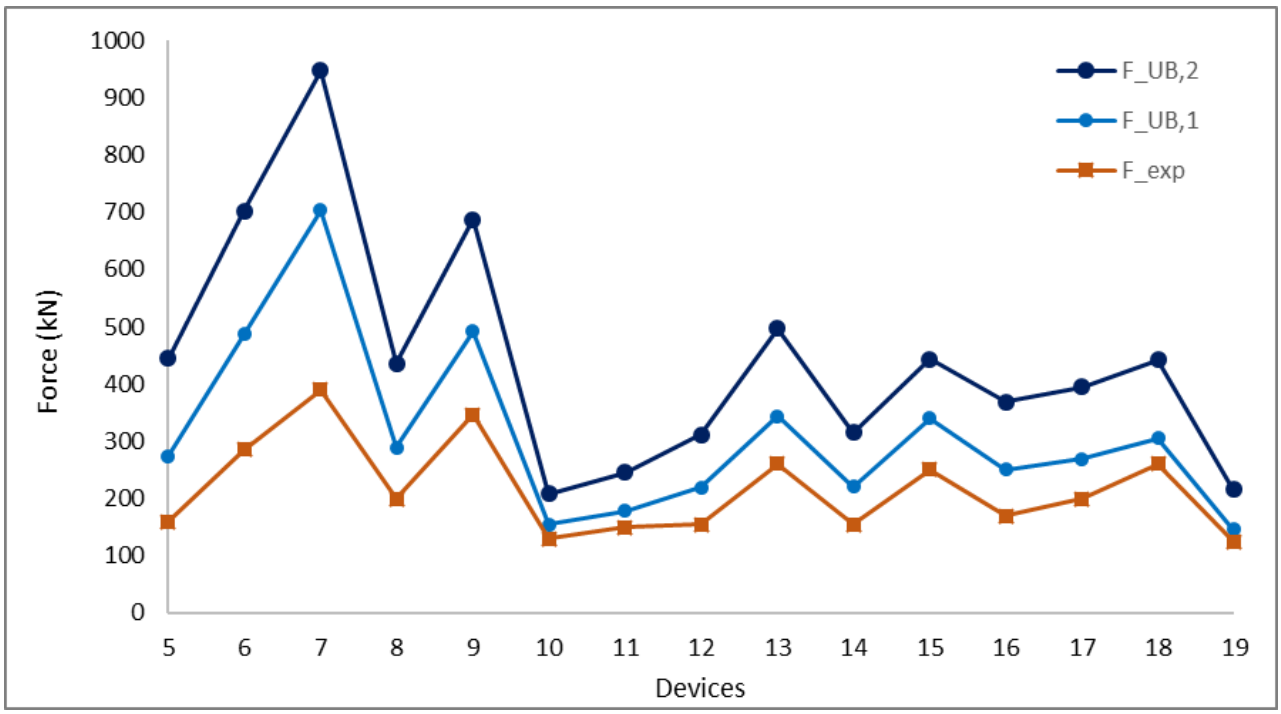

(a) UB force ($F_{UB1,}$ $F_{UB\ 2}$) range from direct extrusion modelling for the HF2V devices.

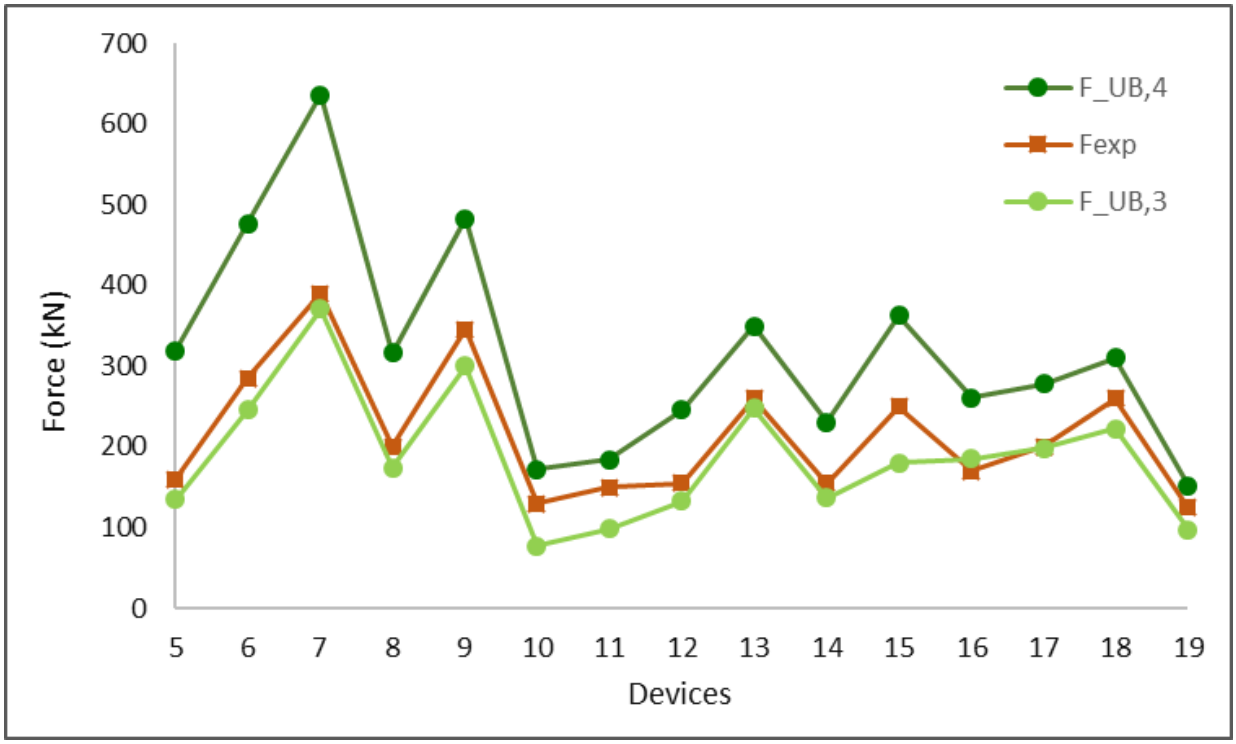

(b) UB force range ($F_{UB,2}$,$F_{UB,3}$) from indirect extrusion modelling for the HF2V devices.

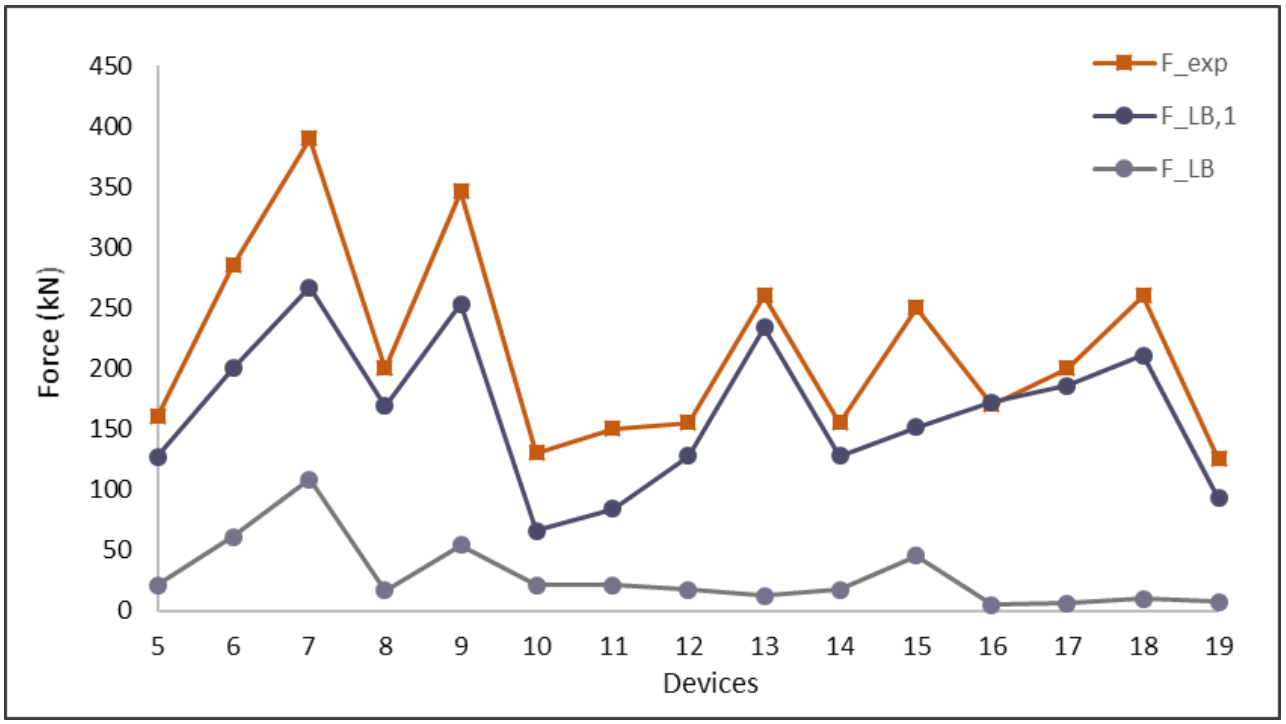

(c) LB force (F_{LB}, $F_{LB,1}$) range from indirect extrusion modelling for the HF2V devices.

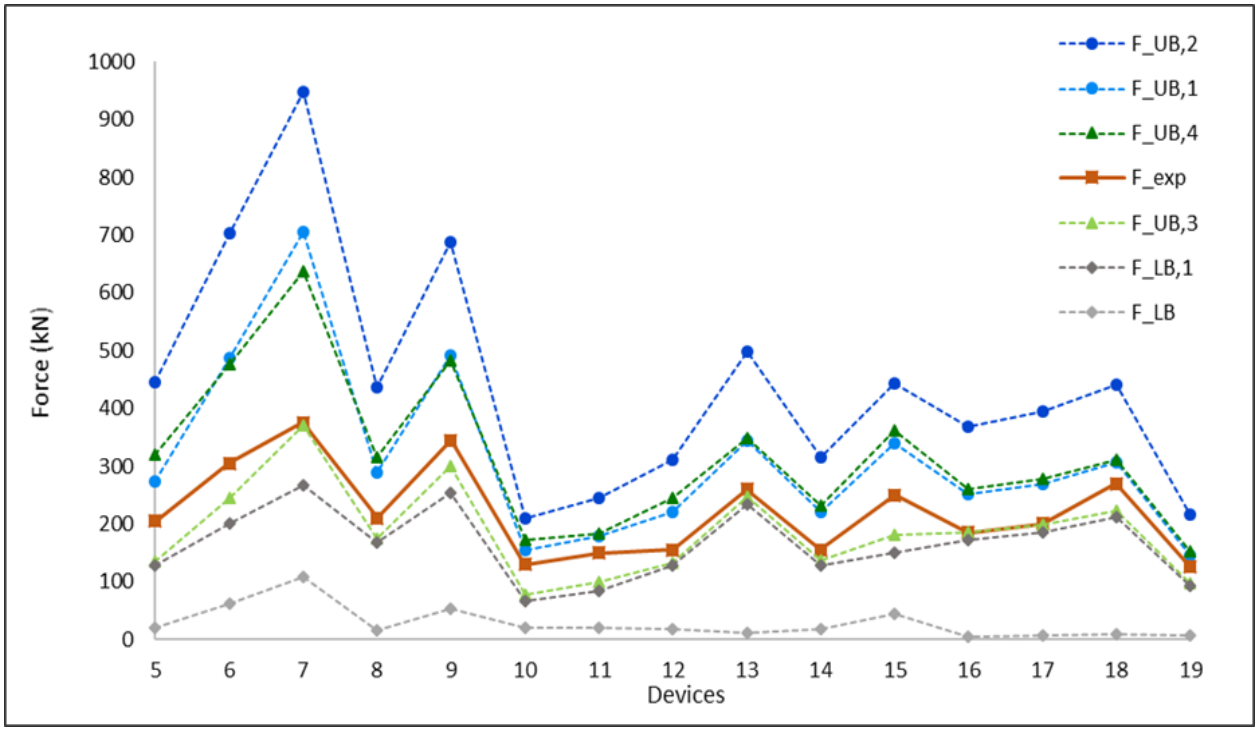

(d) F_{exp} plotted along with all UB and LB force ranges for HF2V devices.

Figure 3.5. Plots for HF2V device UB and LB force ranges from results in Table 3.5.

3.4.2. Key Design Parameters

In Chapter 2, modelling parameters capturing extrusion and friction forces from HF2V devices in the empirical model (Model 4) were: D_{cyl}, AB and SA. In Figure 3.6. (a-c) the force outcomes from the UB, LB models and experimental forces are plotted in ascending values of these device parameters. The numbers above the data points indicate the device identification numbers and the numbers labelled below the plots along horizontal axis indicate the values of the corresponding device parameter considered for sorting. The values along the horizontal axis are only representative of increasing values of the respective parameters and are plotted at fixed intervals representing rank. The horizontal spacing of the data points is not related to the values of the parameters. . However, the vertical position of the data points against the vertical axis values represents the device forces, which increase relative to the magnitude of

the force prediction. This plot shows the UB and LB model forces and device experimental forces for corresponding devices indicated above the plots, given previously in Table 3.5.

In Figure 3.6. (a), when the results are ranked by the value of D_{cyl}, UB and LB values for all the models are observed to monotonically increase, except for devices 5, 8 and 15. This result strongly indicates D_{cyl} has a large influence on overall extrusion force. In particular, D_{cyl} broadly determines the volume of lead available for deformation. Thus, cylinder internal diameter can be used as a rough indicator of device scale, where larger devices typically produce more resistive force.

Devices sorted on increasing order of bulge area *AB*, as shown in Figure 3.6 (b), also indicate larger *AB* values result in larger resistive forces, as expected. A larger bulge area, AB, means more lead can be displaced and sheared by the shaft bulge, thus producing larger deformation, and larger compressive and shearing forces. The forces from Devices 10, 11, 12 and 14 do not fit the overall linear trend of increasing device force with increasing values of AB. The SA of these devices are relatively small as seen in Figure 3.6 (c), which is significant because friction force also contributes to HF2V device force, as discussed previously in Chapter 2. Thus, there is a trade-off between increases in some values and reductions in others in this case.

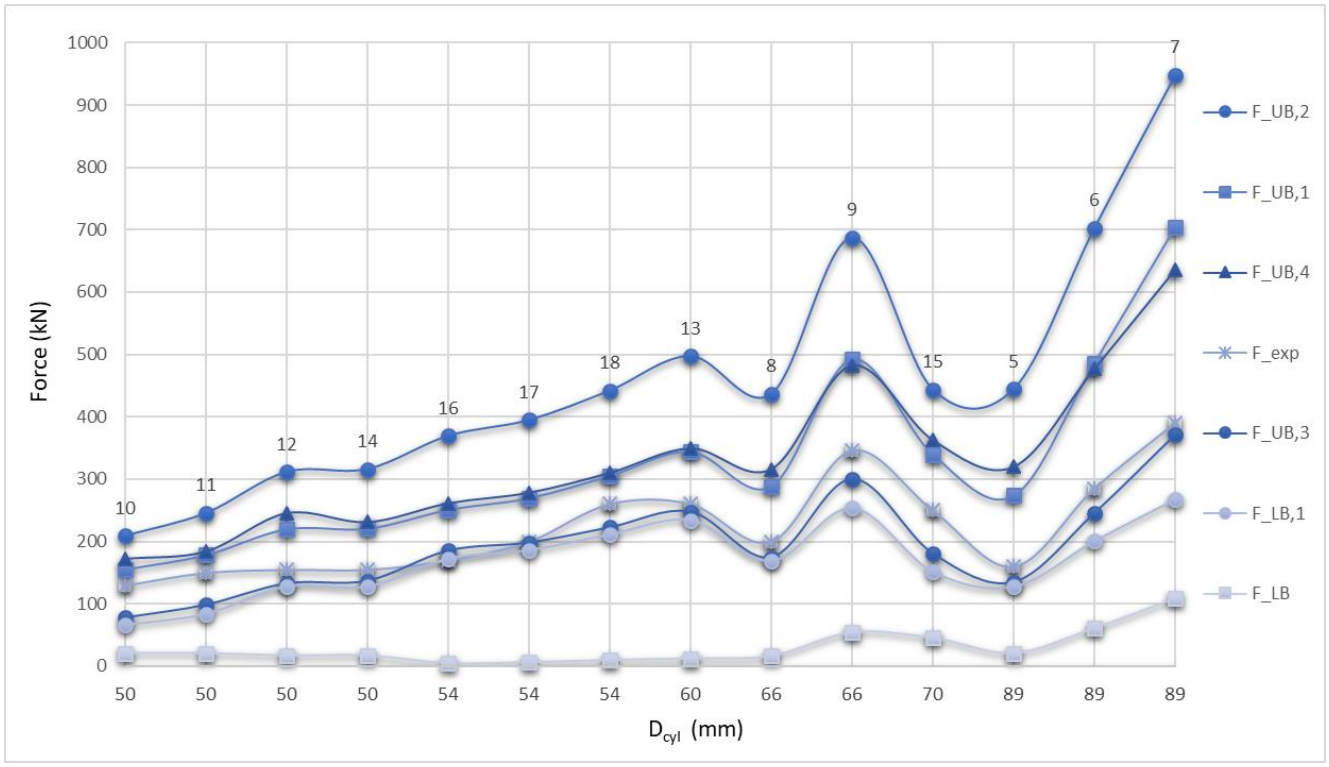

(a) Devices sorted by increasing values of cylinder diameter (D_{cyl}).

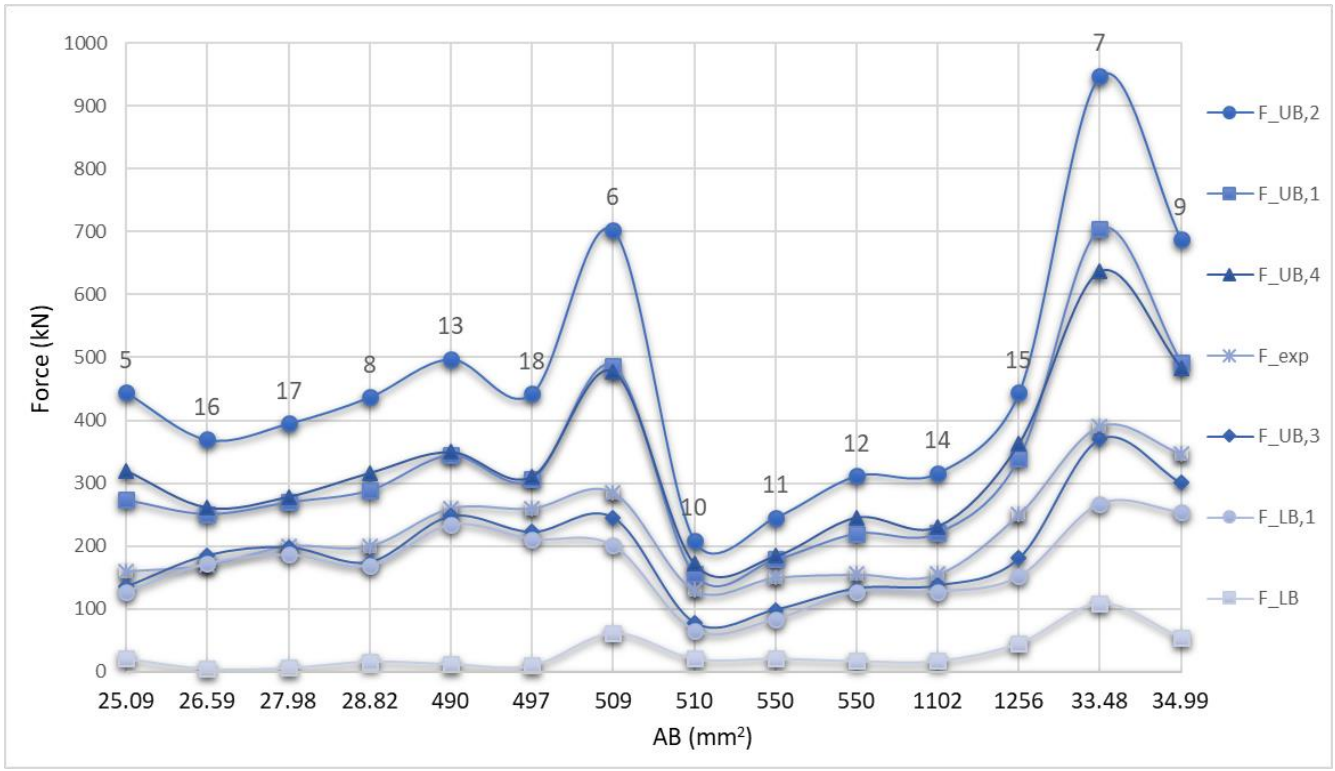

(b) Devices sorted by increasing values of bulge area (AB).

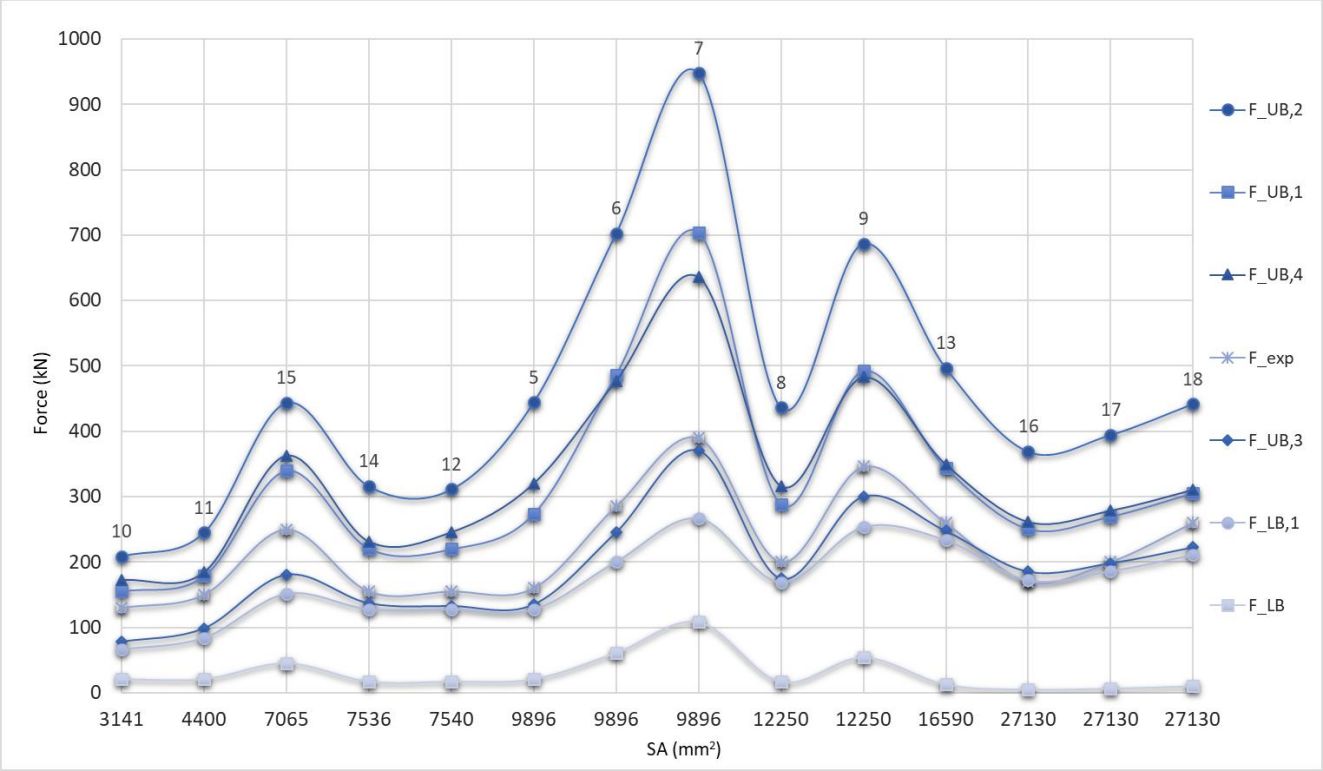

(c) Devices sorted by increasing values of surface area. (SA)

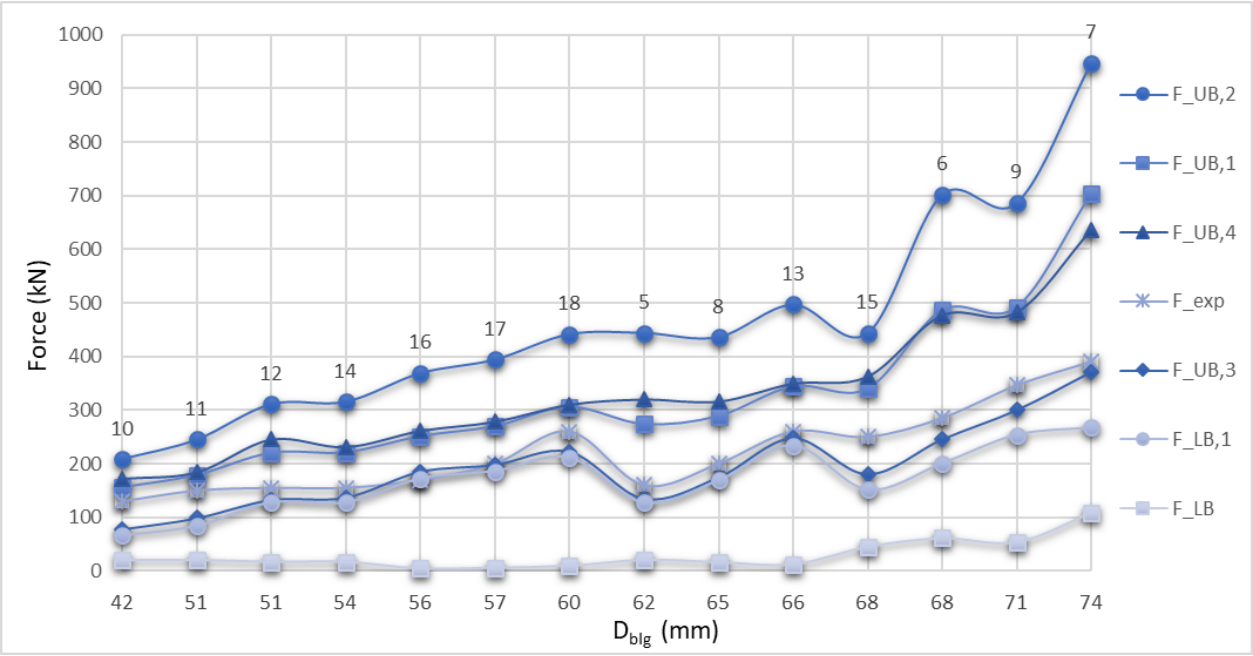

(d) Devices sorted based on increasing values of bulge diameter.

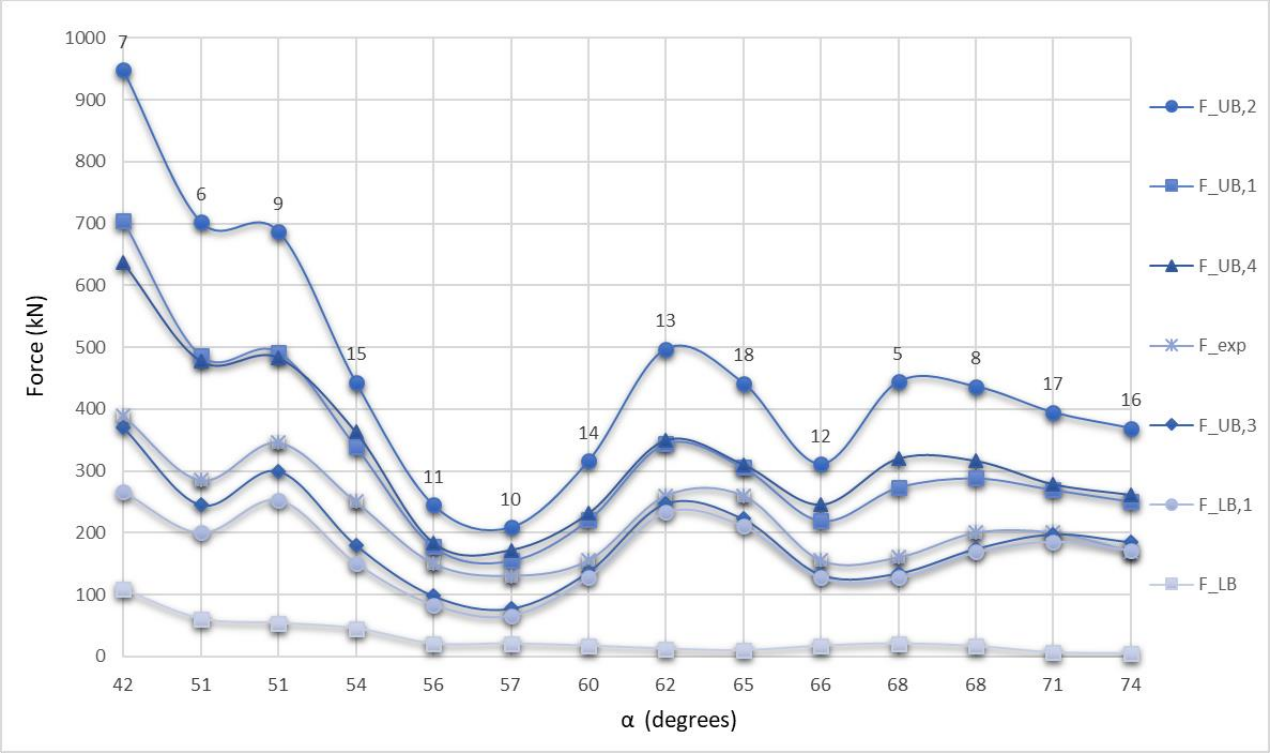

(e) Devices sorted based on increasing values of bulge angle.

Figure 3.6. Devices ranked on values of key device parameters.

However, correlation between resistive force and SA is less clear. Two devices with the same cross sectional properties, one designed to accommodate more stroke length, and with a larger L_{cyl}, may increase the *SA* and frictional force due to addition of contact area, but not the extrusion force. Thus, devices with design constraints in length, could attain higher force capacities by increasing D_{cyl} or AB. Similarly, large devices requiring lower design force capacities for larger surface area could adjust D_{cyl} and *AB* values for desired force capacities. The UB models can thus also be used as a reference in safely designing HF2V devices within a desired force range.

Device forces, when sorted by increasing values of D_{blg}, shows almost a linear relationship between D_{blg} and HF2V device forces in Figure 3.6 (d). Hence, based on this plot, it can be deduced that D_{blg} values directly influence HF2V device forces. A large bulge diameter induces

larger strain or reduction percentage and deformation during loading, leading to production of large resistive forces [161]. However, the direct correlation between force and strain can only be expected upto 40-50% strain of the lead working material, beyond which the values may be constant or decrease, depending on strain rate [87, 230, 236, 237].

Another bulge related attribute is bulge angle (α), which is one of the parameters in direct extrusion UB force models ($F_{UB,1}$ *and* $F_{UB,2}$). From Figure 3.6 (e), decreasing device force is seen with increasing values of α for devices except for Devices 10-12 and 14. Similar trends are observed in the metal forming industry, where bulge angle is a key parameter in designing extrusion dies [238-240]. From previous research on metal extrusion processes, it is noted the extrusion forces increase for increasing small die angle until approximately 35 - 45 degrees and decreases with further increase in bulge angle [240].

According to research in the field of metal extrusion processes, the other parameters related to bulge size, which are important, are the die fillet [239], die length [241], die flat length. These values correspond to bulge arc, bulge length and bulge flat length respectively in the HF2V devices. The bulge angle value is dependent on the bulge flat length (die flat length) [240].

An increasing value of bulge flat length means the metal in contact with the die has to overcome larger values of friction for motion along the die. For bulges of the same length and size, the bulge angle can be reduced by increasing the bulge flat length. This change results in increase in area of contact between the lead and the shaft bugle. Thus, the force required to overcome friction becomes higher and the resulting overall peak extrusion forces are higher.

The bulge arc in HF2V devices can be considered the bulge arc or curve from the shaft to the bulge flat length at the top of the bulge. The effect of the bulge arc radius is particularly prominent in smaller bulge devices, as it allows larger contact area for small bulged devices. The bulge arc factor along with large bulge length of the *Small* devices, Devices 2 and 4, can be attributed to their higher than expected device forces, despite the small size in Chapter 2.

The importance of bulge size is also evident from Device 21 which is a small device with SA smaller than Devices 2 and 4. However, the device produces considerably larger forces from extrusion due to a relatively large value of AB. Overall, bulge related parameters are most crucial in determining the HF2V device forces in addition Precise force calculation method from UB and LB models

3.4.3. Method 1 : Average of forces

The average forces obtained from the analytical models (UB and LB) are given in Table 3.6. The error is calculated for the average forces and the experimental forces from the devices. The overall results from this calculation shows errors ranging from ~1% to ~30% for all the model average forces. The experimental forces considered in Table 3.6 is the mean of peak forces of the HF2V devices from multiple experimental tests.

The UB forces are generally indicative of the maximum achievable force by a device due to the consideration of yield stress for calculation. The large errors could be due to consideration of average peak force. On considering the maximum value of force produced during cyclic testing of device, the errors are reduced by a large percentage, shown in Table 3.7. The cyclic

test data for Devices 10 to 14 were not available. Hence, the known peak force is considered in Table 3.7. Therefore, there is no change in overall errors for Devices 10-14.

Table 3.6. Average model forces and corresponding errors for HF2V devices with respect to mean HF2V peak force.

Devices	F_{exp} (kN)	$F_{UB,1}$ & $F_{LB,1}$		$F_{UB,2}$ & F_{LB}		$F_{UB,4}$ & $F_{LB,1}$		$F_{UB,3}$ & $F_{UB,4}$	
		F_{avg} (kN)	Error (%)	F_{avg} (kN)	Error (%)	F_{avg} (kN)	Error (%)	F_{avg} (kN)	Error (%)
5.	160	200.3	20%	232.6	31%	223.4	28%	28%	30%
6.	285	343.4	17%	381.8	25%	338.7	16%	16%	21%
7.	390	485.6	20%	528.1	26%	451.7	14%	14%	23%
8.	200	228.6	13%	226.6	12%	242.3	17%	17%	18%
9.	346	372.9	7%	370.6	7%	368.0	6%	6%	12%
10.	130	110.5	18%	114.8	13%	118.9	9%	9%	4%
11.	150	131.1	14%	133.1	13%	133.8	12%	12%	6%
12.	155	173.7	11%	164.3	6%	186.4	17%	17%	18%
13.	260	288.9	10%	254.8	2%	291.4	11%	11%	13%
14.	155	174.1	11%	166.6	7%	179.2	14%	14%	16%
15.	250	245.5	2%	244.5	2%	257.0	3%	3%	8%
16.	170	211.5	20%	187.0	9%	216.6	22%	22%	24%
17.	200	227.8	12%	200.5	0%	232.1	14%	14%	16%
18.	260	258.2	1%	225.9	15%	260.5	0%	0%	2%
19.	125	119.5	5%	111.3	12%	122.1	2%	2%	0%

From the results of average forces in Table 3.7**,** the average of forces from $F_{UB,1}$ & $F_{LB,1}$ and $F_{UB,4}$ & $F_{LB,1}$ show smaller errors compared to average model forces from $F_{UB,3}$ & $F_{UB,4}$ and $F_{UB,2}$ & $F_{LB,1}$. Average model forces from $F_{UB,4}$ & $F_{LB,1}$ have the smallest errors when compared to all other average model forces. The maximum force error is 17% and the minimum force error is 2%. Similar errors are observed for average forces of $F_{UB,4}$ & $F_{LB,1}$ with all errors under 23%. In both the cases, the average force values are still over the experimental peak force values. However, they vary by only small percentages and provide a more precise prediction of the maximum attainable device force value.

Table 3.7. Comparison of maximum achieved experimental device force to average analytical model forces and corresponding errors for HF2V devices.

Device	F_{exp} (kN)	$F_{UB,1}$ & $F_{LB,1}$		$F_{UB,2}$ & F_{LB}		$F_{UB,4}$ & $F_{LB,1}$		$F_{UB,3}$ & $F_{UB,4}$	
		F_{avg} (kN)	Error (%)	F_{avg} (kN)	Error (%)	F_{avg} (kN)	Error (%)	F_{avg} (kN)	Error (%)
5.	205	200.3	2%	223.4	12%	223.4	8%	227.3	10%
6.	305	343.4	11%	338.7	20%	338.7	10%	361.3	16%
7.	395	485.6	19%	451.7	25%	451.7	17%	503.6	26%
8.	210	228.6	8%	242.3	7%	242.3	13%	245.3	14%
9.	350	372.9	6%	368.0	6%	368.0	5%	391.5	12%
10.	130	110.5	18%	118.9	13%	118.9	9%	124.9	4%
11.	150	131.1	14%	133.8	13%	133.8	12%	141.2	6%
12.	155	173.7	11%	186.4	6%	186.4	17%	188.9	18%
13.	260	288.9	10%	291.4	2%	291.4	11%	298.4	13%
14.	155	174.1	11%	179.2	7%	179.2	14%	183.9	16%
15.	265	245.5	8%	257.0	8%	257.0	-3%	271.6	2%
16.	185	211.5	13%	216.6	1%	216.6	15%	223.2	17%
17.	200	227.8	12%	232.1	0%	232.1	14%	238.1	16%
18.	270	258.2	5%	260.5	20%	260.5	4%	266.3	1%
19.	125	119.5	5%	122.1	12%	122.1	2%	124.5	0%

Hence, for an approximation of HF2V force device, the average of forces from Models $F_{UB,1}$ & $F_{LB,1}$ or Models $F_{UB,3}$ & $F_{UB,4}$ may be chosen. As expected, the forces from the UB models are indicative of the maximum achievable force by a HF2V device for the given conditions/ assumptions.

3.4.4. Method 2: Linear equation from plots

As the UB models closely predict the maximum device forces, the maximum experimental forces from the devices are plotted against the models forces in Figure 3.7**,** where the horizontal axis represents UB or LB model forces and and the vertical axis represents experimental forces.

Each plot identifies an equation based on the trendline given in Figure 3.7**,** drawn for the plots and shows the correlation between the data. All four plots indicate very good R^2 values with $R^2 \geq 0.81$. The best $R^2 \geq 0.90$ values are observed for plots (b) and (d) in Figure 3.7. Thus, the equations relating experimental forces and model forces for $F_{UB,2}$ vs F_{exp} and $F_{UB,4}$ vs F_{exp} are considered for application of predicting approximate HF2V device forces. The forces calculated form the equation is given in Table 3.8**.**

The overall errors from both the equations are similar, except for Devices 15 and 19, which have and errors of -7% and 2% from the equation for $F_{UB,4}$ and -19% and 10% for the $F_{UB,2}$ equations, respectively. Both the models consider the wall friction effects and predict well above the experimmental force levels. Although equation from $F_{UB,4}$ equations predict more precisely than $F_{UB,2}$ equation, $F_{UB,2}$ model may be chosen for simplicity and ease of calculation.

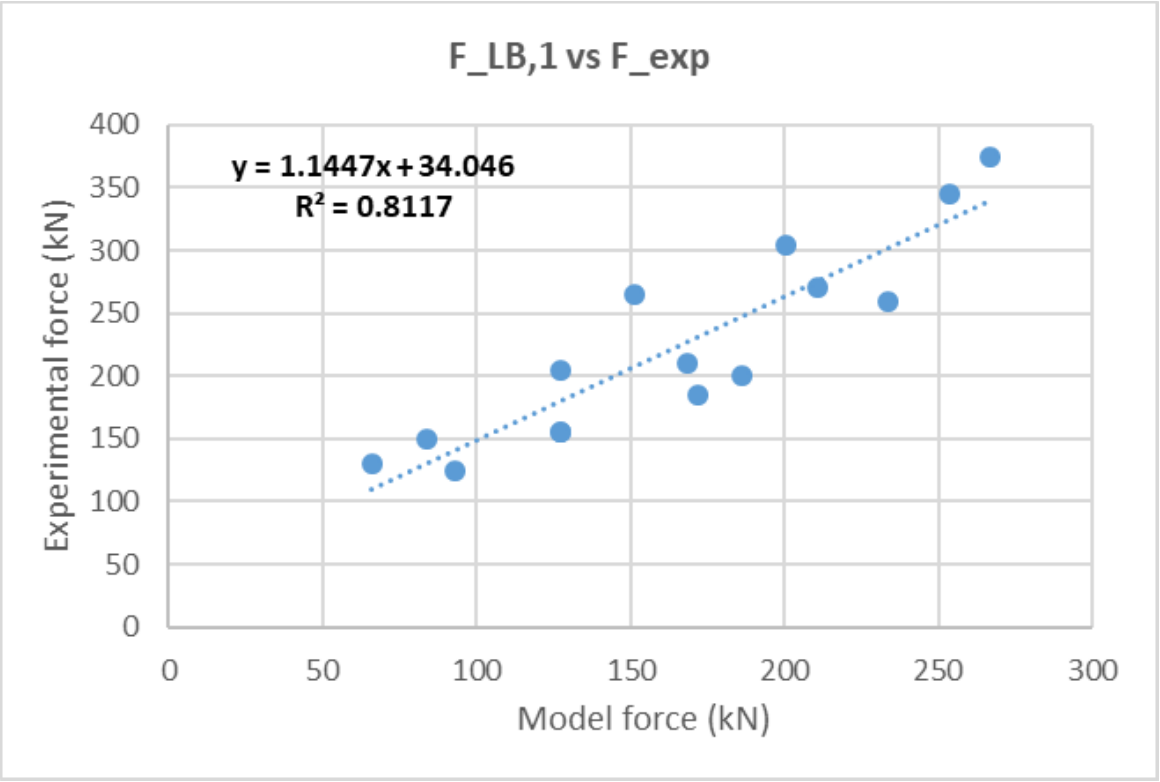

(a) Plot for $F_{LB,1}$ vs F_{exp}

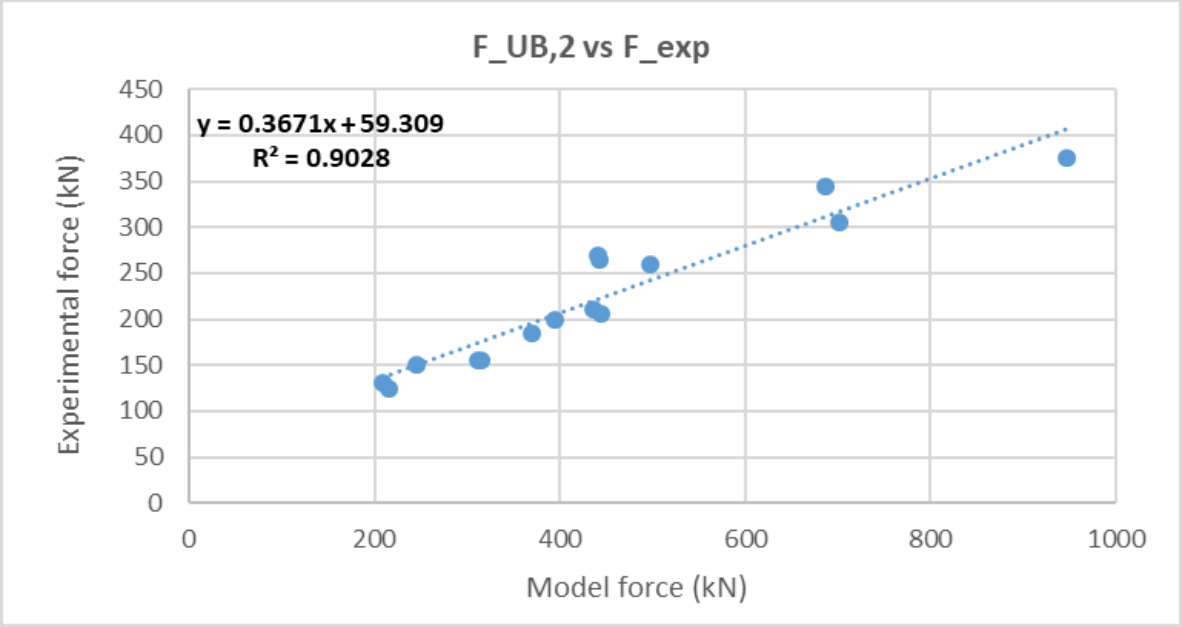

(b) Plot for $F_{UB,2}$ vs F_{exp}

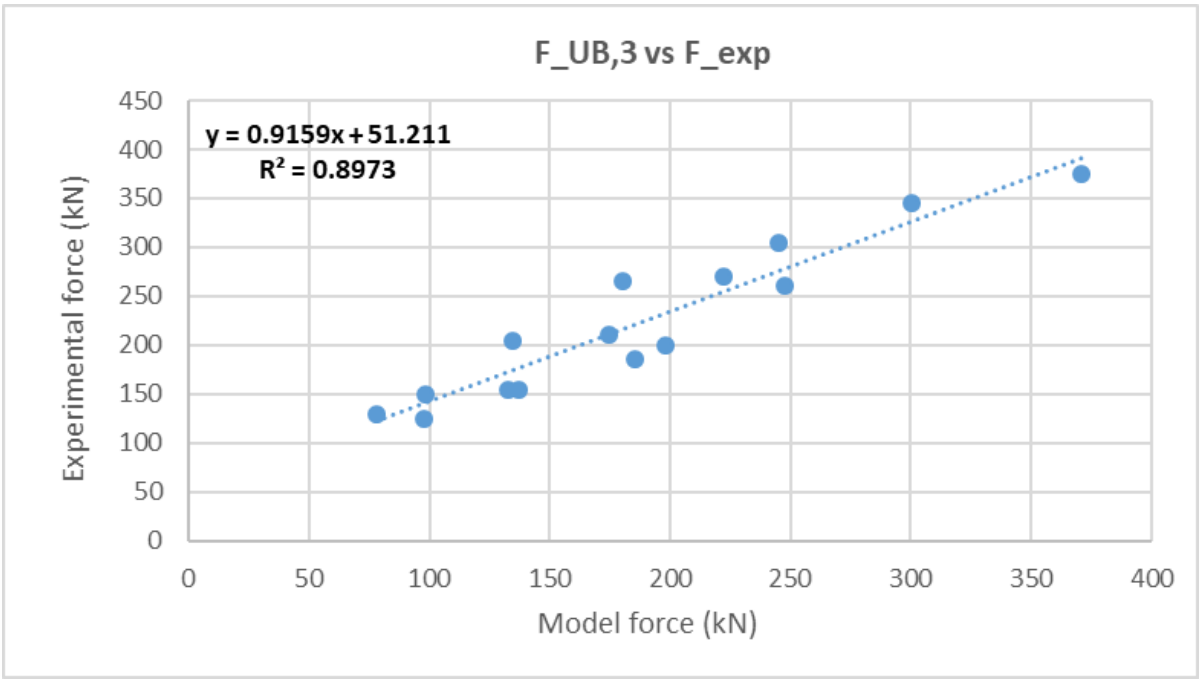

(c) Plot for $F_{UB,3}$ vs F_{exp}

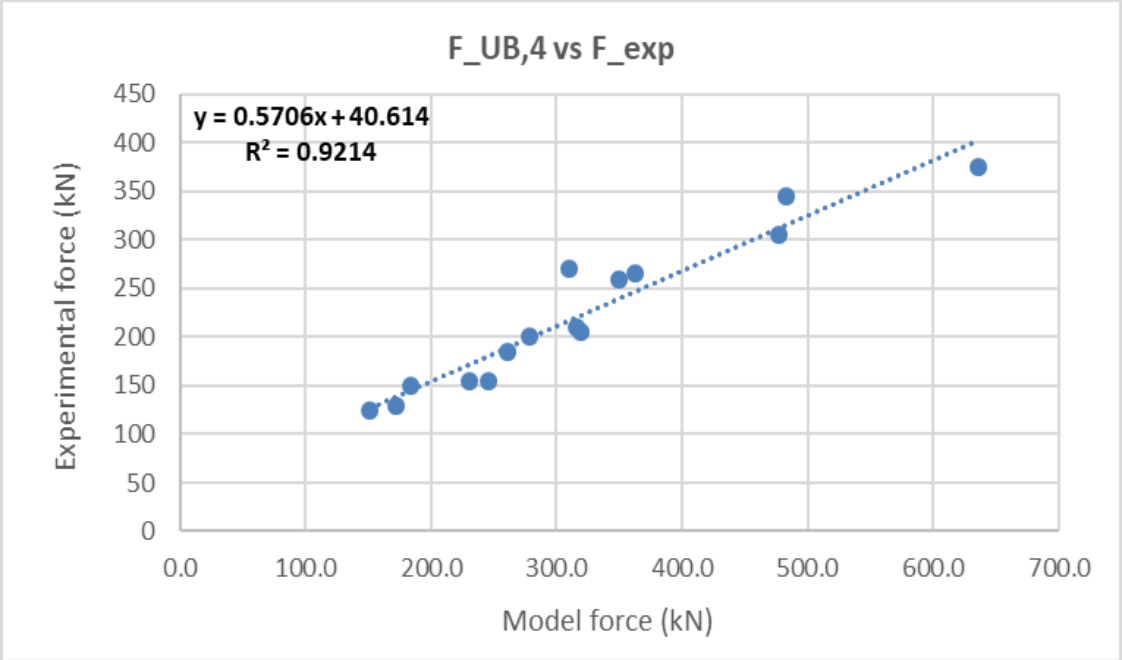

(d) Plot for $F_{UB,4}$ vs F_{exp}

Figure 3.7. Plots for UB and LB model forces vs $F_{exp.}$

Table 3.8. HF2V force approximation based on linear equations from plots.

Devices	F_{exp} (kN)	$F_{UB,2}$ vs F_{exp}		$F_{UB,4}$ vs F_{exp}	
		y = 0.37x + 59.31 (kN)	Error (%)	y = 0.57x + 40.61 (kN)	Error (%)
5.	205	223.4	8%	223.1	8%
6.	305	318.9	4%	312.8	3%
7.	395	409.7	3%	403.7	2%
8.	210	220.5	5%	220.9	5%
9.	350	313.2	-11%	316.0	-11%
10.	130	136.3	5%	138.8	6%
11.	150	149.8	0%	145.5	-3%
12.	155	174.2	11%	180.6	14%
13.	260	243.0	-7%	239.9	-8%
14.	155	175.9	12%	172.4	10%
15.	265	223.1	-19%	247.6	-7%
16.	185	195.6	5%	189.7	2%
17.	200	205.0	2%	199.4	0%
18.	270	222.5	-21%	217.6	-24%
19.	125	138.6	10%	127.0	2%

3.4.5. Method 3: Specific force from direct extrusion UB model ($F_{UB,1}$)

The UB model predictions using the direct extrusion model varied largely from the experimental force predictions, as seen in previous sections. The results obtained using the modified Equation (3-3) for HF2V devices are given in Table 3.9. In Figure 3.8, the model forces are compared to the average HF2V device forces recorded in Table 3.9 for comparison.

The modified direct extrusion based specific model predicts devices force errors ranging from -42% to +17% when compared to the average experimental forces of the devices. As seen in Figure 3.8, the force range of the specific $F_{UB,1}$ model lies very close to the experimental device forces when compared to the $F_{UB,1}$ force range seen in

Figure 3.5(a) and (d).

Table 3.9. Comparison of precise force from $F_{UB,1}$ and average F_{exp}

Devices	$F_{UB,1\_precise}$ (kN)	$F_{exp\_average}$ (kN)	Error
5.	153.6	140	10%
6.	263.6	250	5%
7.	374.5	320	17%
8.	173.4	175	-1%
9.	281.5	310	-9%
10.	75.8	130	-42%
11.	97.5	150	-35%
12.	122.8	155	-21%
13.	236.5	260	-9%
14.	130.6	155	-16%
15.	172.2	250	-31%
16.	176.8	145	22%
17.	188.8	165	14%
18.	211.3	185	14%
19.	94.0	125	-25%

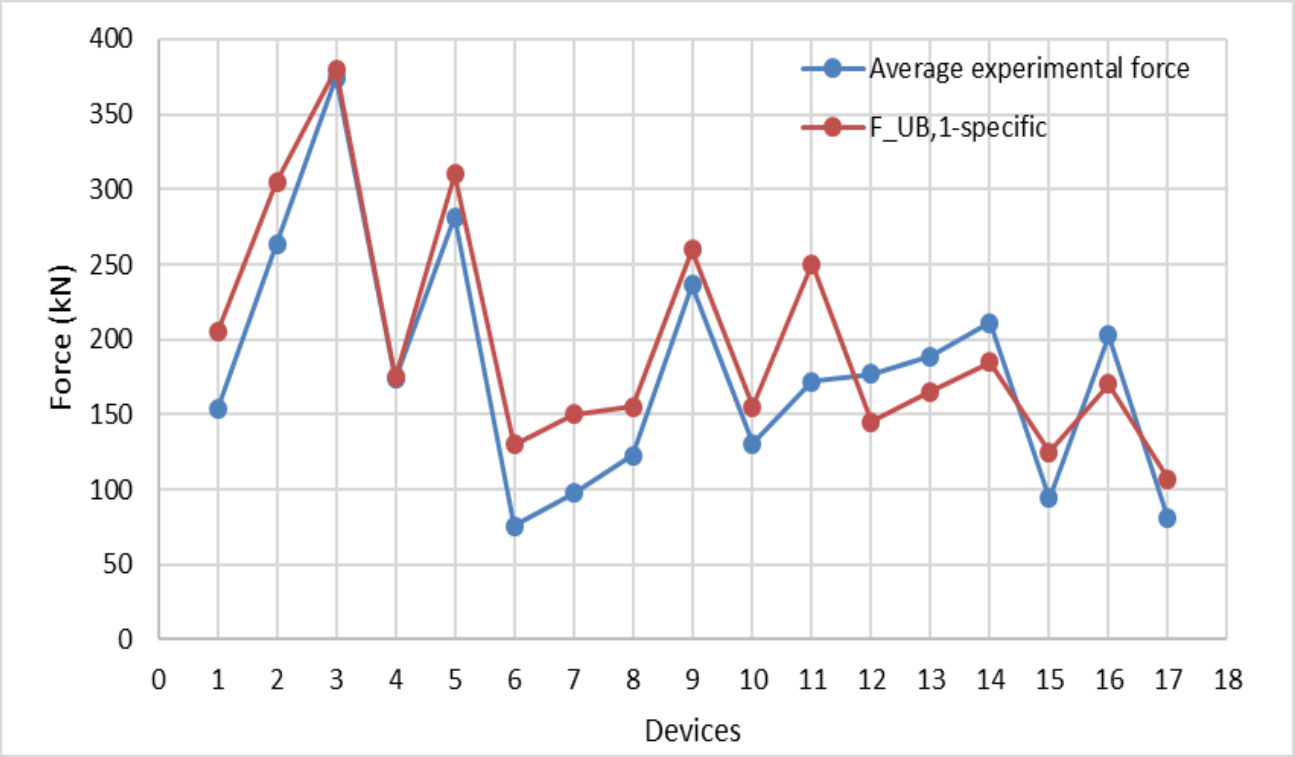

Figure 3.8. Comparison of model ($F_{UB,1\_specific}$) outcome to experimental device forces.

3.5. UB Model Improvement

From **Figure 3.5**, similar trends in plots are observed for UB forces from direct and indirect extrusion. The UB ($F_{UB,\,1,2,4}$) estimates are largest with biggest variation from the experimental forces for Devices 6, 7 and 9 that have the largest bulge and cylinder sizes in comparison to other devices considered in this analysis. Devices 6, 7 and 9 have large bulge diameters. Therefore, they shear larger areas of lead and consequently producing more heat.

During repeated cycles, heat is produced in the HF2V devices [148, 155]. The yield stress values for the same reduction percentages vary with temperature [230] and the lead extrusion pressure has been observed to decrease with increase in temperature [148, 161, 207]. However,

there is no record of the testing temperatures during the experimental HF2V tests or the heat produced during these device experiments, as none were measured. Measuring true lead temperature inside the HF2V device would be a challenge as a thermocouple placed against the cylinder wall during tests will measure the temperature of the cylinder wall, not the actual temperature of lead. Despite good thermal conductivity through lead and steel, a temperature gradient will exist and mean that an external thermocouple is likely to provide an inaccurate indication of internal lead temperature.

However, as explained, the model does not account for the thermal effects due to high amount of shearing occurring in the larger devices that may cause decrease in flow stress and friction factor [161, 218, 242-244]. The modelling of friction forces is of measurable importance, as they play a major role in producing the overall extrusion forces. Friction forces during an extrusion process are influenced by flow stress, area of contact, relative velocity, temperature and material properties [218, 243, 245]. The friction coefficient varies with area of contact, velocity and increasing load [208, 224, 245, 246]. In this study, because of the simplified assumptions made for mathematical reasons and lack of data, friction force modelling cannot be considered fully accurate. For greater accuracy, empirical models or advanced friction models based on dependent parameters [218, 244, 247, 248] or extrusion specific friction models may be used [222, 227, 243, 249-251], but add more complexity for bounds which already work well. In addition, theoretical values from Equations (3-11) and (3-13) show the average flow stress values increase with increasing strain [87, 215, 252]. However, it is experimentally observed the flow stress and yield strength may remain constant or decrease after 40-50% strain of lead [87, 230, 236]. Thus, there is also uncertainty on the exact level of need for such modification to the model.

Another phenomenon associated with strain and temperature is softening, causing a decrease in stress with increasing strain or loading due to adiabatic heating of working material [87, 253]. While strain hardening effects causing increase in forces during lead deformation is captured by the Holloman Equation (3-22) for flow stress, the strain softening parameters are excluded. Thus, the over prediction of forces for Devices 6, 7 and 9 by UB models ($F_{UB,\,1,2,4}$) can be explained by negligence of strain and temperature related parameters.

Thus, it is advisable to consider the strain related effects and strain softening in lead occurring during the HF2V extrusion for UB and LB force estimations [186]. More accurate flow stress estimations could be obtained from equations capturing softening effects [213, 229, 242, 254-256] or from reliable data from experimental tests on lead properties under various strain and temperatures [230, 236, 257] under all forms of deformation. In addition, the HF2V UB forces could thus be better estimated with knowledge of strain rates, velocity and temperature and heating effects during HF2V operations.

3.6. Summary

This chapter has presented upper bound (UB) and lower bound (LB) limit force modelling methods by relating direct and indirect extrusion parameters to HF2V lead extrusion devices. Four analytical UB models and two LB models were proposed by modifying existing direct extrusion and indirect extrusion force models to match the mechanisms in HF2V devices. The models predicted forces well with all the models predicting UB forces above the experimental forces, except $F_{UB,3}$. UB and LB model forces provide limits of operational range of HF2V devices based on devices design parameters and deformation of lead in the devices. The $F_{UB,2}$ and $F_{LB,1}$ create tight bounds along the experimental forces. Furthermore, three methodologies

to obtain precise forces for the HF2V devices were suggested for easy application during device design of which Method 2 : Linear equation from plots, provides precise Hf2V device forces. The UB- LB models predict very well for *Typical* and *Large* devices and need to be tested and refined for *Small* devices.

Chapter 4: Nonlinear finite element modelling for HF2V device force prediction: A Computational Model

4.1. Introduction

Chapters 2 and 3 presented empirical and analytical modelling methods more precisely predict HF2V device forces by design. While the single number representing the nominal yield force is predicted, the knowledge of the exact internal mechanisms resulting in these device forces is lacking, limiting insight and predictive accuracy in device design. Finite element modelling would allow visualization of stress distributions inside the devices and provide a method of computationally determining HF2V device forces, which could be more accurate at relatively low added cost. This method is also capable of producing a full hysteresis loop, rather than just a single number that represents the yield plateau force.

This study develops a generic finite element modelling approach using ABAQUS, to better understand force generation and aid in precision device design. The goal is to create a tool to increase the speed of the overall design and implementation process for uptake and use. A general approach without any human tuning or oversight enables a transferrable design approach, removing any subjectivity or bias that can hinder repeatable use and uptake. The model is applied to 19 experimental HF2V devices of various sizes and force capacities. The overall predictability of the model is assessed with comparison to experimental results.

4.2. Methods

4.2.1. Finite element modelling

Finite element (FE) analysis is an effective method for simulating complex nonlinear mechanics of device operations and computing resulting force capacities [258, 259]. There are numerous FE software packages available for simulating metal forming, such as MARC [260], LS-DYNA [261], PAM-STAMP [260], ADINA [262], ANSYS [263], along with specialist tools like DEFORM [264], HyperXtrude [265], MSC/SuperForge [266] and FORGE [267] . However, ABAQUS is popular for simulating complex contact problems with large deformation, as well as similar highly nonlinear problems [268] like cutting, machining and extrusion [269-274]. ABAQUS is also widely used to estimate forces produced during cutting, machining, milling, forming and extrusion [259, 275-280]. It is highly efficient in simulating quasi-static, complex contact, non-linear and dynamic problems [280]. Using device-specific material properties and the design dimensions of a device, it can be expected to realistically simulate HF2V internal lead deformation mechanics within a device, and thus estimate device capacity in the device and building design phases.

Thus, computer simulations could be used to predict device forces to optimize HF2V device design and performance, which has not been done before. Furthermore, such parametric design studies can be undertaken on broader range of devices without the time and cost involved with experimentally testing every configuration. This goal thus adds precision to the device design process itself, where a detailed device design can be produced to match desired overall response behaviour.

HF2V device operation involves large strain inelastic deformations due to displacement of the shaft during an earthquake. Large deformation analysis is challenging and requires advanced FE coding or use of other FE packages to describe material behaviour models and parameters. This study aims to create a generalizable and repeatable FE modelling technique for the HF2V devices which does not require advanced FEA or input to apply the model. This approach thus enables easy uptake by engineers or researchers.

This research uses ABAQUS to model and validate a general modelling nonlinear FE approach to predict HF2V device forces, where a validated general approach allows any user to apply it with confidence and without specialized operator inputs to the modelling, eliminating error due to subjectivity or bias.

4.2.2. FE model description

4.2.2.1. Modelling

A 2D axisymmetric model of an HF2V device is created using ABAQUS/CAE [281], where the lead extrusion damper is symmetric along the vertical (Y) axis. The model is comprised of three parts: 1) an analytical rigid shaft; 2) an analytical rigid wall; and 3) a deformable volume of lead. These elements are illustrated in Figure 4.1**.**

A 2D model leveraging axial symmetry ensures faster computation than using a full 3D model. The parts are modelled to experimental device dimensions, based upon the CAD models used to manufacture the physical prototypes. The shaft and cylinder are non-deforming and modelled as analytical rigid parts. Analytically rigid surfaces provide better convergence for

curved line segments in complex contact problems [282, 283] and are computationally less expensive than analysis with discrete rigid parts [283, 284].

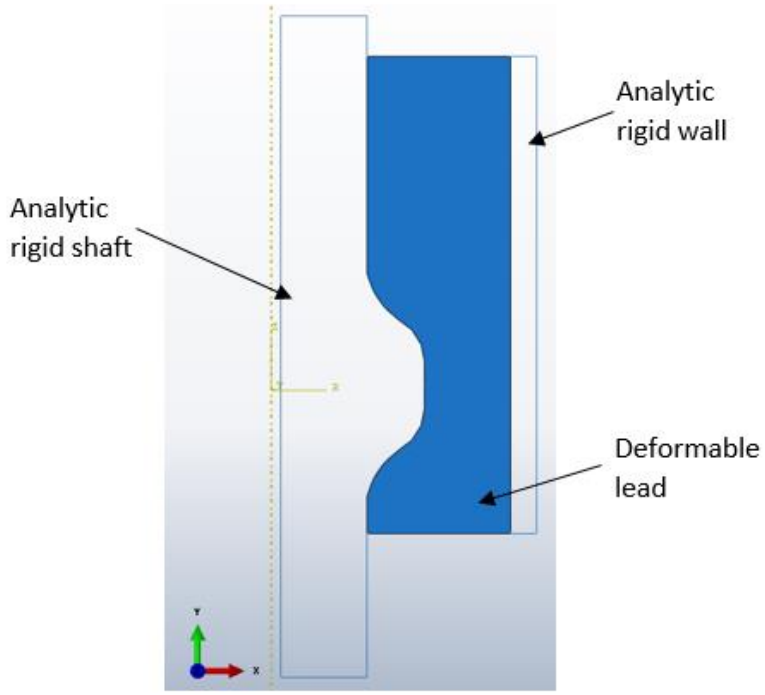

Figure 4.1. Axisymmetric 2D model of HF2V damper

4.2.2.2. Material properties

Material properties are assigned only to the lead, as the endcaps and thick cylinder walls are effectively rigid to ensure all energy is dissipated by moving lead, as with real devices [127]. The material properties of pure lead used are recorded in Table 4.1. The mechanical properties of lead are very sensitive to temperature, chemical composition, strain rate and loading conditions, among other factors [237, 285-287]. From previous research, the plastic data for pure lead during compression at quasi-static velocities are those shown in Table 4.2. [230, 285], where the experimental tests were also performed at very slow, quasi-static velocities similar

to the experimental data used in this work. Use of experimental data for analysis accounts for strain hardening and temperature effects.

Table 4.1. Elastic properties of lead used for modelling [288]

Density (kg/m^3)	Young's Modulus (GPa)	Poisson's Ratio
11,340	16	0.44

Table 4.2. Plastic data of lead used for models [285]

Plastic Strain	Yield Stress (Pa)
0	689,476
0.01	5,810,000
0.02	89,63,184
0.04	1,24,00,000
0.08	15,100,000
0.12	17,000,000
0.16	18,000,000
0.2	19,000,000
0.24	21,000,000
0.28	22,000,000
0.32	22,750,000
0.36	22,854,426

4.2.2.3. Loads and Boundary Conditions

The boundary conditions on analytical rigid parts in ABAQUS can be applied only at reference points. Hence, reference points are attached at the shaft (RP-1) and wall (RP-2). The shaft is fixed for rotation (UR1, UR2, UR3), and displacement along X (U1) and Z (U3) directions.

Then, a fixed condition is applied at RP-2 on the wall allowing zero degrees of freedom. The lead ends are fixed for any displacements to signify the endcaps. The assembly of parts and the boundary conditions applied are shown in Figure 4.2.

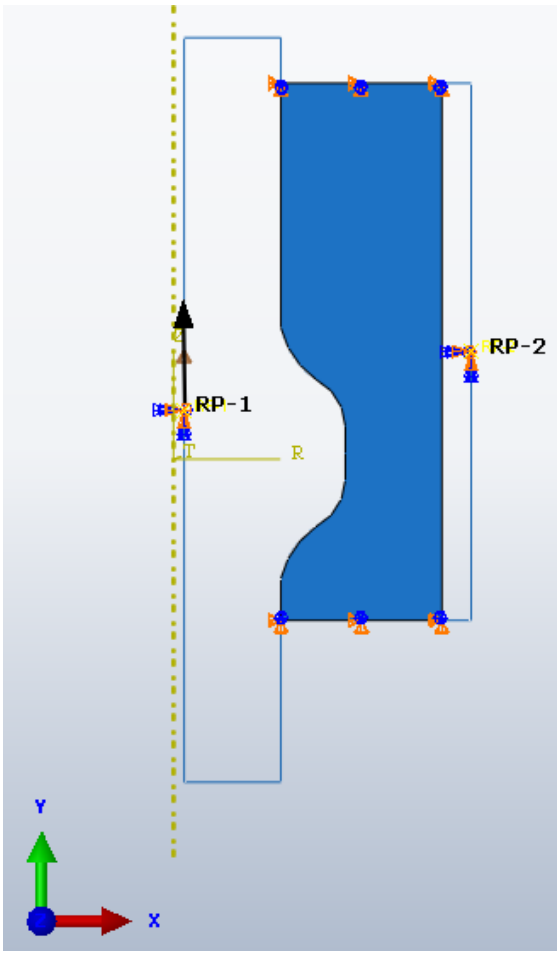

Figure 4.2. Boundary conditions applied on HF2V model

For quasi-static simulations, a velocity of 0.5 mm/s is applied to the reference node attached to the rigid shaft. This input velocity matches the typical loading rate applied during experimental tests. The shaft has degrees of freedom only in the longitudinal (Y) direction, as shown in Figure 4.2. It thus pushes the bulged shaft through the working material.

4.2.2.4. Interaction

Contact simulations calculate contact pressures and related friction forces at the area of contact [280]. Shear forces are created between the lead working material and shaft surfaces during tangential motion. ABAQUS employs several friction models to estimate friction forces at contact surfaces such as coulomb, rough and user defined subroutines [289-293]. Two types of formulations are available in ABAQUS to define contact between parts under Coulomb friction law: penalty and kinematic formulations [281]. The Coulomb friction law assumes shear stresses are proportional to contact pressures [294].

A penalty or kinematic algorithm may be chosen for computing shear forces produced at the lead-shaft and lead-wall interface. A kinematic algorithm provides more accurate results [280] and avoids large fluctuations, which may be observed in the resulting plots [272]. For a surface-to-surface contact between the lead surface and the shaft, 'master-slave' formulations are defined for the interactions between the rigid shaft and the lead, and between the rigid wall and lead. A default master-slave interaction is applied for shat-lead and wall- lead interactions. The analytically rigid parts are assigned as 'master' as they cannot be deformed or penetrated [281, 295].

The friction coefficient (μ) is the ratio between the friction force and normal force. The static friction coefficient between the lead and steel surface is given as 0.5 without lubrication [296]. The transition from a static friction coefficient to lower values at quasi-static velocities is measured as 0.3 for pure lead [208]. Taking into account the pre-stressing of lead and the resulting increase in normal forces, the decreased coefficient of friction is taken as 0.25, with no lubrication [207, 297, 298].

4.2.2.5. Meshing

A ‘free’ axisymmetric quad dominated CAX4R reduced integration 4 node quadrilateral and CAX3 linear triangular node mesh is applied on the lead working material in ABAQUS/Explicit. The mesh is shown in Figure 4.3. This mesh type is automatically chosen for an axisymmetric explicit analysis. No element deletion is chosen in the mesh controls to avoid mesh deletion.

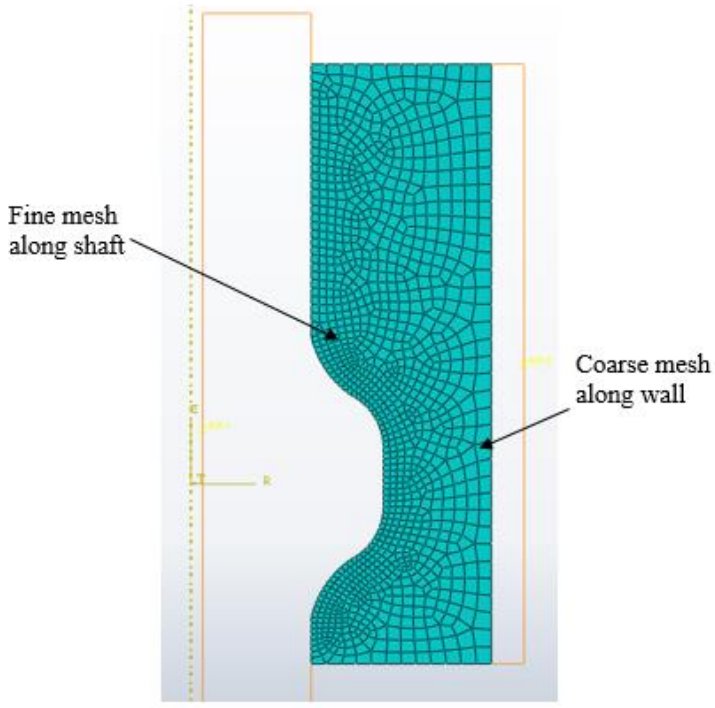

Figure 4.3. Mesh applied on deformable lead part.

A fine mesh is applied on lead along the shaft, where large deformations are expected, for higher accuracy in force outputs, and a coarse mesh is used along the walls. Though computationally expensive, this choice assures no severe mesh distortion which might cause analysis failure. The overall mesh is verified for good quality and modified if required. No meshing is required for analytic rigid as they do not undergo any deformations [281]. This choice saves computational cost and problems from mesh interactions.

4.2.2.6. Moving Mesh

HF2V devices continuously generate a relatively constant force while moving by virtue of the fact lead recrystallizes quickly at room temperature. A great deal of research has focused on simulating this unique property of lead to retain its original mechanical properties by dynamic recovery [299-301]. The forces developed in the HF2V devices can accurately be computed only if the model can replicate the flow and interaction of lead with the shaft behind the bulge. This behaviour of lead in the device is difficult to simulate due to severe mesh distortions during plastic deformations occurring during extrusion.

The Arbitrary Lagrangian–Eulerian (ALE) method, combining the Lagrangian and Eulerian formulations traditionally used for finite element simulations, is applied on the lead region [302-304]. It is an efficient formulation used in highly non-linear, quasi-static, large deformation and contact problems [305-309]. An unstructured/free mesh is applied to the lead surface to allow better remeshing of elements under deformation [310]. The ALE finite element method is used to simulate large deformation problems, allowing a moving mesh along the moving part without distortion [311-314]. The motion of the mesh is only constrained at the boundaries, and is allowed to move under high strain within these fixed boundaries. This re-meshing allows the simulation of lead flow within the cylinder and around the shaft, providing visual guide to the evolution of stress distributions with changing strain/strain rates in the devices, as the shaft moves and dissipative device forces are generated.

In the ALE adaptive mesh domain, the value for the frequency of mesh updates and number of iterations per each adaptive mesh increment, referred to as remeshing sweep per increment, are chosen as 10 and 1, respectively, as a best trade off [314, 315]. The nodal positions are

remapped based on the defined value of frequency of mesh for each time step [259]. An ‘improved aspect ratio’ is chosen for the mesh controls where the smoothing algorithm is based on ‘enhanced algorithm based on evolving geometry [281]. The meshing prediction is obtained based on position from the previous ALE adaptive mesh increment. However, there are trade-offs with this choice, device test velocity, and device capacity or lead strain.

4.2.2.7. Steps

The analysis is run using ABAQUS/Explicit, in multiple small step times of 1 second with automatic increments, to balance higher accuracy and computational time. In explicit analysis, with large strain and inelastic deformation, it is important to keep step times small to maintain equilibrium and simulation accuracy [316-318].

4.2.2.8. Output

The force-time response is obtained from the history output of the contact pressure forces including the normal and friction forces on the lead along the shaft. The contact pressure and frictional shear at the lead-shaft interface integrated over the lead area of contact to the shaft are resolved to give the total forces generated at the interface [281, 295]. These values are used to calculate the resistive force on the shaft as it moves through the lead, and thus the device force. Analytical methods are available for calculating contact pressure forces and friction forces [319]. The overall result is a force-displacement profile, representing the force-deflection results for a single monotonic displacement input

A short moving average filter is used to eliminate small computational errors and computational noise which arise due to remeshing each time step. Hence, a filter with exponential moving average, using smooth2 function in ABAQUS is applied. This filter does not alter results, but eliminates small computational errors and noise due to remeshing during each time step.

4.2.3. Device information

The data for 19 experimental devices used in this study is recorded in Table 4.3.

Table 4.3. Device data used for modelling and analysis. Device design parameters are defined and illustrated in Chapters 2-3.

DeviceNo.	D_{cyl} (mm)	D_{blg} (mm)	D_{shaft} (mm)	L_{cyl} (mm)	L_{blg} (mm)	$L_{blg\ flat}$ (mm)
3	17	13	12	56	10	3
4	20	17	16	68	20	6
5	89	40	30	110	30	5
6	89	50	30	110	30	5
7	89	58	30	110	30	5
8	66	40	30	130	30	6
9	66	50	30	130	30	5
10	50	32	20	50	23	5
11	50	32	20	70	20	2
13	60	42	33	160	30	3
14	50	35	24	100	23	5
15	70	48	30	75	30	5
16	54	35	30	160	20	3
17	54	36	30	160	20	3
18	54	38	30	160	20	3
19	40	27	20	100	17	3
20	62	45	30	155	23	5
21	40	32	20	47	15	0.5
22	89	62.5	36	250	35	3.5

.In Table 4.3., a total of 3 *Small*, 12 *Typical* and 4 *Large* devices are modelled in this study. Device 22 included in this study is a very large device with large surface and force of ~500kN. The HF2V device design parameters are previously illustrated in Chapters 2 and 3.

4.2.4. Analysis

The model approach is applied the same way to all devices without any changes, a generalized easily repeatable modelling approach. The use of device-specific geometry is the only variation between the analyses. Results are analysed for accuracy in prediction of experimental peak device forces, and their capacity to replicate the experimental hysteretic force-displacement behaviour of the given HF2V dampers. Specifically:

a) Qualitative Validation:

The model's capacity to accurately simulate the lead flow in the device is assessed as a qualitative assessment based on expected behaviour. An ideal model should be able to simulate the lead flow around the bulge with the shaft displacement in the HF2V damper in accordance with existing research and provide a visual representation of stress distribution inside the devices. Capturing stresses from the flow of lead behind the bulge is a challenge and is difficult to model without the knowledge of actual lead area of contact to the shaft at all stages of operation. FEM is expected to accurately simulate this behaviour of lead for precise force determination for the HF2V device.

b) Quantitative Validation:

Contact forces (tangential and normal) can be contoured for slave surfaces in contact modelling using analytic rigid shafts. Plots are automatically generated in ABAQUS for the force produced during simulations with each time steps [281]. The hysteretic force-displacement plots of the devices obtained from previous experiments are compared to simulated plots for each device. The FEM plots are expected to be similar to the experimental plots from the corresponding device. However, strain hardening or softening effect is not expected in the FEM plots as no strain hardening or softening parameters were included in the material properties of lead in the FE modelling method presented.

In addition, the force capacity of the device is determined by summing the contact pressure forces (extrusion forces) and frictional forces output by the model. The resulting device force is compared to average peak forces from specific HF2V devices. This comparison is made relative to +/-14% standard error seen in testing 96 HF2V devices of 250kN force capacity, which is thus used as manufacturing variability to assess the results in context [149].

4.3. Results and Discussion

4.3.1. HF2V Simulations and Qualitative Validation

(a) During simulations, the shaft is displaced upwards in small steps of 1s. The flow of lead in a device is shown in

Figure 4.4. A swept mesh is shown in the figures for ease of visualization of node reattachment to the shaft with bulge displacement. The colours in the images indicate maxima or minima of stresses in the devices with displacement of shaft from initial position. The red colour on the spectrum indicates the highest stresses and blue represents the lowest stresses.

(b) In the first steps, the lead is strained under compression by the bulge, causing a rise of stress on the top surface of the bulge and along the shaft above the bulge. As the shaft moves further through the lead, the mesh is observed to move opposite to the direction of shaft. The mesh/nodes move around the shaft and attach to the shaft behind the bulge as the shaft moves further up through the lead. As seen in

(c) **Figure 4.4**., the stresses developed in the devices are due to lead displacement by the bulged shaft. In the first image in

Figure 4.4(a), small displacement of the bulged shaft develops stresses on the upper ends of the shaft. This behaviour could be due to stresses developed from compression of lead in the direction of shaft motion. With increased displacement, higher stresses are observed at the upper fixed ends, which signify the endcaps.

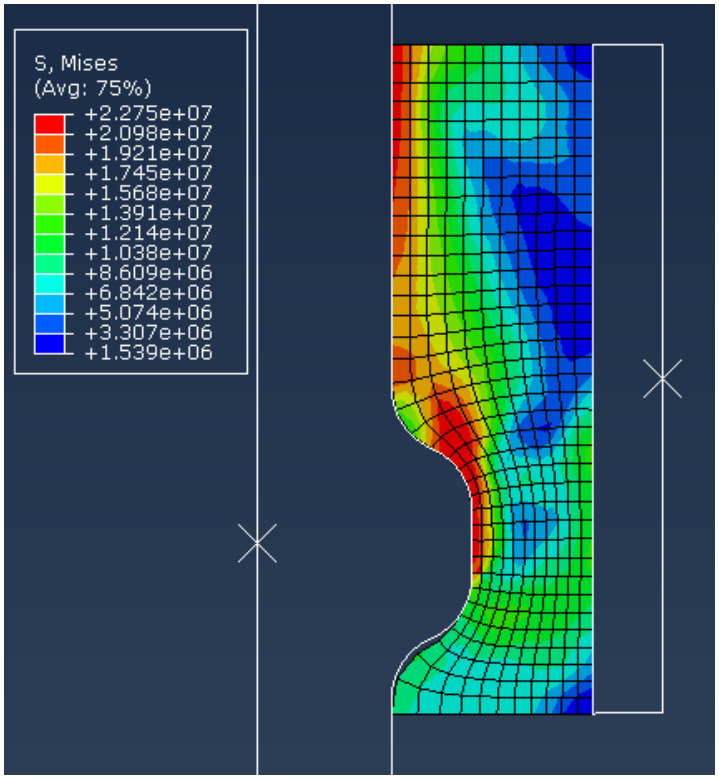

(d) At 0.5 mm displacement of shaft

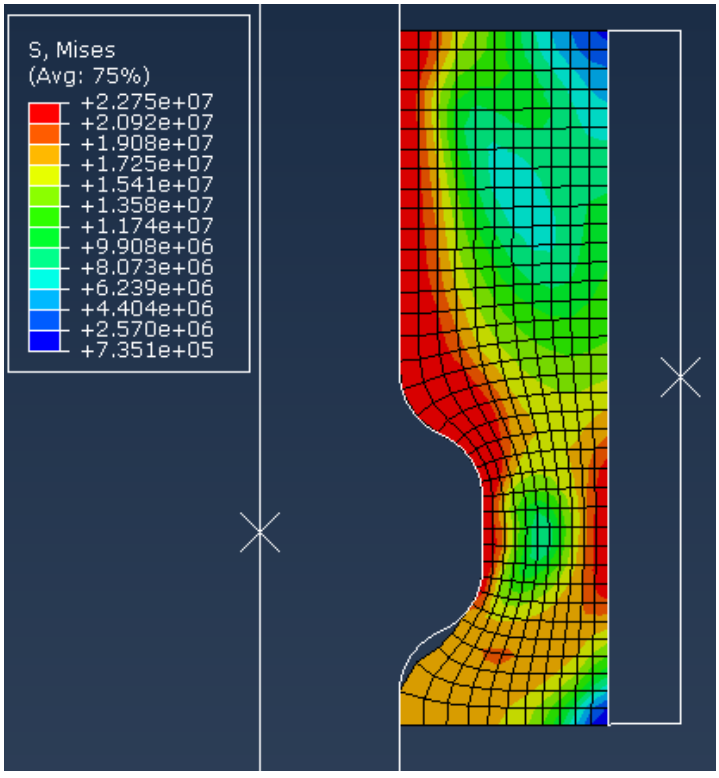

(e) At 1 mm displacement of shaft

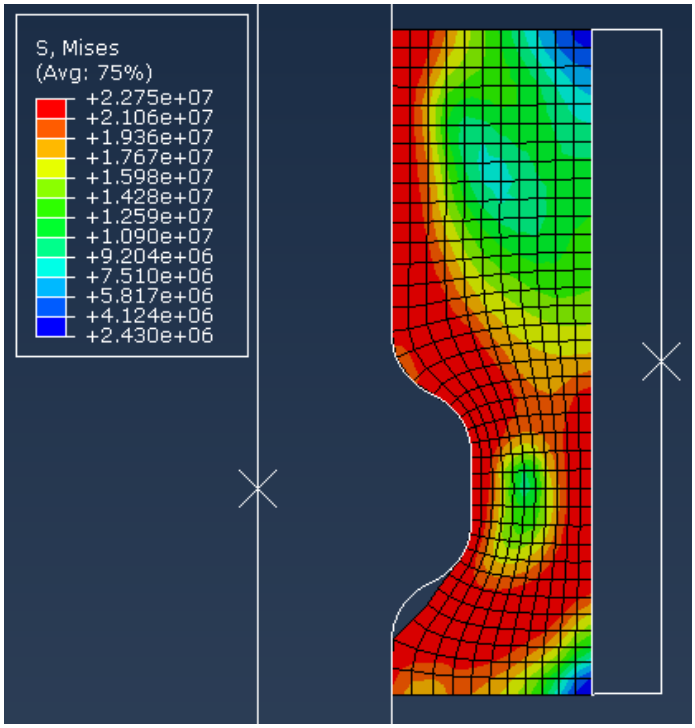

(f) At 2mm displacement of shaft

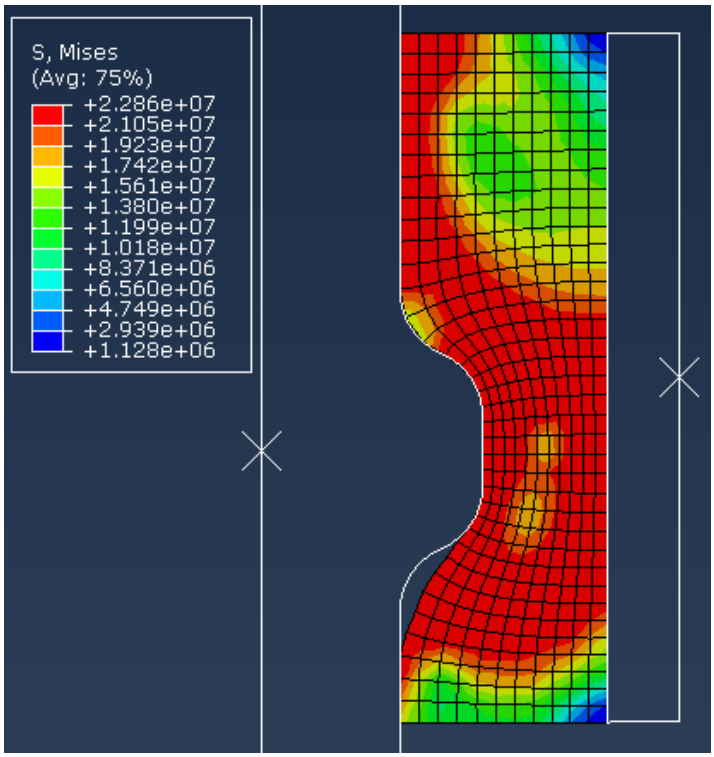

(g) At 4mm displacement of shaft

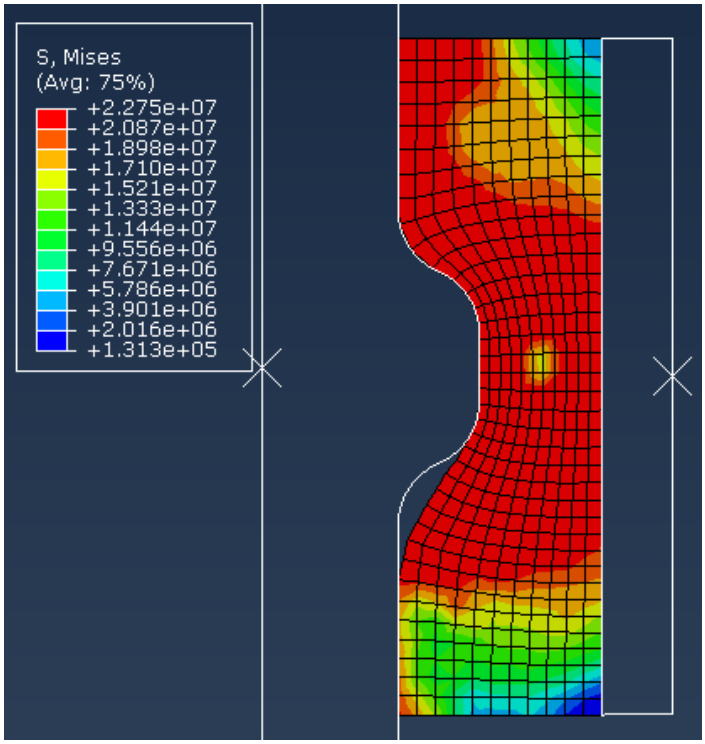

(h) At 7mm displacement of lead

Figure 4.4. Stress distribution in lead with shaft displacement (upwards) at the input displacements noted for Device 10.

(i) The elements move opposite to the direction of shaft motion and reattach to the shaft behind the bulge, as desired and as seen in

Figure 4.4. (c)-(e). This result captures the expected shearing and displacement of lead by the bulge, and the flow of lead around the bulge onto the shaft. Stresses build behind the shaft as more lead is pushed behind the bulge through the annular orifice between the bulge and the wall. As expected, maximum stress is observed around the bulge during all stages of HF2V operations. The maximum stress areas move along with the bulge.

The simulations replicate the expected actual behaviour of lead in the lead extrusion damper under loading. With no element deletion, the mesh is not distorted to failure and the number of elements before and after the analysis is the same. Thus, the overall qualitative validation matched expected

plastic flow mechanics, and, similarly, was good for this device and all others simulated (not shown). The overall modelling approach thus appears credible with no specific means to measure internal stresses in the HF2V devices from experiments for direct qualitative comparison.

4.3.2. Force Deflection Plot comparisons: Quantitative Validation

Force - displacement hysteresis plots are made for each device with eight shown in Figure 4.5. The experimental plots are compared to the plots from FEM results. The FEM plots for Devices 6 and 19 show a very good match with the experimental plots with overall similarity in the plot shapes and average forces achieved.

The plots for Devices 7 and 18 show an experimental plot similar to the FEM plots, but the peak forces do not closely match. In this case, the cause is less certain, but likely due to relatively small differences between real and assumed material properties. In addition, the potential friction force coming from shaft to endcap friction is not captured in the FEM model.

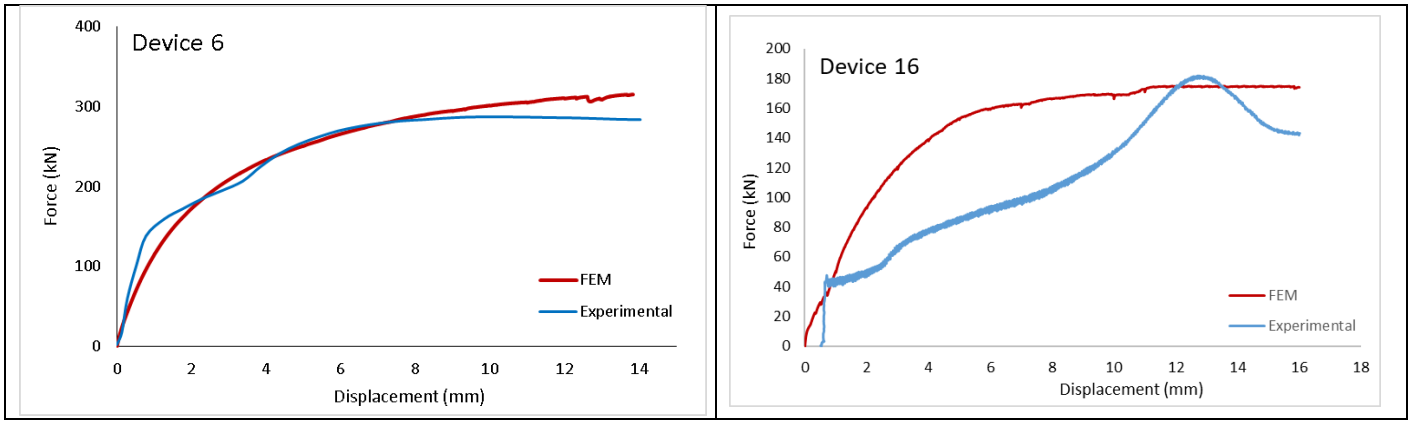

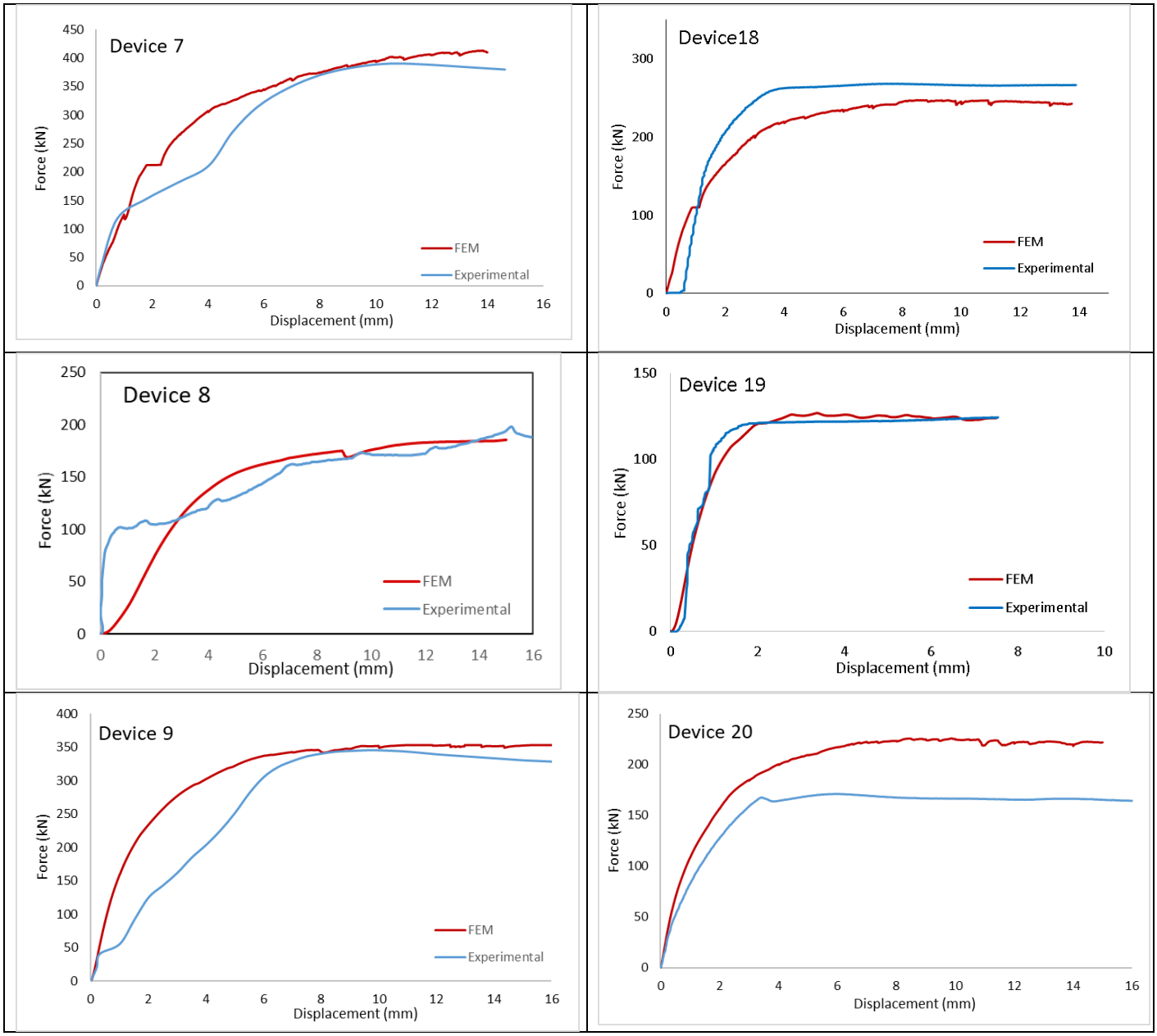

Figure 4.5. Comparisons of plots between experimental results and finite element models for few HF2V devices**.**

The overall peak forces from the experimental and FEM plots for Devices 8, 9 and 16 are close. The FEM plots for these devices are similar to FEM plots from other devices in Figure 4.5. However, they do not match well with their respective experimental plots. The experimental plots for Devices 8, 9 and 16 show a delay in achieving peak forces due to lack of prestressing forces for the devices. As discussed in Chapter 1, inadequate prestressing can cause a delay in attaining peak experimental forces. This problem is specific to experimental tests results only as FE models assume perfectly filled lead dampers. This mismatch is therefore attributed to experimental errors rather than modelling issues. In the case of Device 20, a square shaped plot is obtained from experimental and FE modelling results. However, the overall forces vary largely. These results thus show a full range of model prediction quality.

(j) Oscillations or fluctuations in result plots is a common problem in simulations involving master-slave interactions and penalty friction formulations at interface [272, 320]. The FEM plots for Device 17 is shown in Figure 4.6., resulting from various modelling choices**.** The computational noise observed in Figure 4.6**.** (a) is as a result of penalty friction formulation at interface along with a swept mesh (shown in

Figure 4.4.) for the lead surface. This computational noise in the plots for time based force output plots can be reduced by improved modelling choices, such as using a kinematic friction formulation, which produces less chatter due to its friction force computation methods.

(a) Penalty friction + Swept mesh	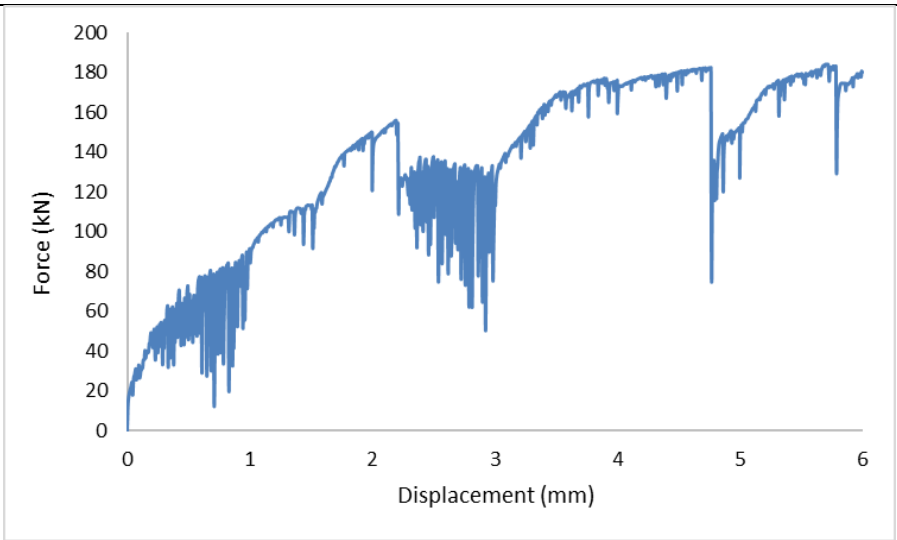
(b) Kinematic friction + Fine mesh along shaft + No filter on results	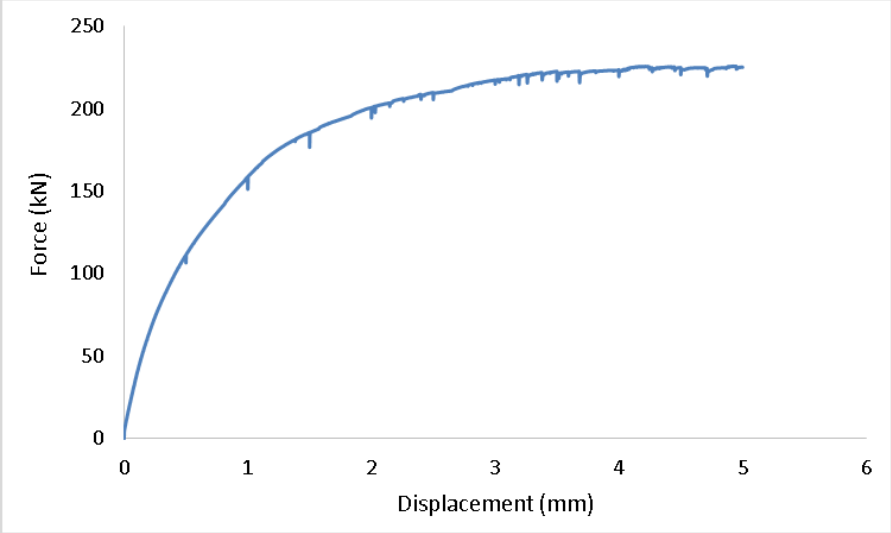
(c) Kinematic friction + Fine mesh along shaft + Filter on results	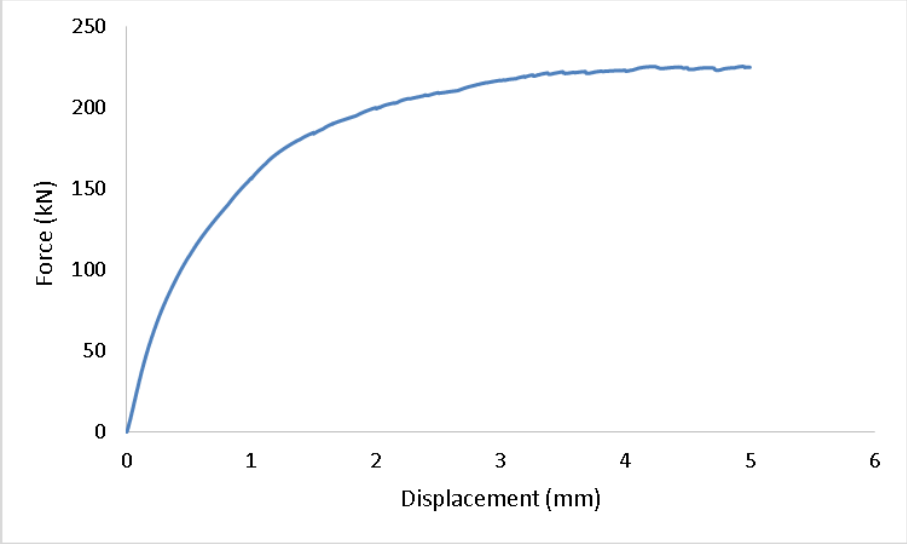

Figure 4.6. Plots of the FEM results for Device 17 for different modelling choices

The very small ‘noise’ at regular inetrvals in the FEM plots are due to the stiction or stick- slip mechanism of lead at the cylinder walls or due to “snagging” along the analytical rigid shaft surfaces [281]. Spikes observed at the end of each time step signifying the end of computation in Figure 4.6 (b). However, with each progressing step, the computation begins where the time step ended. This issue can be resolved by adding filters to the history output after identifying the correct cut off frequencies required for the analysis, such that the peak forces are not modified. Smooth2(X,Y) filter is applied on the total force output at the shaft-lead interface. The modified plot with the filter are shown in Figure 4.6 (c) to illustrate the small computational noise and impact of filtering.

4.3.3. FEM: Force prediction: Quantitative Validation

The force prediction results from the FE model and experimental data are in Table 4.4. The total device forces are calculated by summing the contact pressure forces and friction forces formed during interaction between the rigid shaft and deformable lead. For context, the standard error (SE) of manufacturing for HF2V devices is based on other unrelated experimental data for 64 identical devices [149].

The forces obtained from the FEM have forces within ±10% for 14 of 19 devices (74%), which is within ± 1 SD of manufacturing variability of ±14%. Between ±14-28% or ± 2 SEs there are 3 of 19 devices (21%). Finally, 1 of 19 devices has -39% error, which is within ± 3 SE = ± 42%. This outcome and each $\pm$ SD variation is visually represented in Figure 4.7., where experimental forces are plotted against the forces obtained from the FEM analyses. The black line in the centre signifies a perfect case 1:1 line, where experimental forces and FEM results would exactly match. Each grey line away from the 1:1 line represents ± 1 SE. The red dots

represent the experimental device forces plotted against the FEM model forces of the HF2V devices. Thus, all 19 devices are within ± 3 SE (99.4%) of possible experimental variation in manufacture. These outcomes match reasonable statistical expectations of being within the expected variability due to manufacture for this smaller sample number, providing a further quantitative validation.

Table 4.4. Comparison of forces from experiments and finite element modelling

Device	F_{exp} (kN)	F_{model} (kN)	$F_{contact\ pr}$ (kN)	$F_{friction}$ (kN)	Error %
3	55	46	12	34	16
4	85	52	8	44	39
5	160	167	54	106	-4
6	285	310	130	170	-8
7	390	400	135	265	-3
8	200	185	60	125	8
9	346	345	145	190	0
10	130	125	67	58	4
11	150	152	78	74	-1
13	260	245	68	177	6
14	155	155	45	110	0
15	250	200	115	85	20
16	170	175	27	148	3
17	200	220	65	155	10
18	260	245	45	140	6
19	125	130	59	71	-4
20	190	213	70	150	-12
21	107	107	62	45	0
22	520	650	265	385	20

In particular, this SE can be attributed to assembly and manufacturing variance. The model does not have manufacturing or assembly variability. Therefore, the errors in experiments compared to the (perfect) model should be within the same distribution. Hence, a perfect 1:1

match would not be expected, but the spread shown in Figure 4.7. meets expected statistical variation given this previously mentioned manufacturing variability. It thus validates the model's accuracy since each ± SE variability captures expected numbers of devices. Specifically, if the model had a notable bias error, this result would not have occurred.

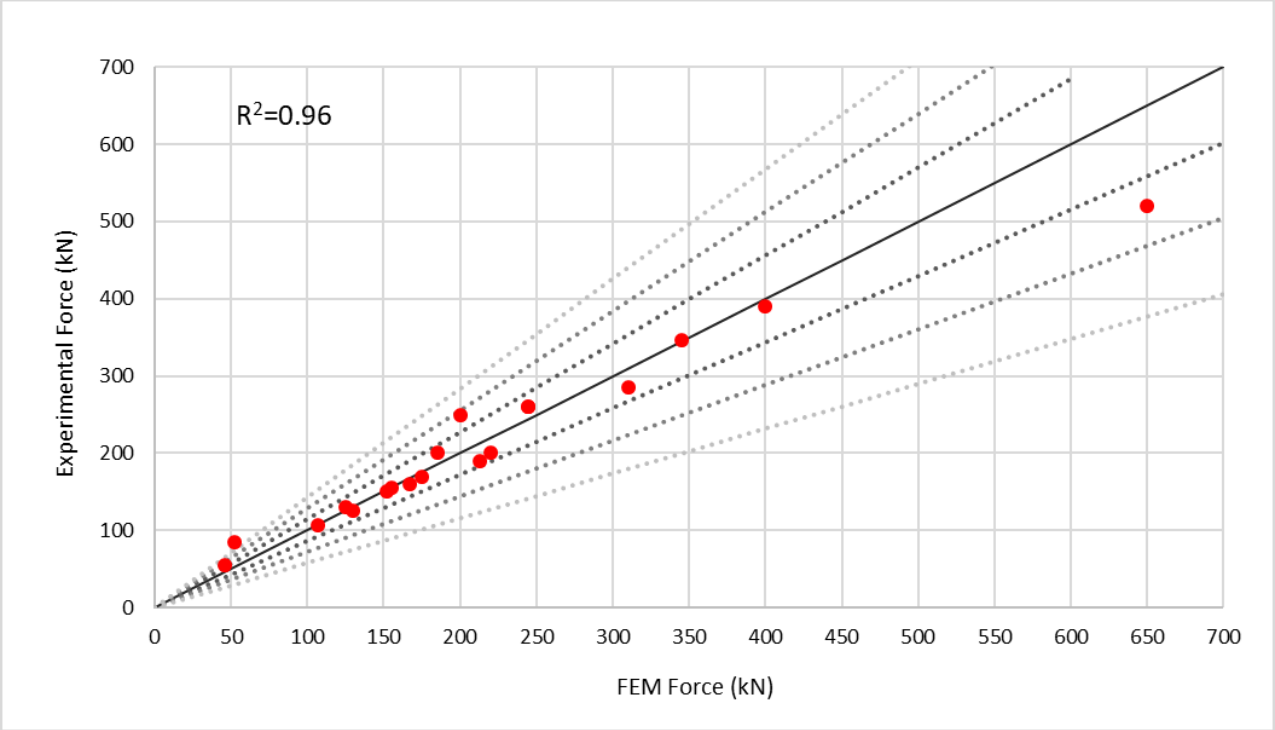

Figure 4.7. Plot of the experimental device forces against FEM analysis results. Standard Deviation representation of the devices. R^2=0.96 for the linear 1:1 line. The spread accounts for variability in device force due to manufacturing variability by ± 1, 2, 3 SEs.

Some of the errors in the results can be attributed to insufficient device design data and testing data available for finite element modelling, such as the specific device testing velocity, exact bulge profile data, bulge curvature radius, bulge angles, and bulge length. Previous studies suggest these parameters can potentially influence the extrusion forces outcomes [163, 164, 321, 322]. The understrength of the experimental results in comparison to the FEM results can

be explained by irregularity in pre-stress and can be addressed by further pre-stressing in manufacture.

4.3.4. Overall assessment

The material property values and boundary conditions were the same for all devices modelled, with only the specific device geometry changing. No calibrations or user inputs were made for simulating any devices for fitting or excluded due to large errors. The results from the FEM model are comparable to the forces from the design based force prediction model for the same HF2V devices modelled in this study, and the statistical distribution of results around the 1:1 line in Figure 4.7. indicates no specific error or bias. Hence, the approach is entirely general, objective, and replicable.

The most important aspect of precise device design is the input material parameters help in replicating the actual device operations. Identifying the exact material properties helps accurately simulate device operations. Several models and parameters are proposed for FE modelling of lead were applied for developing this HF2V model [279, 323, 324]. However, these models could not replicate HF2V device operations and predict forces accurately without this information.

HF2V damper behaviour can possibly be more accurately modelled by considering temperature dependent Young's Modulus [325], stress-strain rate-temperature-load dependent yield stresses [229], an experimentally derived coefficient of friction value [217, 243] or friction factor [218], and strain softening and hardening models [212, 213, 326]. However, the built-in models in many Finite Element (FE) packages are incapable of capturing many of these

phenomena. Given such values, user-defined materials can be implemented through user subroutines inside VUMAT and FE coding [281] to improve model performance. VUMAT is a user subroutine allowing implementation of user defined constitutive material behaviour laws for large deformation processes which are complex to model [327]. However, this approach and addition requires considerable expertise for effective implementation [281, 327], and may not add significant model accuracy.

A last limitation is computational time. Each simulation required about 8-10 hours using a 3.60 GHz Intel Core i7-470 computer with 32GB of RAM for shaft displacement of 10-12 mm. Highly nonlinear models are computationally expensive. However, more powerful computers or faster algorithms would improve this issue significantly.

Overall, the resulting finite element modelling approach yields a generic model, which can predict device forces well within the range for all types of HF2V lead extrusion dampers. Therefore, it can be used as a design tool along with the design-based model to obtain the precise force capacity range of the desired device, limiting the need for extensive prototype validation and possible device redesign. However, due to the safety-critical nature of the implementation of these devices, some level of final experimental testing to prove the design is likely to remain a necessary step before installation in the field.

4.4. Summary

Finite element modelling and analysis of the internal reaction mechanisms of HF2V lead extrusion dampers is done for the first time. This chapter presents a generalizable and objective finite element modelling methodology for HF2V lead extrusion dampers to accurately predict

device force capacities within the ±14% standard error derived from experimental testing. This chapter details all the finite element modelling parameters and methodology used in modelling the HF2V lead extrusion dampers, so the work is replicable.

The model is generic and modelling parameters are kept consistent. The same modelling approach is applied to all devices and only device geometry is changed. The model predicts device forces most precisely for *Typical* and *Large* devices. The model can be used as a design tool and can be used as a reference of expected HF2V device behaviour and force capacities before manufacturing. The device parameters can be modified to observe corresponding force changes and a design can be generated to yield optimum force outputs required for a particular application.

Chapter 5: Summary of HF2V models proposed

5.1. Introduction

HF2V devices have been modelled using empirical, analytical and computational methods in Chapters 2-3. While the techniques identified for modelling the devices were different, the objective of precise HF2V device force was estimation common. As seen in previous chapters, the models deliver approximate measures of expected device force for design consideration and provide expected force ranges. This chapter compares outcomes from the three key models identified in Chapters 2-4 to ascertain if the calculated model forces from empirical and FE models lie within the UB and LB models. This comparison of different models is intended to confirm whether there is generalizability of the UB and LB models for other device design methodologies. Furthermore, the main characteristics, advantages and disadvantages of each modelling method is briefly discussed. Finally, this chapter also provides a concise summary of all the device force models in this thesis.

5.2. Model comparison

5.2.1. Force estimation

In this chapter, 22 HF2V lead extrusion dampers from Chapters 2-4 are modelled using the three modelling techniques. The empirical (Model 4) and analytical models are simple and easily applicable for a HF2V device if all the device parameters are known. The forces from all the models of Chapters 2-4 are calculated and recorded for direct comparison in Table 5.1.

Table 5.1. HF2V device forces from all the proposed models

	Chapter 3		**Chapter 2**		**Chapter 4**	**Chapter 3**			
Device	F_{LB} (kN)	$F_{LB,1}$ (kN)	$F_{Empirical}$ (Model 4) (kN)	F_{exp} (kN)	F_{FEM} (kN)	$F_{UB,3}$ (kN)	$F_{UB,1}$ (kN)	$F_{UB,4}$ (kN)	$F_{UB,2}$ (kN)
1	-	-	8	55	-	-	-	-	-
2	-	-	14	74	-	-	-	-	-
3	-	-	30	55	46	-	-	-	-
4	-	-	49	85	52	-	-	-	-
5	21	127	120	160	167	135	274	320	444
6	61	200	230	285	310	245	487	477	702
7	108	267	338	390	400	371	704	636	948
8	17	169	160	200	185	175	289	316	437
9	54	253	315	346	345	300	492	483	687
10	21	66	140	130	125	78	155	172	209
11	21	84	145	150	152	98	179	184	245
12	17	127	171	155	160	133	220	245	311
13	12	234	187	260	245	248	344	349	497
14	17	127	171	155	155	137	221	231	316
15	45	151	247	250	200	181	340	363	444
16	5	172	157	170	175	185	251	261	369
17	6	186	184	200	220	198	270	278	395
18	10	211	217	260	245	222	306	310	442
19	7	93	112	125	130	98	146	151	215
20	17	141	192	190	213	229	283	329	436
21	19	93	183	107	107	78	143	147	160
22	88	403	446	520	650	526	1315	970	1859

Figure 5.1. visually represents the device force from models in a plot. The plot consists of device forces from all the models given in Table 5.1. The UB and LB force ranges are not calculated for devices 1-4 due to a lack of accurate device geometry values for calculations. All the device forces lie between the F_{LB} and $F_{UB,4}$ models, as seen in Chapter 3, except for the empirical model force value of Device 22. However, as discussed in Chapter 2, the empirical model predicts the forces for *Small* devices less well in this case.

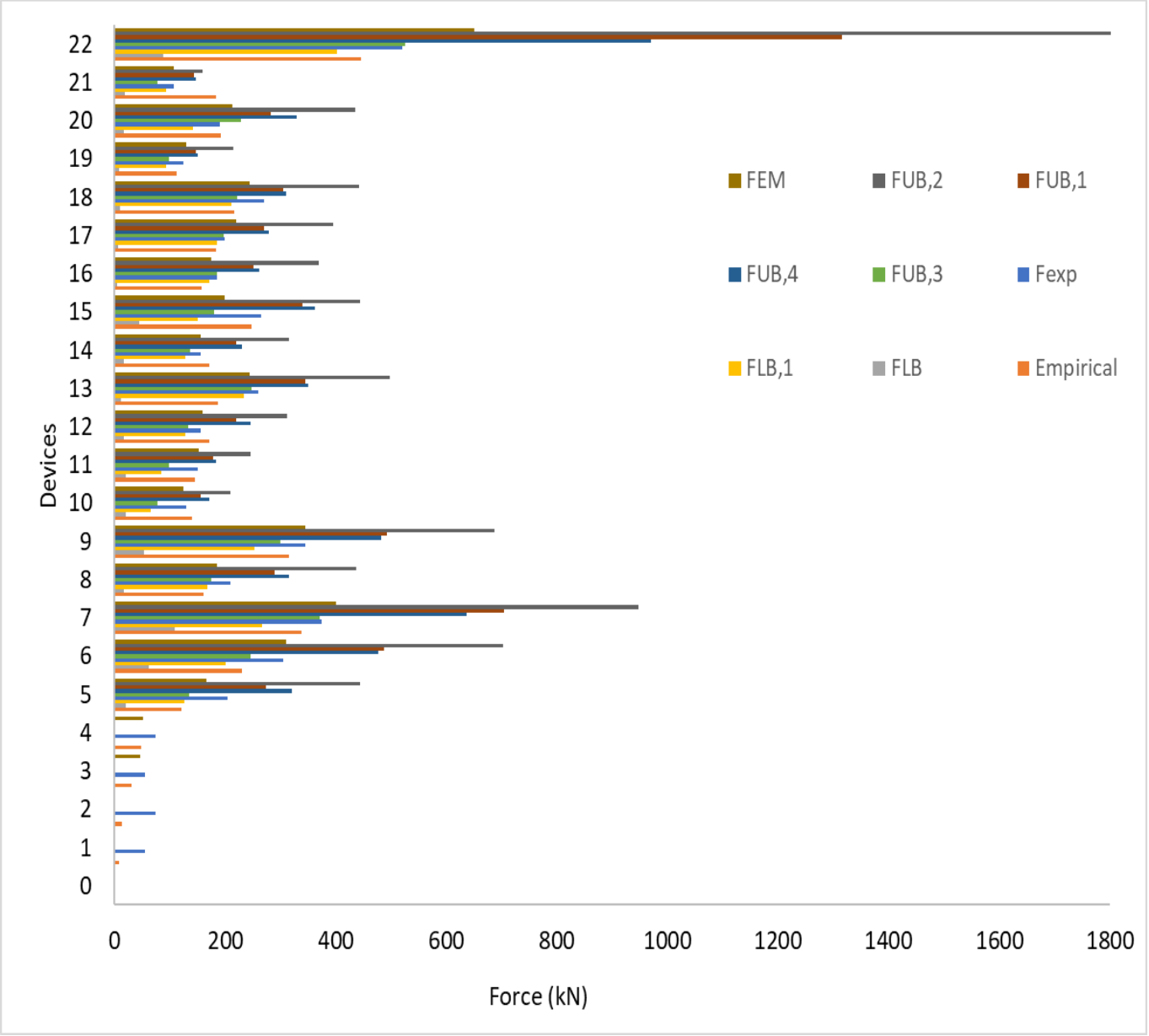

Figure 5.1. Empirical, FEM, UB and LB forces for Devices 1-22.

For better understanding of the correlation between the model forces and experimental forces, the force predictions from the empirical and finite element models are plotted against the experimental forces, along with the UB and LB forces in Figure 5.2. A linear fit line is drawn for the UB and LB model forces. The line of linear fit, broadly indicates the UB and LB force ranges. The correlation coefficient (R^2) values of the linear fit lines for the $F_{UB,1,2,3,4}$ models and $F_{LB,1}$ range between 0.81-0.96, as seen in Figure 5.2. This indicates strong correlation

between the model forces and experimental forces. While the F_{LB} has relatively lower R^2 = 0.63, as the F_{LB} model does not capture the device friction forces.

A 1:1 line is drawn for the plots, which indicate the theoretically perfect model predictions where model forces and experimental forces exactly match. The better model with more precise predicted values will lie closer to the 1:1 line.

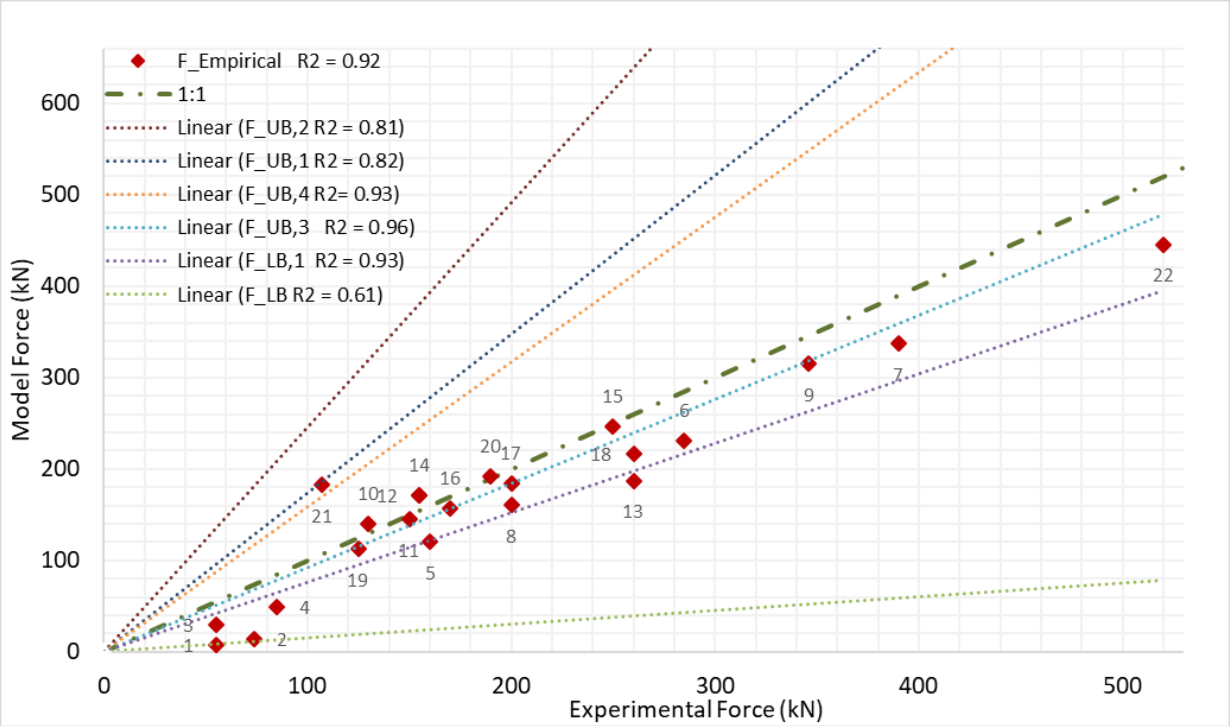

(a) F_{exp} vs $F_{empirical}$

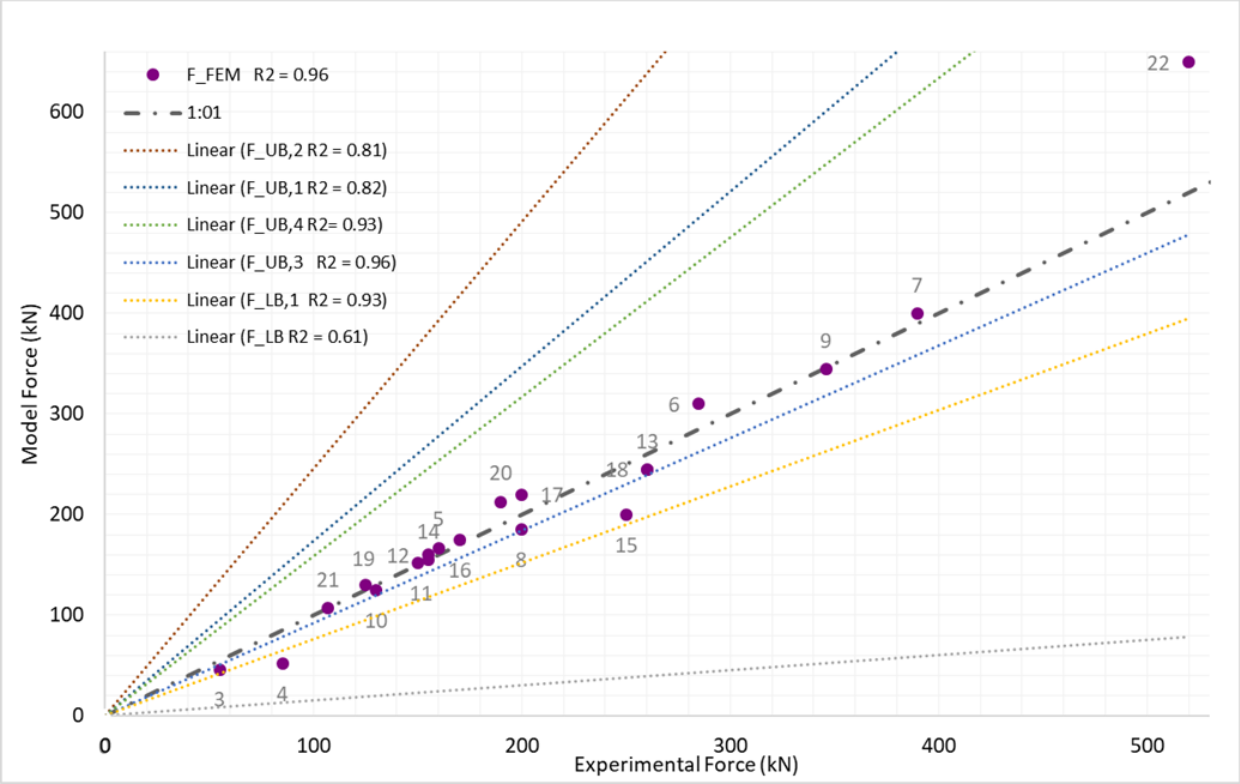

(b) F_{exp} vs F_{FEM}

Figure 5.2. Plots of $F_{empirical}$ and $\mathbf{F_{FEM}}$ plotted against F_{exp} along with UB and LB model forces

In Figure 5.2.(a), the empirical model force predictions lie close to $F_{LB,2}$, $F_{UB,3}$ model linear fit lines and the 1:1 line. The correlation coefficient value for the F_{exp} vs $F_{empirical}$ values along the 1:1 line is $R^2 = 0.92$ indicating very good correlation between the peak experimental forces and the empirical model forces. Overall, the empirical model predicts poorly for *Small* devices, those with no bulge, small bulges or large bulges. However, it performs well for very *Large* and *Typical* devices, as defined in Chapter 2..

The computational FE model predicts the forces for *Small* bulged devices better than the empirical model. Figure 5.2.(b) shows the F_{exp} values plotted aginst the F_{FEM} values. The

overall force prediction of device forces in Figure 5.2.(b) from the FEM model shows strong correlation $R^2 = 0.96$, lying tightly around the 1:1 line, except for Device 22.

Figure 5.3. shows the *Typical* device forces from the FE model, empirical model and experimental results of Table 5.1. against the LB and UB force ranges. The devices are presented on the plots in order of increasing values of experimental forces for better visualization. As seen in Chapters 2 and 4, and Figure 5.2**,** both the empirical model and the FEM predict device design force relatively precisely.

The empirical force predictions lie very close to the $F_{UB,3}$ and $F_{LB,1}$ ranges. The empirical model is more indicative of the steady forces achieved during HF2V device operations as shown in **Figure** 1**.**2 in Chapter 1. FEM predicted forces are greater than the empirical model forces for *Typical* devices with exceptions of Devices 10, 12 and 14.

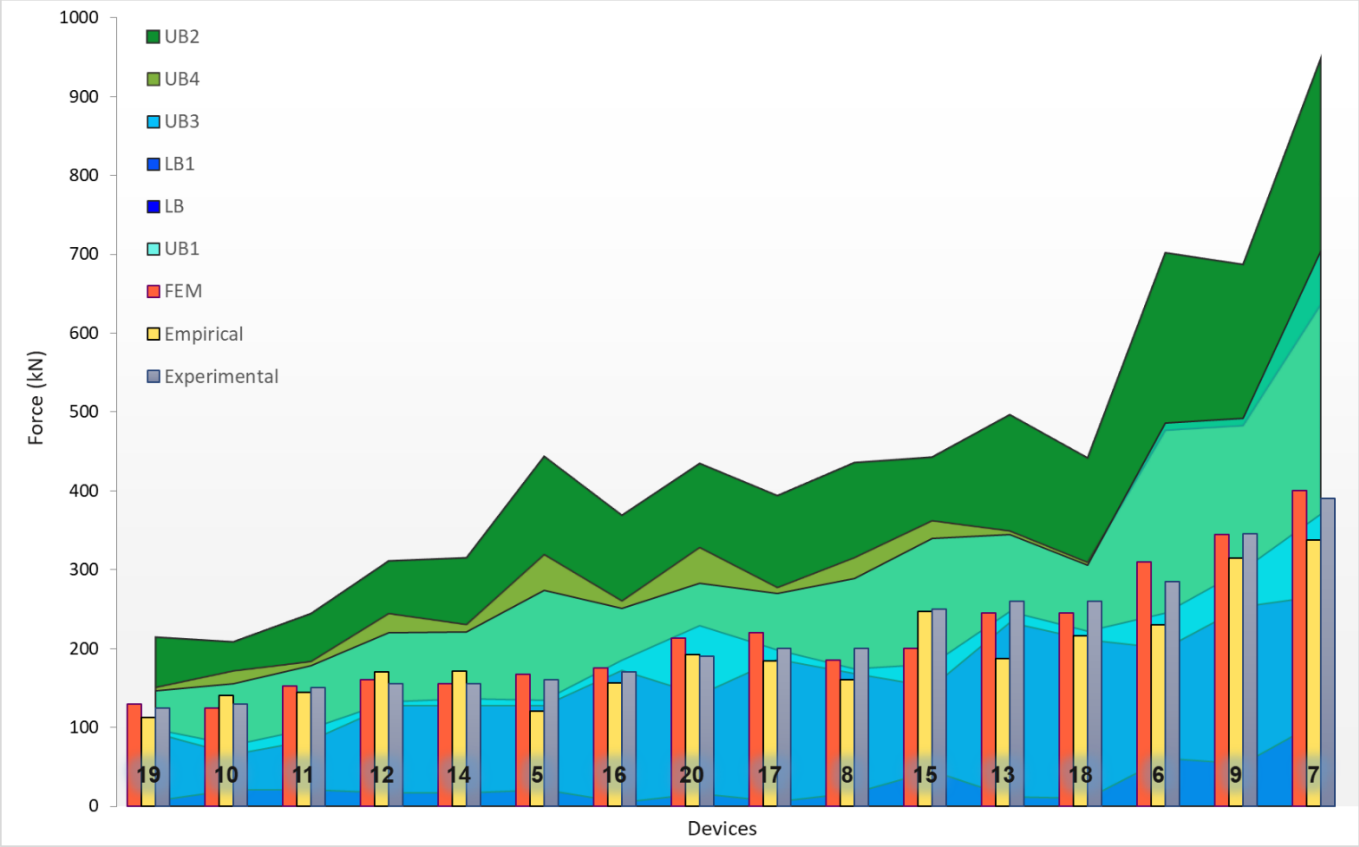

Figure 5.3. HF2V device forces for *Typical* HF2V devices from empirical, FEM, experimental, UB and LB models

Thus, the UB and LB ranges can be used for comparison and, critically for design, prediction of upper and lower force limits of *Typical* and *Large* device forces from other HF2V modelling techniques. In Figure 5.4, the model forces for Devices 9 and 18 are plotted in the hysteresis loop for the HF2V device to better understand where the model forces are estimating device force. This plot shows that although the forces predicted from the different models differ, the experimental results do not show a single force for the device. The experimental device behaviour does not follow an elastic-perfectly-plastic (EPP) response and there is some variation in the experimental force within the nominal yield plateau region. Therefore, the goal of an exact match of model and experimental results need to be considered in this context.

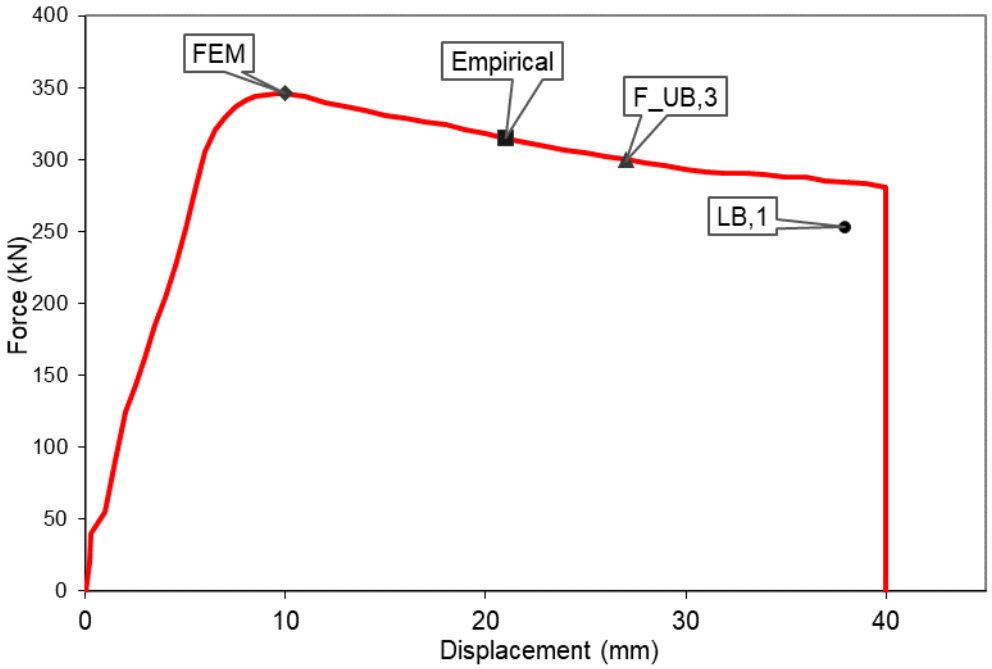

(a) Model forces plotted for Device 9

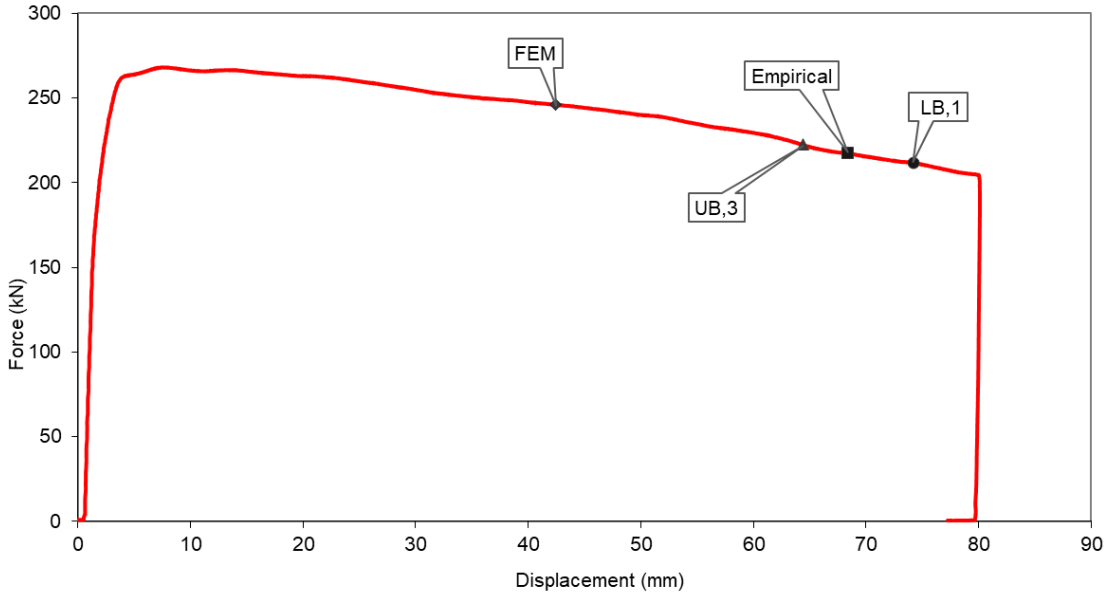

(b) Model forces plotted for Device 18

Figure 5.4. Model forces (FEM, $F_{empirical}$, $F_{UB,3}$ and $F_{LB,1}$) plotted over the hysteresis plots from experimental test data**.**

5.2.2. Advantages and Disadvantages

The empirical model is a linear design based prediction tool with very few parameters involved in determining the average forces from the HF2V dampers. The model is simple and encompasses key device design parameters identified in Chapter 3, applicable to a wide range of devices except, *Small* devices. However, the model lacks in ability to capture the velocity dependence of HF2V devices.

In contrast, the analytical modelling method calculates device force using yield stress corresponding to the strain-rate of deformation of lead in the HF2V devices. The UB and LB models are dependent on almost all key device design parameters to determine device forces directly. The models can be used to approximate the precise device forces produced from HF2V devices during plastic deformation using the $F_{UB,1,2,4}$ models and pure extrusion forces from the F_{LB} model in Chapter 3. The steady forces after the initial strain hardening of lead in the devices can be broadly estimated by $F_{LB,1}$ and $F_{UB,3}$ model forces. Although comprising of many parts, the indirect extrusion UB modelling technique not only provides an overall measure of the force capacity of the devices, but also encapsulates the individual contributions from all relevant HF2V device geometric parameters.

While the LB, UB and empirical models provide an estimation of specific forces achievable from the HF2V devices, the FE model produces an estimation of peak expected device force and a hysteresis plot showing increments in force due to induced strain during shaft displacement. The force-displacement plots from the FE method provide an insight to the mechanisms involved during the nonlinear behaviour of dampers during operations. Additionally, it is an excellent tool for visualizing the changing flow patterns, stress

concentration and distributions of load within the lead with varying geometric device parameters. This FE method can also be applied as an optimization tool where the key damper parameters identified in Chapter 3 can be modified to understand the changes in force outputs and ease of achieving peak force. Although the model serves as a design and a precision force forecasting tool, the modelling method is expensive compared to other models in terms of computation time, software requirement and technology.

Overall, the choice of model for HF2V device modelling application can be done for model simplicity, prediction accuracy, ease of uptake, size of the device, target force capacity, visualization of device operations and optimization. All approaches offer benefits and provide relatively accurate prediction. Thus, it is a choice of need and desired use or speed to govern this choice in design process.

5.3. Summary

This chapter has compared the empirical, analytical and computational models proposed for the HF2V devices by highlighting distinct characteristic of each modelling method and their suitability depending on HF2V damper size and force capacity. The limitations of each modelling process are briefly described to provide a guideline for HF2V model uptake depending complexity, expertise, accuracy, time and modelling objective.

Chapter 6: Conclusion

The research within this thesis explores the development of design and modelling methodologies for the lead extrusion dampers. The outcomes of this study are HF2V lead extrusion damper empirical design, upper and lower force range and finite element models, which can all precisely estimate the force capacities of devices. The modelling process has provided an insight into the factors contributing the overall resistive force response from the HF2V devices.

The empirical equation modelled on associated device parameters predicts device forces predicts device design forces with ± 80% (average) precision for *Small* and *Large* devices. This model provides an insight into the force contributions of overall extrusion forces and friction forces. Friction forces contribute to the overall HF2V device forces significantly with an average of 22% in *Typical* devices and 50% in *Large* devices. In *Small* HF2V devices, the size of the bulge or area ratio is pivotal in determining the overall device forces generated. The key design parameters identified for a HF2V lead extrusion device design are cylinder diameter, surface area and bulge area.

The HF2V device design and operation principles were then matched to industrial bulk forming extrusion parameters and processes. Based on existing extrusion models, a methodology to obtain an operational ranges for the bulged shaft HF2V devices was derived. Four models provided upper bound force range models for the devices based on direct and indirect extrusion processes. Two models give lower bound forces of the HF2V devices, one of which shows pure extrusion force developed in devices. The experimental, empirical and computational model forces are within the UB and LB ranges for all but one device signifying generalizability of

models. The overall analytical modelling encompasses almost all design parameters in an HF2V device to predict the likely bounding forces for a given design. Several additional key design aspects of the extrusion damper were identified from analytical modelling which matched the parameters identified through empirical modelling.

The finite element model developed is a promising tool that is capable of predicting device forces based on input parameters and provides a new insight into the internal reactions and plastic deformations within a lead extrusion damper, which otherwise is not possible to observe experimentally. All the modelling methods followed are accurately described and can be taken up to design device forces for *Typical* and *Large* devices for precise calculations. This method computes the device force automatically using finite element methods and is a reliable tool for design optimization.

The three proposed models have distinct characteristics and can be used individually or as an integrated design tool to achieve the best of every model. The devices can be applied through all stages of device modelling as follows:

- The empirical model is simple design tool which can be used for initial approximation of device forces using only few key geometric device parameters to achieve precise average force capacity of the device.
- The analytical models are more complex design tools consisting of more HF2V design parameters and is effective to determine the maximum and minimum force capacity of the HF2V device. This provides a better overview of how the device behaves.

- The computational model can be used achieve a better understanding of the device operation mechanics and estimate the force produced by the HF2V device model at every stage of operation.

Overall, this thesis has developed design and modelling technique for the HF2V lead extrusion dampers that are generic and offers different models for uptake and application for designers, engineers and researchers depending on complexity, aim and availability of design data. New insight has been obtained regarding specific contributions to the overall device response behaviour.

Chapter 7: Future Work

The research within this thesis has provided significant insight into development of design models for application to high force-to-volume lead extrusion devices. Contributions to the overall response behaviour have been delineated within the models presented. However, there remain areas requiring further research to address limitations and refine recommendations. Several areas of further interest to expand HF2V device design knowledge have been identified as a result of this work. Some areas of particular interest for future work are detailed within this chapter.

7.1. Experimental testing and validation

Due to the limited availability of the SATEC machine during laboratory refurbishment, prospective experimental tests were not conducted to validate the models created. The design and building of new HF2V devices for specific force capacities for a wide range of devices with varying force capacities and sizes can better establish the limitations of each modelling technique beyond the cross validations done in this thesis. The most reliable model can be determined by extensive testing of devices and comparison to the force predictions from the models. Based on the test outcomes and comparisons, models can be modified and calibrated to suit devices of varying sizes and capacities.

This research relied largely on devices with AR< 0.5 for analysis and understanding device mechanisms. Testing devices with large area ratio (AR > 0.5) for all sizes of devices would be beneficial in providing an insight into discrete behaviour of Device 21, not captured well by the empirical and analytical models.

7.2. Study of frictional effects

Friction during extrusion is the main concern in the metal extrusion industry, as it adds to the overall force required for extruding the material. In all 3 types of HF2V device modelling in Chapters 2, 3 and 4, friction is seen to be the essential in HF2V device force contributions. An extensive investigation of devices forces for various friction coefficients and the effect on overall device forces is an area of interest.

Friction coefficients and resulting friction forces during extrusion largely depends on the interacting metals. Varying the steel type, surface finish and sliding speed has shown improvements in friction forces in several studies [298, 328]. Experimental studies to observe improvements or loss in friction forces for various steel type shafts and cylinders will be of particular interest. Furthermore, testing HF2V devices with lubrication of the shaft and/or cylinder to determine how reducing friction at these interfaces influences both the model and experimental results, would add value.

7.3. Velocity Dependence

The rate dependence of mechanical properties of lead has been established in previous research [87, 252]. Existing research suggests the HF2V lead extrusion dampers are weakly velocity dependant and Rodgers et al suggest a velocity dependant model for the HF2V devices with velocity exponent $\sim\alpha = 0.1$ [112, 121]. Further, assessing the velocity dependence of experimental devices and calibrating the models to attain device forces at high speed would allow the models for applications at higher velocities. Analysis of experimental observations

to modify the empirical, analytical and finite element models will help match the models to high velocity performance.

7.4. Design of Experiments and Optimization

A parametric study to understand the sensitivity of HF2V devices to specify key geometric changes would allow better prediction of device forces. Taguchi proposed an optimization method for determining and analysing optimal manufacturing parameters [329-332]. Design of experiments is a widely used method in the manufacturing industry to maximize the understanding effect of parametric variation and corresponding changes in results. To attain functional relationships between response of HF2V operations to independent parameters an orthogonal array can be designed on basis of which experiments can be conducted. Taguchi optimization methods can then be used to find the degree of variation in force with variation of specific parameters of HF2V devices.

The variation of bulge shape on force outputs is of particular interest as the bulge causes maximum deformation. The various features of the shaft bulge need to be investigated separately to completely understand the lead-bulge interaction. The bulge parameters are bulge flat length, bulge radius, bulge angle and bulge length. It is expected that changes to these variables will alter device performance, but the level of sensitivity to such changes is not currently known.

7.5. Automated HF2V modelling

The finite element model developed in Chapter 4 using ABAQUS can act as an effective design tool for understanding changes in HF2V forces with changing device design parameters. Key parameters that effect the device forces are identified in Chapter 5**.** Varying the key parameters, the devices can be modified for achieving specific forces. However, this approach is a trial and error methodology. An optimization model automatically generating a HF2V device design for a target device force would be desirable.

Based on existing design knowledge of HF2V devices and experimental test results an input file can be generated for HF2V design values for target force capacities. The analysis results can be used to generate an optimization algorithm to resize HF2V device geometry by automatic optimization cycles to achieve specific device forces. By applying required constraints on maximum and minimum allowable geometric change based on design requirements, a parametric design model can be automatically generate using commercial finite element packages and scripting tools like the ABAQUS CAE Python interface [281]. This method has been widely applied for automated parametric shape optimizations [333-336].

To perform this modelling, the models developed in Chapters 2 and 3 can be used as reference input model for the material properties identified for FE model in Chapter 4. The FE model developed in Chapter 4 cannot be used for this automated parametric modelling as all the involved parts need to be meshed for this analysis. Additionally, there is a need to assess the strength and stiffness of all steel components during analysis to prevent buckling during loading. It should be noted that methodology requires advanced scripting and FE analysis skills and wide range of experimental data for accuracy.

References

1. Geller, R.J., *Earthquake prediction: a critical review.* Geophysical Journal International, 1997. **131**(3): p. 425-450.
2. Ouzounov, D., S. Pulinets, K. Hattori, and P. Taylor, *Pre-earthquake processes: A multidisciplinary approach to earthquake prediction studies*. Vol. 234. 2018: John Wiley & Sons.
3. Zhang, Y., Z. Wu, X. Zhang, and G. Li, *Annual Earthquake Potential Consultation: A Real Forward Prediction Test in China*, in *Earthquake and Disaster Risk: Decade Retrospective of the Wenchuan Earthquake*. 2019, Springer. p. 117-134.
4. Kaiser, A., C. Holden, J. Beavan, D. Beetham, R. Benites, A. Celentano, D. Collett, J. Cousins, M. Cubrinovski, and G. Dellow, *The Mw 6.2 Christchurch earthquake of February 2011: preliminary report.* New Zealand journal of geology and geophysics, 2012. **55**(1): p. 67-90.
5. Chiarabba, C., A. Amato, M. Anselmi, P. Baccheschi, I. Bianchi, M. Cattaneo, G. Cecere, L. Chiaraluce, M. Ciaccio, and P. De Gori, *The 2009 L'Aquila (central Italy) MW6. 3 earthquake: Main shock and aftershocks.* Geophysical Research Letters, 2009. **36**(18).
6. Kuwata, Y., S. Takada, and M. Bastami, *Building damage and human casualties during the Bam-Iran earthquake.* Asian journal of civil engineering (building and housing, 2005. **6**(1-2): p. 1-19.
7. Abidi, S., S. Akbar, and F. Bioret. *Post-Event Reconstruction in Asia since 1999: An Overview Focusing on the Social and Cultural Characteristics of Asian Countries*. in *International Conference on Earthquake Engineering and Seismology*. 2011.
8. Parker, M. and D. Steenkamp, *The economic impact of the Canterbury earthquakes.* Reserve Bank of New Zealand Bulletin, 2012. **75**(3): p. 13-25.
9. Seville, E., J. Vargo, and I. Noy, *Economic recovery following earthquakes disasters.* Encyclopedia of Earthquake Engineering, 2014: p. 1-14.
10. Kenny, C., *Why do people die in earthquakes? The costs, benefits and institutions of disaster risk reduction in developing countries*, in *Policy Research Working Paper 4823*. 2009, The World Bank: Washington, DC.
11. Mumtaz, H., S.H. Mughal, M. Stephenson, and J.K. Bothara, *The challenges of reconstruction after the October 2005 Kashmir earthquake.* Proceedings of the New Zealand Society for Earthquake Engineering. Wairakei, New Zealand, 2008.
12. Williams, G., *Study on disaster risk reduction, decentralization and political economy*. 2011, The global assessment report on disaster risk reduction
13. *Routledge Companion to Global Heritage Conservation*. 1st Edition ed, ed. V. Bharne and T. Sandmeier. 2019, London: Routledge.
14. Bhagat, S., H. Samith Buddika, R. Kumar Adhikari, A. Shrestha, S. Bajracharya, R. Joshi, J. Singh, R. Maharjan, and A.C. Wijeyewickrema, *Damage to cultural heritage structures and buildings due to the 2015 Nepal Gorkha earthquake.* Journal of Earthquake Engineering, 2018. **22**(10): p. 1861-1880.
15. McClean, R., *Heritage Buildings, Earthquake Strengthening and Damage: The Canterbury Earthquakes September 2010-January 2012*, in *Report for the Canterbury Earthquakes Royal Commission*. 2012.
16. King, S.A., A.S. Kiremidjian, N. Basöz, K. Law, M. Vucetic, M. Doroudian, R.A. Olson, J.M. Eidinger, K.A. Goettel, and G. Horner, *Methodologies for evaluating the*

socio-economic consequences of large earthquakes. Earthquake spectra, 1997. **13**(4): p. 565-584.
17. Shinozuka, M., A. Rose, and R. Eguchi, *Engineering and socioeconomic impacts of earthquakes*. 1998, Multidisciplinary Center for Earthquake Engineering Research: New York.
18. Amini Hosseini, K., S. Hosseinioon, and Z. Pooyan, *An investigation into the socioeconomic aspects of two major earthquakes in Iran.* Disasters, 2013. **37**(3): p. 516-535.
19. Lebowitz, A.J., *Cross-Sectional Data Within 1 Year of the Fukushima Meltdown: Effect-Size of Predictors for Depression.* Community Mental Health Journal, 2016. **52**(1): p. 94-101.
20. Xu, J., L. Xie, B. Li, N. Li, and Y. Yang, *Anxiety symptoms among children after the Wenchuan earthquake in China.* Nordic journal of psychiatry, 2012. **66**(5): p. 349-354.
21. Kılıç, C. and M. Ulusoy, *Psychological effects of the November 1999 earthquake in Turkey: an epidemiological study.* Acta Psychiatrica Scandinavica, 2003. **108**(3): p. 232-238.
22. Gluckman, P. and K.F.F. FRS, *The psychosocial consequences of the Canterbury earthquakes: A briefing paper.* New Zealand: Office of the Prime Minister's Science Advisory Committee Publishing, 2011.
23. Wu, J., N. Li, S. Hallegatte, P. Shi, A. Hu, and X. Liu, *Regional indirect economic impact evaluation of the 2008 Wenchuan Earthquake.* Environmental Earth Sciences, 2012. **65**(1): p. 161-172.
24. Dorahy, M.J., C. Renouf, A. Rowlands, D. Hanna, E. Britt, and J.D. Carter, *Earthquake aftershock anxiety: An examination of psychosocial contributing factors and symptomatic outcomes.* Journal of loss and trauma, 2016. **21**(3): p. 246-258.
25. Javanmardi, A., Z. Ibrahim, K. Ghaedi, H.B. Ghadim, and M.U. Hanif, *State-of-the-Art Review of Metallic Dampers: Testing, Development and Implementation.* Archives of Computational Methods in Engineering, 2019: p. 1-24.
26. Symans, M., F. Charney, A. Whittaker, M. Constantinou, C. Kircher, M. Johnson, and R. McNamara, *Energy dissipation systems for seismic applications: current practice and recent developments.* Journal of structural engineering, 2008. **134**(1): p. 3-21.
27. Naeim, F. and J.M. Kelly, *Design of seismic isolated structures: from theory to practice*. 1999: John Wiley & Sons.
28. Scawthorn, C. and W.-F. Chen, *Earthquake engineering handbook*. New directions in civil engineering. 2002, Boca Raton, FL : CRC Press, c2003: CRC press.
29. Lindeburg, M.R. and K.M. McMullin, *Seismic design of building structures: A professional's introduction to earthquake forces and design details*. 11th edition ed. 2014, Belmont, CA: Professional Publications, Inc.
30. Fajfar, P., *Seismic design methodologies for the next generation of codes*. 2019: Routledge.
31. Datta, T.K., *A state-of-the-art review on active control of structures.* ISET Journal of earthquake technology, 2003. **40**(1): p. 1-17.
32. Nath, S. *Methods for Improving the Seismic Performance of Structures-A Review*. in *IOP Conference Series: Materials Science and Engineering*. 2018. IOP Publishing.012141
33. Soong, T.T., Spencer, B.F. Jr., *Supplemental Energy Dissipation: State-of-the-Art and State-of-the-Practice.* Engineering Structures, 2002. **24**(3): p. 243-259.

34. Constantinou, M.C., Soong, T. T, Dargush, G. F, *Passive Energy Dissipation Systems for Structural Design and Retrofit*. Monograph No. 1, Multidisciplinary Center for Earthquake Engineering Research. 1998, Buffalo (NY) 324.
35. Hanson, R.D. and T.T. Soong, *Seismic design with supplemental energy dissipation devices*. Vol. Monograph No. 8. 2001, Oakland: Earthquake Engineering Research Institute (EERI).
36. Torunbalci, N. *Seismic isolation and energy dissipating systems in earthquake resistant design*. in *Proc. 13thWorld conference on earthquake engineering, 13WCEE*. 2004. Vancouver, Canada.Paper No. 3273
37. Dyke, S.J., B.F. Spencer Jr, M.K. Sain, and J.D. Carlson, *Modeling and Control of Magnetorheological Dampers for Seismic Response Reduction.* Smart Materials and Structures, 1996. **5**(5): p. 565-575.
38. Symans, M.D. and M.C. Constantinou, *Semi-active control systems for seismic protection of structures: a state-of-the-art review*. Engineering structures, 1999. **21**(6): p. 469-487.
39. Spencer Jr, B. and T. Soong. *New applications and development of active, semi-active and hybrid control techniques for seismic and non-seismic vibration in the USA*. in *Proceedings of international post-SMiRT conference seminar on seismic isolation, passive energy dissipation and active control of vibration of structures*. 1999. Cheju, Korea
40. Yoshioka, H., J. Ramallo, and B. Spencer Jr, *"Smart" Base Isolation Strategies Employing Magnetorheological Dampers.* Journal of Engineering Mechanics, 2002. **128**(5).
41. Heaton, T.H., Hall. J. F., Wald. D. J., Halling, M. W., *Response of High-Rise and Base-Isolated Buildings to Hypothetical Mw 7.0 Blind Thrust Earthquake.* Science, 1995. **Volume 267**(5195): p. 206 - 211.
42. Constantinou, M.C. and M.D. Symans, *Seismic response of structures with supplemental damping*. The Structural Design of Tall Buildings, 1993. **2**(2): p. 77-92.
43. Moghaddasi, M., M. Cubrinovski, J.G. Chase, S. Pampanin, and A. Carr, *Stochastic Quantification of Soil-Shallow Foundation-Structure Interaction.* Journal of Earthquake Engineering, 2012. **16**(6): p. 820-850.
44. Moghaddasi, M., G.A. MacRae, J.G. Chase, M. Cubrinovski, and S. Pampanin, *Seismic design of yielding structures on flexible foundations.* Earthquake Engineering & Structural Dynamics, 2015. **44**(11): p. 1805-1821.
45. Sadek, F., A.W. Taylor, and R.M. Chung, *Passive energy dissipation devices for seismic applications*. 1996, Building and Fire Research Laboratory, National Institute of Standards and Technology: Gaithersburg.
46. Cimellaro, G.P. and S. Marasco, *Passive Energy Dissipating Systems*, in *Introduction to Dynamics of Structures and Earthquake Engineering*. 2018, Springer International Publishing: Cham. p. 391-419.
47. Hazaveh, N.K., G.W. Rodgers, J.G. Chase, and S. Pampanin, *Passive direction displacement dependent damping (D3) device.* Bulletin of the New Zealand Society for Earthquake Engineering, 2018. **51**(2): p. 105-112.
48. Borzouie, J., G.A. MacRae, J.G. Chase, G.W. Rodgers, and G.C. Clifton, *Experimental studies on cyclic performance of column base weak axis aligned asymmetric friction connection.* Journal of Constructional Steel Research, 2015. **112**: p. 252-262.
49. Lin, W.H. and A.K. Chopra, *Earthquake response of elastic SDF systems with non-linear fluid viscous dampers.* Earthquake Engineering & Structural Dynamics, 2002. **31**(9): p. 1623-1642.

50. Hazaveh, N.K., G.W. Rodgers, J.G. Chase, and S. Pampanin, *Reshaping structural hysteresis response with semi-active viscous damping.* Bulletin of Earthquake Engineering, 2017. **15**(4): p. 1789-1806.
51. Chanchi, J., G.A. MacRae, J.G. Chase, G.W. Rodgers, A. Mora, and G.C. Clifton. *Design Considerations for Braced Frames with Asymmetric Friction Connections*. in *STESSA 2012 – Behaviour of Steel Structures in Seismic Areas*. 2012. Santiago, Chile. 8-pages
52. Golondrino, J.C., MacRae, G.A, Chase, J.G, Rodgers, G.W, and Clifton, C., *Behaviour of Asymmetrical Friction Connections using different shim materials*, in *New Zealand Society of Earthquake Engineers Annual Conference (NZSEE 2012)*. 2012: Christchurch, New Zealand.
53. Rodgers, G.W., J.G. Chase, R. Causse, J. Chanchi, and G.A. MacRae, *Performance and Degradation of Sliding Steel Friction Connections: Impact of Velocity, Corrosion Coating and Shim Material.* Engineering Structures, 2017. **141**: p. 292-302.
54. Clifton, G.C., *Semi-rigid Joints for Moment-Resisting Steel Framed Seismic-Resisting Systems*. 2005, The University of Auckland, Auckland, New Zealand.
55. Borzouie, J., G. MacRae, J. Chase, G. Rodgers, and G. Clifton, *Experimental studies on cyclic performance of column base strong axis–aligned asymmetric friction connections.* Journal of Structural Engineering, 2015. **142**(1): p. 04015078.
56. Borzouie, J., MacRae, G.A., Chase, J.G., Rodgers, G.W. and Clifton, G.C, *Experimental studies on cyclic performance of column base weak axis aligned asymmetric friction connection.* Journal of Constructional Steel Research, 2015: p. 252-262.
57. Housner, G., L.A. Bergman, T.K. Caughey, A.G. Chassiakos, R.O. Claus, S.F. Masri, R.E. Skelton, T. Soong, B. Spencer, and J.T. Yao, *Structural Control : Past, Present, and Future.* Journal of Engineering Mechanics, 1997. **123**(9): p. 897 - 971.
58. Mulligan, K.J., J.G. Chase, J.B. Mander, G.W. Rodgers, and R.B. Elliott, *Nonlinear Models and Validation for Resetable Device Design and Enhanced Force Capacity.* Structural Control and Health Monitoring, 2010. **17**(3): p. 301-316.
59. Mulligan, K.J., J.G. Chase, J.B. Mander, G.W. Rodgers, R.B. Elliott, R. Franco-Anaya, and A.J. Carr, *Experimental Validation of Semi-active Resetable Actuators in a 1/5th Scale Test Structure.* Earthquake Engineering and Structural Dynamics, 2009. **38**(4): p. 517-536.
60. Rodgers, G.W., J.B. Mander, J.G. Chase, K.J. Mulligan, B.L. Deam, and A. Carr, *Re-shaping Hysteretic Behaviour—Spectral Analysis and Design Equations for Semi-active Structures.* Earthquake Engineering & Structural Dynamics, 2007. **36**(1): p. 77-100.
61. Spencer Jr, B.F., S.J. Dyke, M.K. Sain, and J.D. Carlson, *Phenomenological Model for Magnetorheological Dampers.* Journal of Engineering Mechanics, 1997. **123**(3): p. 230-238.
62. Jansen, L.M. and S.J. Dyke, *Semiactive Control Strategies for MR Dampers: Comparative Study.* Journal of Engineering Mechanics, 2000. **126**(8): p. 795-803.
63. Filiatrault, A., Tremblay, R., Wanitkorkul, A., *Performance Evaluation of Passive Damping Systems For the Seismic Retrofit of Steel Moment-Resisting Frames Subjected to Near-Field Ground Motions.* Earthquake Spectra, 2001. **17**(3): p. 427-456.
64. Constantinou, M.C.S., M. D., *Seismic Response of Structures with Supplemental Damping.* The Structural Design of Tall Buildings. **2**(2): p. 77-92.

65. Hazaveh, N.K., Rodgers, G.W.,Chase, J.G.,Pampanin, S., *Experimental test and validation of a direction-and displacement-dependent viscous damper*. Journal of Engineering Mechanics, 2017. **143**(11): p. 04017132.
66. Hazaveh, N.K., A.A. Rad, G.W. Rodgers, J.G. Chase, S. Pampanin, and Q.T. Ma. *Shake Table Testing of a Low Damage Steel Building with 2-4 Displacement Dependent (D3) Viscous Damper*. in *Key Engineering Materials*. 2018. Trans Tech Publ.331-338
67. Reddy, G.R., D.K. Jha, and G. Verma, *Retrofitting of Structures and Equipments*, in *Textbook of Seismic Design: Structures, Piping Systems, and Components*, G.R. Reddy, H.P. Muruva, and A.K. Verma, Editors. 2019, Springer Singapore: Singapore. p. 457-519.
68. Makris, N., *Seismic isolation: Early history*. Earthquake Engineering & Structural Dynamics, 2019. **48**(2): p. 269-283.
69. Aghlara, R. and M.M. Tahir, *A passive metallic damper with replaceable steel bar components for earthquake protection of structures.* Engineering structures, 2018. **159**: p. 185-197.
70. El-Bahey, S. and M. Bruneau, *Bridge Piers with Structural Fuses and Bi-Steel Columns. I: Experimental Testing.* Journal of Bridge Engineering, 2012. **17**(1): p. 25-35.
71. Saravanan, M., R. Goswami, and G.S. Palani, *Replaceable Fuses in Earthquake Resistant Steel Structures: A Review*. International Journal of Steel Structures, 2018. **18**(3): p. 868-879.
72. Robinson, W.H., Greenbank, L. R., *An Extrusion Energy Absorber Suitable for the Protection of Structures During an Earthquake.* Earthquake Engineering & Structural Dynamics, 1976. **4**(3): p. 251-259.
73. Skinner, R.I., Tyler, R.G., Heine, A.J., Robinson, W.H., *Hysteretic dampers for the protection of structures from earthquakes.* Bulletin of the New Zealand National Society for Earthquake Engineering, 1980. **13**(1): p. 22-36.
74. Robinson, W.H., *Cyclic energy absorber, US4117637 A*. 1978, Google Patents.
75. Avitzur, B., *Analysis of metal extrusion.* Journal of Engineering for Industry, 1965. **87**(1): p. 57-69.
76. Rowe, G.W., *Elements of metalworking theory*. 1979, London, UK: Hodder Arnold.
77. Jacques, S. and L. Louis, *Extrusion of metals*, U.S.P. Office, Editor. 1951, Google Patents: United States of America.
78. Robinson, W.H., *Recent research and applications of seismic isolation in New Zealand.* Bulletin-New Zealand National Society For Earthquake Engineering, 1995. **28**: p. 253-264.
79. Robinson, W., *Recent applications of high-damping hysteretic devices for the seismic isolation of buildings and bridges.* Journal of alloys and compounds, 1994. **211**: p. 592-595.
80. Monir, H.S. and A. Naser. *Seismic design of steel structures with lead-extrusion dampers as knee braces*. in *AIP Conference Proceedings*. 2008. AIP.1433-1440
81. Parulekar, Y.M., Reddy, G.R., Vaze, K.K., Kushwaha, H.S., *Lead extrusion dampers for reducing seismic response of coolant channel assembly.* Nuclear engineering and design, 2004. **227**(2): p. 175-183.
82. Rodgers, G.W., Chase, J.G., Mander, J.B., Leach, N.C., Denmead, C.S., Cleeve, L. , Heaton, D. *High Force-to-Volume Extrusion Dampers and Shock Absorbers for Civil Infrastructure*. in *Proceedings of 19th Australasian Conference on the Mechanics of Structures and Materials*. 2006.

83. Rodgers, G.W., J.G. Chase, J.B. Mander, N.C. Leach, and C.S. Denmead, *Experimental development, tradeoff analysis and design implementation of high force-to-volume damping technology*. 2007.
84. Soydan, C., E. Yüksel, and E. İrtem, *Retrofitting of pinned beam–column connections in RC precast frames using lead extrusion dampers.* Bulletin of Earthquake Engineering, 2018. **16**(3): p. 1273-1292.
85. Muramatsu, M., M. Koyama, and I. Watanabe, *Tensile testing with cyclic strain holding to analyze dynamic recrystallization of pure lead.* Advances in Materials Science and Engineering, 2014. **2014**.
86. Hotta, S., K. Matsumoto, T. Murakami, T. Narushima, and C. Ouchi, *Dynamic and static restoration behaviors of pure lead and tin in the ambient temperature range.* Materials transactions, 2007. **48**(No.10): p. 2665-2673.
87. Hofmann, W., *Lead and lead alloys*, in *Lead and Lead Alloys*. 1970, Springer. p. 25-320.
88. Robinson, W.H., *Lead-rubber hysteretic bearings suitable for protecting structures during earthquakes.* Earthquake Engineering & Structural Dynamics, 1982. **10**(4): p. 593-604.
89. Robinson, W. and A. Tucker, *A lead-rubber shear damper.* Bull. New Zealand Natl. Soc. Earthquake Engrg, 1976. **4**: p. 251-59.
90. Robinson, W.H. and W.J. Cousins. *Lead dampers for base isolation*. in *Proceeding of the 9thWorld Conference on Earthquake Engineering*. 1988.427-432
91. Eskandari, M. and E.P. Najafabadi, *Experimental and analytical study of telescopic lead yielding damper.* Journal of Constructional Steel Research, 2018. **150**: p. 371-383.
92. Horikiri, M., M. Ooka, H. Machida, and S. Ishikura, *Compressive/Tensile-Load-Type Damper made of lead and seismic isolation apparatus using the same, 6,164,023, 2000*. 2000, United States Patent
93. Zhou, Y., C. Wu, X. Deng, and Y. Wu. *Research and application of lead viscoelastic damper*.
94. Gong, S. and Y. Zhou, *Experimental study and numerical simulation on a new type of viscoelastic damper with strong nonlinear characteristics.* Structural Control and Health Monitoring, 2017. **24**(4): p. e1897.
95. Xin, Y., H. Wang, and S. Cheng, *Experimental study on new combined steel-lead damper*. Eng Mech, 2007. **24**(3): p. 126-130.
96. Yan, X.Y., A. Qi, W. Lin, and S.G. Wang. *Research on Design Method of Combined Steel Lead Energy Dissipation Structure*. in *Applied Mechanics and Materials*. 2011. Trans Tech Publ.526-530
97. Cheng, S., S. Du, X. Yan, Q. Guo, and Y. Xin, *Experimental study and numerical simulation of clapboard lead damper*. Proceedings of the Institution of Mechanical Engineers, Part C: Journal of Mechanical Engineering Science, 2017. **231**(9): p. 1688-1698.
98. Curadelli, R.O. and J.D. Riera, *Reliability based assessment of the effectiveness of metallic dampers in buildings under seismic excitations.* Engineering structures, 2004. **26**(13): p. 1931-1938.
99. Curadelli, R. and J. Riera, *Design and testing of a lead damper for seismic applications.* Proceedings of the Institution of Mechanical Engineers, Part C: Journal of Mechanical Engineering Science, 2007. **221**(2): p. 159-164.
100. Robinson, W.H., *Damper*, U.S. Patent, Editor. 2001, Damping Systems Limited, Auckland New Zealand.

101. Robinson, W. *Key developments: Seismic isolation*. in *The 1855 Wairarapa Earthquake Symposium*. 2005.150
102. Skinner, R., W. Robinson, and G. McVerry, *Seismic isolation in New Zealand.* Nuclear Engineering and Design, 1991. **127**(3): p. 281-289.
103. Charleson, A., P. Wright, and R. Skinner. *Wellington central police station, base isolation of an essential facility*. in *Pacific Conference on Earthquake Engineering*. 1987.377-388
104. Cousins, W.J., Robinson, W.H., McVerry, G.H. *Recent Developments in Devices for Seismic Isolation*. in *Proc. Pacific Conference on Earthquake Engineering, Christchurch, New Zealand*. 1991.221-232
105. Goto, W., T. Motohi, Y. Sugimura, S. Nagashima, H. Dohi, M. Suzuki, and K. Saito, *A Study on Seismic Response of Buildings in Sendai during the 2011 Great East Japan Earthquake*, in *15 WCEE*. 2012: Lisbon, Portugal. p. 5970-5979.
106. Wataru, G., T. Motohi, Y. Sugimura, S. Nagashima, K. Toyota, M. Suzuki, and K. Saito. *Evaluation of earthquake response of high-rise building with dampers in Sendai during the 2011 off the Pacific coast of Tohoku earthquake*. in *The International Symposium on Engineering Lessons from the the 2011 Great East Japan Earthquake*. 2011. Tokyo, Japan.1077-1086
107. Iwatsubo, T., Y. Sasaki, H. Abe, K. Kuroda, Y. Saito, K. Tai, and H. Sumiya. *NUPEC project: Seismic proving test of heavy component with energy absorbing support*. in *7th Intern. Conf. on Nuclear Engrg*. 1999.1-8
108. Abe, H., I. Ichihashi, K. Kuroda, T. Iwatsubo, and K. Tai, *Seismic proving test of heavy component with energy absorbing support*, in *Proceedings of the International Conference on Global Environment and Advanced Nuclear Power Plants*. 2002. p. 107-111.
109. Shannon, T. *Turanga Library Christchurch - Hybrid Rocking Precast Concrete Wall Panels*. in *Concrete New Zealand Conference*. 2019. Dunedin
110. Cousins, W.J., Porritt, T.E., *Improvements to Lead-Extrusion Damper Technology*. Bulletin of the New Zealand National Society for Earthquake Engineering, 1993. **26**(3): p. 342-348.
111. Robinson, W.H. and L.R. Greenbank, *Properties of an Extrusion Energy Absorber*. Bulletin of the New Zealand Society for Earthquake Engineering, 1975. **8**(3): p. 187-191.
112. Rodgers, G.W., *Next Generation Structural Technologies: Implementing High Force-to-Volume Energy Absorbers*, in *Mechanical Engineering*. 2009, University of Canterbury, Christchurch, New Zealand, Ph.D. thesis.
113. Rodgers, G.W., Denmead, C.S., Leach, N.C., Chase, J.G., Mander, J.B. *Experimental development and analysis of a high force/volume extrusion damper*. in *Proceedings New Zealand Society for Earthquake Engineering Annual Conference*. March 10-12, 2006. Napier, New Zealand
114. Soydan, C., A. Gullu, O. Hepbostancı, E. Yuksel, and E. Irtem. *Design of a Special Lead Extrusion Damper*. in *World Conference on Earthquake Engineering 15th, Portugal Lisboa*. 2012.
115. Soydan, C., E. Yüksel, and E. İrtem, *Determination of the characteristics of a new prestressed lead extrusion damper*, in *Proceedings of the 16th World Conference on Earthquake Engineering*. 2017: Santiago, Chile.
116. Wrzesniak, D., Rodgers, G.W., Fragiacomo, M, Chase, J.G., *Experimental Testing of Damage-Resistant Rocking Glulam Walls with Lead Extrusion Dampers.* Construction and Building Materials. **102**: p. 1145-1153.

117. Solberg, K.M., B.A. Bradley, G.W. Rodgers, J.B. Mander, R.P. Dhakal, and J.G. Chase, *Quasi-Static testing of a damage protected beam-column subassembly with internal lead damping devices*, in *Pacific Conference on Earthquake Engineering (PCEE 2007)*. 2007: Singapore. p. 9.
118. Latham, D.A., A.M. Reay, and S. Pampanin. *Kilmore Street Medical Centre: Application of an Advanced Flag-Shape Steel Rocking System*. in *New Zealand Society for Earthquake Engineering–NZSEE–Conference*. 2013. Wellington, New Zealand.26-28
119. Soydan, C., E. Yuksel, and E. İrtem, *The behavior of a steel connection equipped with the lead extrusion damper.* Advances in Structural Engineering, 2014. **17**(1): p. 25-39.
120. Latham, D., A.M. Reay, and S. Pampanin. *Kilmore street medical centre: Application of a post-tensioned steel rocking system*. in *Steel Innovations Conference 2013*. 2013. Christchurch, New Zealand
121. Rodgers, G.W., Mander, J.B, Chase, J.G, Dhakal, R.P, Leach N.C., Denmead, C.S., *Spectral Analysis and Design Approach for High Force-to-Volume Extrusion Damper-Based Structural Energy Dissipation.* Earthquake Engineering & Structural Dynamics, 2008. **37**(2): p. 207 - 223.
122. Rodgers, G., J. Mander, and J. Chase, *Full-Scale Experimental Validation of a DAD Post-Tensioned Concrete Connection Utilising Embedded High Force-to-Volume Lead Dampers*, in *New Zealand Society for Earthquake Engineering (NZSEE)* 2009: Christchurch
123. Mander, T.J., G.W. Rodgers, J.G. Chase, J.B. Mander, G.A. MacRae, and R.P. Dhakal, *Damage Avoidance Design Steel Beam-Column Moment Connection Using High-Force-to-Volume Dissipators.* Journal Of Structural Engineering, 2009. **135**(11): p. 1390-1397.
124. Bacht, T., Chase, J. G., MacRae, G., Rodgers, G. W., Rabczuk, T., Dhakal, R. P., & Desombre, J., *HF2V Dissipator Effects on the Performance of a 3 Story Moment Frame.* Journal of Constructional Steel Research, 2011. **67**(12): p. 1843 - 1849.
125. Rodgers, G.W., Solberg, K. M., Chase, J. G., Mander, J. B., Bradley, B. A., Dhakal, R. P., & Li, L. , *Performance of a Damage-Protected Beam-Column Subassembly Utilizing External HF2V Energy Dissipation Devices.* Earthquake Engineering & Structural Dynamics, 2008. **37**(13).
126. Rodgers, G.W., J.B. Mander, and J.G. Chase. *Full-Scale Experimental Validation of a DAD Post-Tensioned Concrete Connection Utilising Embedded High Force-to-Volume Lead Dampers*. in *New Zealand Society for Earthquake Engineering (NZSEE 2009)*. 2009. Christchurch
127. Rodgers, G.W., Denmead, C., Leach, N., Chase, J.G., Mander, J.B. *Spectral Evaluation of High Force-Volume Lead Dampers for Structural Response Reduction*. in *Proc. New Zealand Society for Earthquake Engineering Annual Conference*. 2006. Napier, New Zealand
128. Desombre, J.R., G.W.; MacRae, G.A.; Rabczuk, T.; Dhakal, R.P.; Chase, J.G., *Experimentally validated FEA models of HF2V damage free steel connections for use in full structural analyses.* 2011.
129. Rodgers, G. and J. Chase. *Development of combined passive and semi-active damping techniques for net-zero base-shear damping*. in *Proceeding of the New Zealand Society for Earthquake Engineering Annual Conference (NZSEE 2010), Wellington, New Zealand, 26-28 March*. 2010.
130. Roland, T., G. Rodgers, J. Chase, and G. MacRae, *Spectral analysis and Assessment of a net-zero base-shear energy dissipation approach for seismic energy mitigation*, in

Proceedings of the Ninth Pacific Conference on Earthquake Engineering (PCEE 2011). 2011: Auckland, New Zealand p. 9.
131. Rodgers, G., J. Chase, T. Roland, and G. MacRae, *Spectral analysis for a semi-active–passive net-zero base-shear design concept.* Earthquake Engineering & Structural Dynamics, 2012. **41**(8): p. 1207-1216.
132. Golzar, F.G., G.W. Rodgers, and J.G. Chase, *Nonlinear Spectral Analysis for Structures with Re-centring D3 Viscous Dissipaters.* Journal of Earthquake Engineering, 2018: p. 1-17.
133. Golzar, F.G., G.W. Rodgers, and J.G. Chase, *Impact of Hybrid Damping Devices on Structural Response Parameters, Including Base Shear and Peak and Residual Drifts*, in *16th World Conference on Earthquake, 16WCEE 2017*. 2017: Santiago, Chile.
134. Ghahramanian Golzar, F., *Hybrid passive seismic mitigation devices for low-damage structures*, in *Mechanical Engineering*. 2018, University of Canterbury: Christchurch, New Zealand.
135. Kato, F., Rodgers, G.W., MacRae, G.A., Chase, J.G., *Spectral Design Analysis of Sliding Hinge Joints and HF2V Devices for Seismic Dissipation*, in *New Zealand Society of Earthquake Engineers Annual Meeting (NZSEE 2012)*. 2012: Christchurch, New Zealand
136. Rodgers, G.W., Solberg, K.M, Mander J.B, Chase, J.G, Bradley, B.A, Dhakal, R.P., *High-Force-to-Volume Seismic Dissipators Embedded in a Jointed Precast Concrete Frame.* Journal of Structural Engineering, 2012. **138**(3): p. 375-386.
137. Rodgers, G.W., J.B. Mander, and J. Geoffrey Chase, *Modeling cyclic loading behavior of jointed precast concrete connections including effects of friction, tendon yielding and dampers.* Earthquake Engineering & Structural Dynamics, 2012. **41**(15): p. 2215-2233.
138. MacRae, G., C. Clifton, and S. Innovations. *Low damage design of steel structures*. in *Steel Innovations 2013 Workshop* 2013. Christchurch, New Zealand: Steel Construction New Zealand
139. Mander, T.J., Rodgers, G.W., Chase, J.G., Mander, J.B., MacRae, G.A., Dhakal, R.P, *Damage avoidance design steel beam-column moment connection using high-force-to-volume dissipators.* Journal of structural engineering, 2009. **135**(11): p. 1390-1397.
140. Geoffrey W. Rodgers, J.B.M., J. Geoffrey Chase, *Semi-explicit rate-dependent modeling of damage-avoidance steel connections using HF2V damping devices.* Earthquake Engineering & Structural Dynamics, 2011. **40**(9): p. 977-992.
141. Rodgers, G., J. Chase, R. Dhakal, K. Solberg, G. Macrae, J. Mander, and T. Mander, *Investigation of rocking connections designed for damage avoidance with high force-to-volume energy dissipation*, in *14th World Conference on Earthquake Engineering (14 WCEE)*. 2008: Beijing, China
142. Rodgers, G.W., J.B. Mander, J.G. Chase, and R.P. Dhakal, *Beyond ductility: parametric testing of a jointed rocking beam-column connection designed for damage avoidance.* Journal of Structural Engineering, 2015. **142**(8): p. C4015006.
143. Wrzesniak, D., Rodgers, G.W., Fragiacomo, M., Chase, J.G., *Experimental testing and analysis of damage-resistant rocking glulam walls with lead extrusion dampers.* Construction and Building Materials, 2016(102): p. 1145-1153.
144. Rodgers, G.W., Chase, J.G., MacRae, G.A., Bacht, T., Dhakal, R.P., Desombre, J., *Influence Of HF2V Damping Devices On The Performance Of The SAC3 Building Subjected To The SAC Ground Motion Suites*, in *9th U.S. National & 10th Canadian Conference on Earthquake Engineering (9USN-10CCEE)*. 2010: Toronto.
145. Rodgers, G.W., J.G. Chase, G. MacRae, T. Bacht, J. Desombre, and R.P. Dhakal, *Analytical Investigation of the Effects of HF2V Damping Devices on the Seismic*

Performance of the SAC3 Building, in *13th Asia Pacific Vibration Conference (APVC 2009)*. 2009: University of Canterbury, New Zealand.
146. Muir, C., D. Bull, and S. Pampanin. *Seismic testing of the slotted beam detail for reinforced concrete structures*. in *Structures Congress 2013: Bridging Your Passion with Your Profession*. 2013. Pittsburgh.2614-2625
147. Muir, C.A., *Seismic performance of the slotted beam detail in reinforced concrete moment resisting frames*, in *Civil and Natural Resources Engineering*. 2014, University of Canterbury.
148. Rodgers, G.W., Chase, J.G., Heaton, D., Cleeve, L., *Testing of Lead Extrusion Damping Devices Undergoing Representative Earthquake Velocities*, in *New Zealand Society for Earthquake Engineering (NZSEE) Annual Technical Conference*. 2013: Wellington, New Zealand.
149. Rodgers, G.W., Chase, J.G.,Mander, J.B., *Repeatability and High-Speed Validation of Supplemental Lead-Extrusion Energy Dissipation Devices.* Advances in Civil Engineering, 2019. **Vol 2019**: p. 13.
150. Aher, S., Mar, D., Rodgers, G.W, *Rocking walls with lead extrusion dampers protect formerly homeless seniors from earthquake risks* in *17th U.S.-Japan-New Zealand Workshop on the Improvement of Structural Engineering and Resilience* 2018: Queenstown, New Zealand
151. Helm, N. *Rocking and rolling in the Garden City*. Build 2019. **172**, 62- 65.
152. Kordani, R., G. Rodgers, and J. Chase, *Response analysis of hybrid damping device with self-centring*, in *New Zealand Society of Earthquake Engineering (NZSEE 2015)*. 2015: Rotorua, New Zealand.
153. Kordani, R., G. Rodgers, and J. Chase, *Analysis of Hybrid Damping Device with Self-Centring*, in *8th International Conference on Behavior of Steel Structures in Seismic Areas (STESSA 2015)*. 2015: Shanghai, China. p. 8.
154. Golzar, F.G., G.W. Rodgers, and J.G. Chase, *Nonlinear spectral design analysis of a structure for hybrid self-centring device enabled structures.* Structural Engineering and Mechanics, 2017. **61**(6): p. 701-709.
155. Patel, C.C., *Seismic Analysis of Parallel Structures Coupled by Lead Extrusion Dampers.* International Journal of Advanced Structural Engineering. **9**(2).
156. Yang, M., Z. Xu, and X. Zhang, *Experimental study on lead extrusion damper and its earthquake mitigation effects for large-span reticulated shell.* Steel and Composite Structures, 2015. **18**(2): p. 481-496.
157. Jun, Y., *An investigation on extruded lead dampers used to reduce the seismic response of building structures* Building Technique Development, 2001. **4**.
158. YAN, W., Y. LI, Y. CHEN, and L. SU, *Study on Application of Lead Extrusion Dampers in Seismic Control of Viaducts [J]*. Journal of Highway and Transportation Research and Development, 2011. **4**.
159. Tsai, C.S.L., W.S.; Chang, C.W.; Li, M.C. *Testing and analysis of a new lead-extrusion damper*. in *ASME 2002 Pressure Vessels and Piping Conference*. 2002. American Society of Mechanical Engineers.215-220
160. Rodgers, G.W., Chase, J.G., Mander, J.B., Leach, N.C., Denmead, C.S., *Experimental Development, Tradeoff Analysis and Design Implementation of High Force-to-Volume Damping Technology.* Bulletin of the New Zealand Society for Earthquake Engineering 2007, 2007. **40**(2): p. 35-48.
161. Pearson, C.E. and R.N. Parkins, *The Extrusion of Metals*. 1960: Chapman & Hall.

162. Pekcan, G., Mander, J.B., Chen, S.S., *Fundamental Considerations for the Design of Non-Linear Viscous Dampers.* Earthquake Engineering & Structural Dynamics, 1999. **28**(11): p. 1405-1425.
163. Golondrino, J.C., Chase, J.G., Rodgers, G.W., MacRae, G.A., Clifton, C., *Velocity Dependence of HF2V Devices Using Different Shaft Configurations*, in *NZSEE Annual Conference* 2012: Christchurch, New Zealand.
164. Golondrino, J.C., Chase, J.G., Rodgers, G.W., MacRae, G.A., Clifton, C.G. *Velocity Effects on the Behaviour of High-Force-To-Volume Lead Dampers (HF2V) Using Different Shaft Configurations*. in *Proceedings of the Fifteenth World Conference on Earthquake Engineering*. 2012. Lisbon, Portugal
165. Harrell, F.E., K.L. Lee, and D.B. Mark, *Tutorial in biostatistics multivariable prognostic models: issues in developing models, evaluating assumptions and adequacy, and measuring and reducing errors.* Statistics in medicine, 1996. **15**: p. 361-387.
166. Snee, R.D., *Validation of regression models: methods and examples.* Technometrics, 1977. **19**(4): p. 415-428.
167. Steyerberg, E.W. and Y. Vergouwe, *Towards better clinical prediction models: seven steps for development and an ABCD for validation.* European Heart Journal, 2014. **35**(29): p. 1925-1931.
168. Giancristofaro, R.A. and L. Salmaso, *Model performance analysis and model validation in logistic regression.* Statistica, 2007. **63**(2): p. 375-396.
169. Lee, J. and Y.-Y.R. Wang, *On Validation Approaches in Data Production*. 1993: Total Data Quality Management Research Program, Sloan School of Management ….
170. Justice, A.C., K.E. Covinsky, and J.A. Berlin, *Assessing the generalizability of prognostic information.* Annals of internal medicine, 1999. **130**(6): p. 515-524.
171. Mondol, M.H. and M.S. Rahman, *A comparison of internal validation methods for validating predictive models for binary data with rare events.* Journal of Statistical Research, 2017. **51**(2): p. 131-144.
172. Stone, M., *Cross-validatory choice and assessment of statistical predictions.* Journal of the Royal Statistical Society: Series B (Methodological), 1974. **36**(2): p. 111-133.
173. Picard, R.R. and R.D. Cook, *Cross-validation of regression models.* Journal of the American Statistical Association, 1984. **79**(387): p. 575-583.
174. Shao, J., *Linear model selection by cross-validation.* Journal of the American statistical Association, 1993. **88**(422): p. 486-494.
175. Hansen, L.K. and J. Larsen, *Linear unlearning for cross-validation.* Advances in computational mathematics, 1996. **5**(1): p. 269-280.
176. Kramer, C. and P. Gedeck, *Leave-cluster-out cross-validation is appropriate for scoring functions derived from diverse protein data sets.* Journal of chemical information and modeling, 2010. **50**(11): p. 1961-1969.
177. Ballester, P.J. and J.B. Mitchell, *Comments on "leave-cluster-out cross-validation is appropriate for scoring functions derived from diverse protein data sets": Significance for the validation of scoring functions*. 2011, ACS Publications.
178. Cawley, G.C. and N.L. Talbot, *Efficient leave-one-out cross-validation of kernel fisher discriminant classifiers.* Pattern Recognition, 2003. **36**(11): p. 2585-2592.
179. Cawley, G.C. *Leave-one-out cross-validation based model selection criteria for weighted LS-SVMs*. in *The 2006 ieee international joint conference on neural network proceedings*. 2006. IEEE.1661-1668
180. Filzmoser, P., B. Liebmann, and K. Varmuza, *Repeated double cross validation.* Journal of Chemometrics: A Journal of the Chemometrics Society, 2009. **23**(4): p. 160-171.

181. Karasuyama, M., I. Takeuchi, and R. Nakano, *Efficient leave-m-out cross-validation of support vector regression by generalizing decremental algorithm.* New Generation Computing, 2009. **27**(4): p. 307.
182. Koul, A., C. Becchio, and A. Cavallo, *Cross-validation approaches for replicability in psychology.* Frontiers in Psychology, 2018. **9**: p. 1117.
183. Bleeker, S., H. Moll, E. Steyerberg, A. Donders, G. Derksen-Lubsen, D. Grobbee, and K. Moons, *External validation is necessary in prediction research:: A clinical example.* Journal of clinical epidemiology, 2003. **56**(9): p. 826-832.
184. Steyerberg, E.W., S.E. Bleeker, H.A. Moll, D.E. Grobbee, and K.G. Moons, *Internal and external validation of predictive models: a simulation study of bias and precision in small samples.* Journal of clinical epidemiology, 2003. **56**(5): p. 441-447.
185. Steyerberg, E.W. and F.E. Harrell, *Prediction models need appropriate internal, internal–external, and external validation.* Journal of clinical epidemiology, 2016. **69**: p. 245-247.
186. Saha, P.K., *Aluminum extrusion technology*. 2000: Asm International.
187. Chen, C. and F. Ling, *Upper-bound solutions to axisymmetric extrusion problems.* International Journal of Mechanical Sciences, 1968. **10**(11): p. 863-879.
188. Adie, J. and J. Alexander, *A graphical method of obtaining hodographs for upper-bound solutions to axi-symmetric problems.* International Journal of Mechanical Sciences, 1967. **9**(6): p. 349-357.
189. Drucker, D., W. Prager, and H. Greenberg, *Extended limit design theorems for continuous media.* Quarterly of applied mathematics, 1952. **9**(4): p. 381-389.
190. Hosford, W., & Caddell, R., *Mechanics and Metallurgy*. Upper-Bound Analysis. 2007, Cambridge: Cambridge University Press.
191. Kudo, H., *An upper-bound approach to plane-strain forging and extrusion—III.* International Journal of Mechanical Sciences, 1960. **1**(4): p. 366-368.
192. Chen, P.C., *Upper bound solutions to plane-strain extrusion problems.* Journal of Engineering for Industry, 1970. **92**(1): p. 158-164.
193. Hashmi, M., *A lower bound solution for the plane strain extrusion forging process.* Mathematical and Computer Modelling: An International Journal, 1988. **11**: p. 1183-1188.
194. Oluwole, O. and A. Adewumi, *Comparative analysis of analytical and graphical upperbound solutions for 4-high reversing aluminium cold-rolling sheet mill.* Science and Technology, 2012. **2**(1): p. 30-36.
195. Avitzur, B., E.D. Bishop, and W.C. Hahn, *Impact extrusion—Upper bound analysis of the early stage.* Journal of Engineering for Industry, 1972. **94**(4): p. 1079-1086.
196. Tiernan, P., Hillery, M.T.,Draganescu, B.,Gheorghe, M., *Modelling of cold extrusion with experimental verification.* Journal of Materials Processing Technology, 2005. **168**(2): p. 360-366.
197. Pop, M., D. Frunza, and A. Neag, *Experimental and Numerical Aspects Regarding Lead Alloy Plastic Deformation.* Romanian Journal of Technical Sciences Applied Mechanics, 2012. **57**(1): p. 71-82.
198. Pop, M., Frunza, D., Neag, A., Pavel,C., *Researches on forward extrusion of lead alloy.* Metalurgia, 2012. **64**(1 : 10 - III).
199. Socaciu, T., *An analysis regarding the variation of necessary force by the indirect extrusion processes.* Procedia Technology, 2014. **12**: p. 433-438.
200. Ajiboye, J.S., *Upper bound analysis of extrusion from square billets through circular and square/rectangular dies.* Journal of Mechanical Science and Technology, 2009. **23**(2): p. 461-474.

201. Ebrahimi, M., S.N. Tiji, and F. Djavanroodi, *Upper bound solution of equal channel forward extrusion process as a new severe plastic deformation method.* Metallurgical Research & Technology, 2015. **112**(6).
202. Samanta, S., *A new die profile with high process efficiency.* Applied Scientific Research, 1972. **25**(1): p. 54-64.
203. Yang, D.Y. and C.H. Han, *A New Formulation of Generalized Velocity Field for Axisymmetric Forward Extrusion Through Arbitrarily Curved Dies.* Journal of Manufacturing Science and Engineering, 1987. **109**(2): p. 161-168.
204. Pop, M., D. Frunza, and A. Neag, *Experimental and Numerical Aspects Regarding Lead Alloy Plastic Deformation.*
205. Lee, B., Y. Keum, and R. Wagoner, *Modeling of the friction caused by lubrication and surface roughness in sheet metal forming.* Journal of materials processing technology, 2002. **130**: p. 60-63.
206. Yoo, S.-S. and D.-E. Kim, *Minimum lubrication technique using silicone oil for friction reduction of stainless steel.* International Journal of Precision Engineering and Manufacturing, 2013. **14**(6): p. 875-880.
207. GAZZARD, S.T., D.H. ROBERTS, J.C. MOORE, and N.A. RATCLIFF. *Dispersion Strengthened Lead for Cable Sheathing* in *The Second International Conference on Lead*. October 4-7 1965 Arnhem: Elsevier Science
208. Bowden, F.P. and L. Leben, *The nature of sliding and the analysis of friction.* Proceedings of the Royal Society of London. Series A. Mathematical and Physical Sciences, 1939. **169**(938): p. 371-391.
209. Vishnupriya, V., G.W. Rodgers, and J.G. Chase, *Precision Design Modelling of HF2V devices*, in *New Zealand Society of Earthquake Engineering Annual Conference (NZSEE 2017) and the AntiSeismic Systems International Society (ASSISI) 15th World Conference on Seismic Isolation, Energy Dissipation and Active Vibration Control of Structures*. 2017: Wellington, NZ.
210. Vishnupriya, V., G.W. Rodgers, J.B. Mander, and J.G. Chase, *Precision Design Modelling of HF2V Devices.* Structures, 2018. **14**: p. 243-250.
211. Symons, D.D., J. Chen, and P. Alton, *Calculation of optimal jaw geometry for an electronic bond pull test.* Proceedings of the Institution of Mechanical Engineers, Part C: Journal of Mechanical Engineering Science, 2014. **228**(11): p. 1847-1858.
212. Kong, L. and P. Hodgson, *Constitutive modelling of extrusion of lead with cyclic torsion.* Materials Science and Engineering: A, 2000. **276**(1-2): p. 32-38.
213. Kong, L., P. Hodgson, and B. Wang, *Development of constitutive models for metal forming with cyclic strain softening.* Journal of Materials Processing Technology, 1999. **89**: p. 44-50.
214. Horrobin, D. and R. Nedderman, *Die entry pressure drops in paste extrusion.* Chemical Engineering Science, 1998. **53**(18): p. 3215-3225.
215. Groover, M.P., *Principles of Modern Manufacturing: SI Version*. 2013: Wiley.
216. Anand, L. and W. Tong, *A constitutive model for friction in forming.* CIRP annals, 1993. **42**(1): p. 361-366.
217. Childs, T., *Friction modelling in metal cutting.* Wear, 2006. **260**(3): p. 310-318.
218. Flitta, I. and T. Sheppard, *Nature of friction in extrusion process and its effect on material flow.* Materials science and technology, 2003. **19**(7): p. 837-846.
219. Sohrabpour, S., A.H. Shabaik, and E.G. Thomsen, *Local Friction Coefficients in Axisymmetric Extrusions of Aluminum.* Journal of Manufacturing Science and Engineering, 1970. **92**(2): p. 461-467.

220. Evans, W. and B. Avitzur, *Measurement of Friction in Drawing, Extrusion, and Rolling.* Journal of Tribology, 1968. **90**(1): p. 72-80.
221. Liu, Y.F., Li, J. ,Zhang, Z.M., Hu, X.H., Zhang, W.J., *Experimental comparison of five friction models on the same test-bed of the micro stick-slip motion system.* Mechanical Sciences, 2015. **6**(1): p. 15-28.
222. Bakhshi-Jooybari, M., *A theoretical and experimental study of friction in metal forming by the use of the forward extrusion process.* Journal of materials processing technology, 2002. **125**: p. 369-374.
223. Dongare, V.S., *Hot Extrusion of Carbon Nanotube-Magnesium Matrix Composite Wire*. 2014, Ohio University.
224. DePierre, V. and F. Gurney, *A method for determination of constant and varying friction factors during ring compression tests.* Journal of Lubrication Technology, 1974. **96**(3): p. 482-487.
225. Velu, R. and M. Cecil, *Quantifying Interfacial Friction in Cold Forming using Forward Rod Backward Cup Extrusion Test.* Journal of The Institution of Engineers (India): Series C, 2012. **93**(2): p. 157-161.
226. Hosford, W.F. and R.M. Caddell, *Metal forming: mechanics and metallurgy*. 2011: Cambridge University Press.
227. Pradip, K., *Aluminum extrusion technology.* ASM International, Ohio, 2000.
228. Wrzesniak, D., Rodgers, G. W., Fragiacomo, M., Chase, J. G., *Experimental testing of damage-resistant rocking glulam walls with lead extrusion dampers.* CONSTRUCTION AND BUILDING MATERIALS, 2016. **102**: p. 1145-1153.
229. Wong, S., P.D. Hodgson, and P.F. Thomson, *Room temperature deformation and recrystallisation behaviour of lead and lead–tin alloys in torsion and plane strain compression.* Materials science and technology, 1999. **15**(6): p. 689-696.
230. Loizou, N., Sims, R.B., *The yield stress of pure lead in compression.* Journal of the Mechanics and Physics of Solids, 1953. **1**(4): p. 234-243.
231. Phaniraj, C., D. Samantaray, S. Mandal, and A. Bhaduri, *A new relationship between the stress multipliers of Garofalo equation for constitutive analysis of hot deformation in modified 9Cr–1Mo (P91) steel.* Materials Science and Engineering: A, 2011. **528**(18): p. 6066-6071.
232. Wong, S., P.D. Hodgson, and P. Thomson, *Comparison of torsion and plane-strain compression for predicting mean yield strength in single-and multiple-pass flat rolling using lead to model hot steel.* Journal of materials processing technology, 1995. **53**(3-4): p. 601-616.
233. Mukherjee, A.K., *An examination of the constitutive equation for elevated temperature plasticity.* Materials Science and Engineering: A, 2002. **322**(1-2): p. 1-22.
234. Molaei, S., M. Shahbaz, and R. Ebrahimi, *The relationship between constant friction factor and coefficient of friction in metal forming using finite element analysis.* Iranian Journal of Materials Forming, 2014. **1**(2): p. 14-22.
235. Sheppard, T., P. Tunnicliffe, and S. Patterson, *Direct and indirect extrusion of a high strength aerospace alloy (AA 7075).* Journal of Mechanical Working Technology, 1982. **6**(4): p. 313-331.
236. Tober, G., O. Anopuo, and P. Maier. *Lead as Test Rolling Material for Hot Complex Rolling of Steel*. in *Advanced Materials Research*. 2012. Trans Tech Publ.84-88
237. Rack, H.J. and G.A. Knorovsky, *Assessment of stress-strain data suitable for finite-element elastic--plastic analysis of shipping containers*. 1978, Sandia Labs.

238. Syahrullail, S., C. Azwadi, and Y. Najib, *The influences of the die half angle of taper die during cold extrusion process.* Arabian Journal for Science and Engineering, 2013. **38**(5): p. 1201-1207.
239. Wu, C.-Y. and Y.-C. Hsu, *The influence of die shape on the flow deformation of extrusion forging.* Journal of Materials Processing Technology, 2002. **124**(1-2): p. 67-76.
240. Zuan, A., S. Yong, M. Nurul, S. Syahrullail, and E. Rahim, *The Effects Of The Die Half Angle Of Taper Die On Plane Strain Extrusion.* Jurnal Teknologi, 2016. **78**(9-2).
241. Mohapatra, S.K., *Aluminium Based Material Extrusion through Mathematical Contoured Die: Numerical & Experimental Investigation*. 2016.
242. Yadav, S., Repetto, E.A., Ravichandran, G.,Ortiz, M., *A computational study of the influence of thermal softening on ballistic penetration in metals.* International Journal of Impact Engineering, 2001. **25**(8): p. 787-803.
243. Hora, P., Becker, C.,Tong, L.C., Maier, J., Müller, S. *Advanced frictional models for extrusion application*. in *Key Engineering Materials*. 2014. Trans Tech Publ.41-48
244. Saha, P.K., *Thermodynamics and tribology in aluminum extrusion.* Wear, 1998. **218**(2): p. 179-190.
245. Madakson, P.B., *The frictional behaviour of materials.* Wear, 1983. **87**(2): p. 191-206.
246. Rabinowicz, E., *The nature of the static and kinetic coefficients of friction.* Journal of applied physics, 1951. **22**(11): p. 1373-1379.
247. Wang, L., J. Zhou, J. Duszczyk, and L. Katgerman, *Friction in aluminium extrusion—Part 1: A review of friction testing techniques for aluminium extrusion.* Tribology International, 2012. **56**: p. 89-98.
248. Oden, J. and J. Martins, *Models and computational methods for dynamic friction phenomena.* Computer methods in applied mechanics and engineering, 1985. **52**(1-3): p. 527-634.
249. Hsu, T.-C. and C.-C. Huang, *The friction modeling of different tribological interfaces in extrusion process.* Journal of Materials Processing Technology, 2003. **140**(1-3): p. 49-53.
250. Ma, X., M.B. De Rooij, and D.J. Schipper, *Modelling of contact and friction in aluminium extrusion.* Tribology international, 2010. **43**(5-6): p. 1138-1144.
251. Wang, L. and H. Yang, *Friction in aluminium extrusion—part 2: A review of friction models for aluminium extrusion.* Tribology International, 2012. **56**: p. 99-106.
252. Zhang, X., Y. Zhu, Y. Yang, and C. Xu, *Mechanical Behavior of Lead at High Strain Rates.* Journal of Materials Engineering and Performance, 2019: p. 1-7.
253. Kalpakjian, S., S. Schmid, and H. Musa, *Mechanical behavior, testing, and manufacturing properties of materials.* Manufacturing, Engineering & Technology, 6th ed., Pearson Education Inc., Upper Saddle River, NJ, 2008: p. 56-87.
254. DeLo, D. and S. Semiatin, *Finite-element modeling of nonisothermal equal-channel angular extrusion.* Metallurgical and Materials Transactions A, 1999. **30**(5): p. 1391-1402.
255. Liang, R. and A.S. Khan, *A critical review of experimental results and constitutive models for BCC and FCC metals over a wide range of strain rates and temperatures.* International Journal of Plasticity, 1999. **15**(9): p. 963-980.
256. Peroni, L., M. Scapin, C. Fichera, A. Manes, and M. Giglio. *Mechanical properties at high strain-rate of lead core and brass jacket of a NATO 7.62 mm ball bullet*. in *EPJ Web of Conferences*. 2012. EDP Sciences.01060

257. Grunenwald, T., F. Llorca, and J. Farre. *A modeling of visco-plastic behavior of lead and a lead alloy over a wide range of strain rate and temperature*. in *Journal de Physique IV (Proceedings)*. 2003. EDP sciences.99-104
258. Lesar, D.E., *Calculation of contact pressures and frictional effects on mechanical contact surfaces by finite element methods with application to fretting damage prediction*. 1982, DAVID W TAYLOR NAVAL SHIP RESEARCH AND DEVELOPMENT CENTER BETHESDA MD.
259. Jin, X. and Y. Altintas, *Prediction of micro-milling forces with finite element method.* Journal of Materials Processing Technology, 2012. **212**(3): p. 542-552.
260. Heislitz, F., H. Livatyali, M.A. Ahmetoglu, G.L. Kinzel, and T. Altan, *Simulation of roll forming process with the 3-D FEM code PAM-STAMP*. Journal of Materials Processing Technology, 1996. **59**(1-2): p. 59-67.
261. Maker, B.N. and X. Zhu, *Input parameters for metal forming simulation using LS-DYNA.* Livermore Software Technology Corporation, 2000. **4**: p. 43-46.
262. Gierzyńska-Dolna, M. and P. Lacki, *Some aspects of modelling of metal forming processes.* Computers & structures, 2003. **81**(8-11): p. 605-613.
263. Facchinetti, M. and W. Miszuris, *Analysis of the maximum friction condition for green body forming in an ANSYS environment.* Journal of the European Ceramic Society, 2016. **36**(9): p. 2295-2302.
264. Karamyshev, A., I. Nekrasov, V. Parshin, A. Fedulov, and A. Pugin, *Modeling metal-shaping operations in DEFORM-3D in order to efficiently design production processes.* Metallurgist, 2012. **56**(1-2): p. 115-118.
265. Liu, G., K. Huang, J. Zhou, and J. Duszczyk, *Simulation of steady-state extrusion through a hollow die using HyperXtrude FE software.* Computer methods in materials science, 2011. **11**(2): p. 259-264.
266. Mehta, B.V., I. Al-Zkeri, J.S. Gunasekera, and A. Buijk, *3D flow analysis inside shear and streamlined extrusion dies for feeder plate design.* Journal of Materials Processing Technology, 2001. **113**(1-3): p. 93-97.
267. Marie, S., R. Ducloux, P. Lasne, J. Barlier, and L. Fourment. *Inverse Analysis of Forming Processes based on FORGE environment*. in *Key Engineering Materials*. 2014. Trans Tech Publ.1494-1502
268. Chaudhari, S. and M. Chakrabarti, *Modeling of concrete for nonlinear analysis using finite element code ABAQUS.* International Journal of Computer Applications, 2012. **44**(7): p. 14-18.
269. Li, S., Bourke, M.A.M., Beyerlein, I.J., Alexander, D.J., Clausen, B., *Finite element analysis of the plastic deformation zone and working load in equal channel angular extrusion.* Materials Science and Engineering: A, 2004. **382**(1-2): p. 217-236.
270. Nasr, M.N. and M.M. Ammar, *An evaluation of different damage models when simulating the cutting process using FEM.* Procedia CIRP, 2017. **58**: p. 134-139.
271. Lei, S., Y.C. Shin, and F.P. Incropera, *Thermo-mechanical modeling of orthogonal machining process by finite element analysis.* International Journal of Machine Tools and Manufacture, 1999. **39**(5): p. 731-750.
272. Kathirgamanathan, P. and T. Neitzert. *Modelling of metal extrusion using ABAQUS*. in *The Proceedings of 3rd NZ Metals Industry Conference*. 2006.
273. Sevier, M., H. Yang, S. Lee, and S. Chandrasekar, *Severe plastic deformation by machining characterized by finite element simulation.* Metallurgical and Materials Transactions B, 2007. **38**(6): p. 927.

274. Sevier, M., H. Yang, W. Moscoso, and S. Chandrasekar, *Analysis of severe plastic deformation by large strain extrusion machining.* Metallurgical and materials transactions A, 2008. **39**(11): p. 2645-2655.
275. Weber, M., H. Autenrieth, J. Kotschenreuther, P. Gumbsch, V. Schulze, D. Löhe, and J. Fleischer, *Influence of friction and process parameters on the specific cutting force and surface characteristics in micro cutting.* Machining Science and Technology, 2008. **12**(4): p. 474-497.
276. Ali, M.H., B.A. Khidhir, M.N.M. Ansari, and B. Mohamed, *FEM to predict the effect of feed rate on surface roughness with cutting force during face milling of titanium alloy.* HBRC Journal, 2013. **9**(3): p. 263-269.
277. Saffar, R.J. and M.R. Razfar, *Simulation of end milling operation for predicting cutting forces to minimize tool deflection by genetic algorithm.* Machining Science and Technology, 2010. **14**(1): p. 81-101.
278. Adetoro, O. and P. Wen, *Prediction of mechanistic cutting force coefficients using ALE formulation.* The International Journal of Advanced Manufacturing Technology, 2010. **46**(1-4): p. 79-90.
279. Henrard, C., C. Bouffioux, P. Eyckens, H. Sol, J. Duflou, P. Van Houtte, A. Van Bael, L. Duchene, and A. Habraken, *Forming forces in single point incremental forming: prediction by finite element simulations, validation and sensitivity.* Computational mechanics, 2011. **47**(5): p. 573-590.
280. Kang, J.H., G.H. Kim, and W.S. Choi, *Impact-Contact Analysis of Prismatic Graphite Blocks Using Abaqus*. 2010, Korea Atomic Energy Research Institute.
281. ABAQUS-Users-Manual, *Version 6.13-2*. Dassault Systémes Simulia Corp., Providence, Rhode Island, USA, 2013.
282. Nair, A.U., L. Hubert, and A.M. Bestelmeyer. *Characterization of damage in hyperelastic materials using standard test methods and abaqus*. in *2009 SIMULIA Customer Conference*. 2009.1-15
283. Wang, T., J. Platts, and A. Levers. *Finite element impact modelling for shot peen forming*. in *Proceedings of the 8th international conference on shot peening, Garmisch-Partenkirchen, Germany*. 2002.
284. Zeng, G., X.-m. Lai, Z.-q. Yu, and Z.-q. Lin, *Numerical simulation and sensitivity analysis of parameters for multistand roll forming of channel section with outer edge.* Journal of Iron and Steel Research International, 2009. **16**(1): p. 32-37.
285. Lindholm, U., *Some experiments with the split hopkinson pressure bar∗.* Journal of the Mechanics and Physics of Solids, 1964. **12**(5): p. 317-335.
286. Gondusky, J.M. and J. Duffy, *The Dynamic Stress-strain Relation of Lead and Its Dependence on Grain Structure*. 1967, Brown Univ Providence Ri Div Of Engineering.
287. Evans, J., *Structural analysis of shipping casks. Vol. 8. Experimental study of the stress-strain properties of lead under specified impact conditions*. 1970, Oak Ridge National Lab.
288. *Engineering Toolbox*. [cited 2001 15 Sep 2018]; Available from: https://www.engineeringtoolbox.com.
289. King, S. and T. Richards, *Solving contact problems with abaqus.* Dassault Systemes, Coventry, UK, 2013.
290. Ramezani, M. and Z.M. Ripin, *A friction model for dry contacts during metal-forming processes.* The International Journal of Advanced Manufacturing Technology, 2010. **51**(1-4): p. 93-102.

291. Yoshida, H., M. Tada, and M. Mochimaru. *3D Finite Element Analysis of the frictional behavior of the human fingertip*. in *2006 International Conference of the IEEE Engineering in Medicine and Biology Society*. 2006. IEEE.91-94
292. Gorczyca, J.L., J.A. Sherwood, L. Liu, and J. Chen, *Modeling of friction and shear in thermostamping of composites-part I.* Journal of Composite Materials, 2004. **38**(21): p. 1911-1929.
293. Lee, K., *Analysis of static and dynamic frictional contact of deformable bodies including large rotations of the contact surfaces.* KSME international journal, 2002. **16**(10): p. 1276-1286.
294. Li, W., S. Shi, F. Wang, Z. Zhang, T. Ma, and J. Li, *Numerical Simulation of Friction Welding Processes Based on ABAQUS Environment.* Journal of Engineering Science & Technology Review, 2012. **5**(3).
295. Rao, G.V.G., P. Mahajan, and N. Bhatnagar, *Micro-mechanical modeling of machining of FRP composites–Cutting force analysis.* Composites science and technology, 2007. **67**(3-4): p. 579-593.
296. FULLER, D.D., *2d. Coefficients of Friction.* American Institute of Physics Handbook, 1963. **1**: p. 42.
297. Chowdhury, M. and D. Nuruzzaman, *Experimental investigation on friction and wear properties of different steel materials.* Tribology in Industry, 2013. **35**(1): p. 42-50.
298. Chowdhury, M., M. Khalil, D. Nuruzzaman, and M. Rahaman, *The effect of sliding speed and normal load on friction and wear property of aluminum.* International Journal of Mechanical & Mechatronics Engineering, 2011. **11**(1): p. 45-49.
299. Han, F., B. Tang, H. Kou, L. Cheng, J. Li, and Y. Feng, *Static recrystallization simulations by coupling cellular automata and crystal plasticity finite element method using a physically based model for nucleation.* Journal of materials science, 2014. **49**(8): p. 3253-3267.
300. Sztwiertnia, K., *Recrystallization*. 2012: BoD–Books on Demand.
301. Rollett, A., *Overview of modeling and simulation of recrystallization.* Progress in materials science, 1997. **42**(1-4): p. 79-99.
302. Hughes, T.J., W.K. Liu, and T.K. Zimmermann, *Lagrangian-Eulerian finite element formulation for incompressible viscous flows.* Computer methods in applied mechanics and engineering, 1981. **29**(3): p. 329-349.
303. Donea, J., S. Giuliani, and J.-P. Halleux, *An arbitrary Lagrangian-Eulerian finite element method for transient dynamic fluid-structure interactions.* Computer methods in applied mechanics and engineering, 1982. **33**(1-3): p. 689-723.
304. Gadala, M., M. Movahhedy, and J. Wang, *On the mesh motion for ALE modeling of metal forming processes.* Finite Elements in Analysis and Design, 2002. **38**(5): p. 435-459.
305. Wang, J. and M.S. Gadala, *Formulation and survey of ALE method in nonlinear solid mechanics.* Finite Elements in Analysis and Design, 1997. **24**(4): p. 253-269.
306. Rodríguez-Ferran, A., F. Casadei, and A. Huerta, *ALE stress update for transient and quasistatic processes.* International Journal for Numerical Methods in Engineering, 1998. **43**(2): p. 241-262.
307. Benson, D.J., *An efficient, accurate, simple ALE method for nonlinear finite element programs.* Computer methods in applied mechanics and engineering, 1989. **72**(3): p. 305-350.
308. Ghosh, S. and N. Kikuchi, *An arbitrary Lagrangian-Eulerian finite element method for large deformation analysis of elastic-viscoplastic solids.* Computer Methods in Applied Mechanics and Engineering, 1991. **86**(2): p. 127-188.

309. Schreurs, P., F. Veldpaus, and W. Brekelmans, *Simulation of forming processes, using the arbitrary Eulerian-Lagrangian formulation.* Computer Methods in Applied Mechanics and Engineering, 1986. **58**(1): p. 19-36.
310. Tu, J., G.H. Yeoh, and C. Liu, *Computational fluid dynamics: a practical approach*. 2018: Butterworth-Heinemann.
311. Gadala, M.S., Wang, J, *Elasto-plastic finite element simulation of rolling and compression between wedge-shaped dies.* Journal of Materials Processing Technology, 2000. **97**(1-3): p. 132-147.
312. Zhao, H., Wang, He-nan, Wang, Meng-jun, Li, Guang-yao, *Simulation of extrusion process of complicated aluminium profile and die trial.* Transactions of Nonferrous Metals Society of China, 2012. **22**(7): p. 1732-1737.
313. Zhuang, X.-C., Zhao, Zhen, Xiang, Hua, Li, Cong-Xin, *Simulation of sheet metal extrusion processes with Arbitrary Lagrangian-Eulerian method.* Transactions of Nonferrous Metals Society of China, 2008. **18**(5): p. 1172-1176.
314. Yildirim, B., S. Muftu, and A. Gouldstone, *Modeling of high velocity impact of spherical particles.* Wear, 2011. **270**(9-10): p. 703-713.
315. Li, W.-Y. and W. Gao, *Some aspects on 3D numerical modeling of high velocity impact of particles in cold spraying by explicit finite element analysis.* Applied Surface Science, 2009. **255**(18): p. 7878-7892.
316. Orszulik, R.R. and U. Gabbert, *An interface between Abaqus and Simulink for high-fidelity simulations of smart structures.* IEEE/ASME Transactions on Mechatronics, 2015. **21**(2): p. 879-887.
317. Miller, K., G. Joldes, D. Lance, and A. Wittek, *Total Lagrangian explicit dynamics finite element algorithm for computing soft tissue deformation.* Communications in numerical methods in engineering, 2007. **23**(2): p. 121-134.
318. Brewer, J.C., *Effects of angles and offsets in crash simulations of automobiles with light trucks*, in *17th International Technical Conference on Enhanced Safety of Vehicles*. 2001, SAE Technical Paper: Amsterdam, Netherlands. p. 8.
319. Camacho, A., M. Marin, L. Sevilla, and R. Domingo, *Influence of strain hardening on forces and contact pressure distributions in forging processes.* Journal of Achievements in Materials and Manufacturing Engineering, 2006. **15**(1/2): p. 166-173.
320. Kim, J.H., J.H. Lim, J.H. Lee, and S. Im, *A new computational approach to contact mechanics using variable-node finite elements.* International journal for numerical methods in engineering, 2008. **73**(13): p. 1966-1988.
321. Lontos, A.E., Soukatzidis, F.A., Demosthenous, D.A., Baldoukas, A.K. *Effect of extrusion parameters and die geometry on the produced billet quality using finite element method*. in *Proceedings of the 3rd international conference on manufacturing engineering (ICMEN), Chalkidiki, Greece*. 2008.215-28
322. Fereshteh-Saniee, F., N. Fakhar, and M. Karimi, *Experimental, analytical, and numerical studies on the forward extrusion process.* Materials and Manufacturing Processes, 2013. **28**(3): p. 265-270.
323. Sohoni, G., M. Walame, V. Tandon, R. Mahajan, and S. Raju. *Dynamic Behavior Characterization of Lead at High Strain Rates Using High Speed Photography for Finite Element Simulation*. in *ASME 2005 International Mechanical Engineering Congress and Exposition*. 2005. American Society of Mechanical Engineers.525-530
324. Bhat, A.R., *Finite element modeling and dynamic impact response evaluation for ballistic applications*. 2009, Oklahoma State University.

325. Wen, S., Keer, L.A., Vaynman, S. L., Lawrence, R., *A constitutive model for a high lead solder*. IEEE Transactions on Components and Packaging Technologies, 2002. **25**(1): p. 23-31.
326. Ertürk, S., *Thermo-mechanical modelling and simulation of magnesium alloys during extrusion process*. 2009, Christian-Albrechts Universität Kiel.
327. Ming, L. and O. Pantalé, *An efficient and robust VUMAT implementation of elastoplastic constitutive laws in Abaqus/Explicit finite element code.* Mechanics & Industry, 2018. **19**(3): p. 308.
328. Suh, N.P. and H.-C. Sin, *The genesis of friction.* Wear, 1981. **69**(1): p. 91-114.
329. Hsia, S.-Y., *Optimization of microextrusion preforming using taguchi method.* Mathematical Problems in Engineering, 2013. **2013**.
330. Nalbant, M., H. Gökkaya, and G. Sur, *Application of Taguchi method in the optimization of cutting parameters for surface roughness in turning.* Materials & design, 2007. **28**(4): p. 1379-1385.
331. Yang, W.p. and Y. Tarng, *Design optimization of cutting parameters for turning operations based on the Taguchi method.* Journal of materials processing technology, 1998. **84**(1-3): p. 122-129.
332. Jurković, Z., M. Jurković, and S. Buljan, *Optimization of extrusion force prediction model using different techniques.* Journal of Achievements in materials and manufacturing engineering, 2006. **17**(1-2): p. 353-356.
333. Park, C., C.-Y. Joh, and Y.-S. Kim, *Multidisciplinary design optimization of a structurally nonlinear aircraft wing via parametric modeling.* International Journal of Precision Engineering and Manufacturing, 2009. **10**(2): p. 87-96.
334. Lanzi, L., A. Airoldi, and C. Chirwa, *Application of an iterative global approximation technique to structural optimizations.* Optimization and Engineering, 2009. **10**(1): p. 109-132.
335. Shinde, S.D., *Standardization of Jib Crane Design by" FEM Rules" And Parametric Modeling.* International Journal of Recent Trends in Engineering, 2009. **1**(5): p. 145.
336. He, L., C. Liu, and Z.Y. Wu. *Parametric modeling and stability analysis of temporary grandstand*. in *Applied Mechanics and Materials*. 2014. Trans Tech Publ.907-916